INTEGRATION OF ICT AND ARTIFICIAL INTELLIGENCE TECHNIQUES TO ENHANCE TOMATO PRODUCTION

March, 2021

DENIS PASTORY RUBANGA

TOKYO UNIVERSITY OF AGRICULTURE

THESIS DISSERTATION FOR THE DEGREE OF
DOCTOR OF PHILOSOPHY IN AGRICULTURAL ENGINEERING

INTEGRATION OF ICT AND ARTIFICIAL INTELLIGENCE TECHNIQUES TO ENHANCE TOMATO PRODUCTION

DENIS PASTORY RUBANGA

Committee Chair: Professor Dr. Kiyoshi TAJIMA

Supervisors: Professor Dr. Sawahiko SHIMADA

Professor Dr. Katsumori HATANAKA

Associate Professor Dr. Ayako SEKIYAMA

March, 2021

ABSTRACT

This research thesis is structured in six Chapters including the general introduction as Chapter 1 and the general conclusion as Chapter 6 to address the research topics summarized in this section.

In **Chapter 2**, we focused at the problem of abiotic factors (herein microclimate) of labor constrained small-scale farmers in Japan. The approach based on ICT technological transfer of smart agriculture system to labor constrained small-scale horticultural farmers to improve tomato production management. The solution to this was applied usage and deployment of a wireless sensor network. The real-time information composed of commercial inexpensive wireless sensor network devices and developed database for crop environment monitoring and management.

In **Chapter 3**, we studied factors to enhance impactful use of computer vison based early detection approach to tackle tomato pest *Tuta absoluta* (*T. absoluta*). A comprehensive study of the demography and farmer information flow was done in the areas mostly affected by *T. absoluta*. We examined tomato farmers knowledge on tomato pest *T. absoluta* damage that could be used to devise recommended platform for introduction of computer vision (CV) based approach to tackle *T. absoluta*. With the field experiments we carried out, we showed a high correlation of decreased marketable tomato due to *T. absoluta* damages. Therefore to solve this problem, a need for early detection was required which was the basis for Chapter 4 and 5.

In **Chapter 4**, we detailed the need for early pest detection for effective management

option at early stages of tomato production to avoid economic losses. The main goal was to develop computer vision based tomato pest early identification and quantification tools that could be used to strengthen phytosanitary capacity and systems for effective management option of *T. absoluta*. In this Chapter, the specific research's objectives was: (1) to develop a *T. absoluta* early identification Convolutional Neural Network (CNN) model under commonly practiced agriculture practices. (2) to develop early detection and quantification CNN models for tomatoes infested by *T. absoluta* damage characteristics and quantification to enhance early detection.

In **Chapter 5**, we focused on using multispecral image analysis to investigate spectral characteristics and applied in detection of *T. absoluta* infested tomato plants under commonly practices agriculture practices using gradient boosting approach. Results showed that the CatBoost model of vegetation index NDVI, GNDi, NRI, and MARI imafeg could be used to detect diseased leaves. Further, Tree Explainer algorithm adopted on SHAP values showed that NDVI and GNDI were the indicators with the highest contribution to the trained model, and that NIR reflection information would be effective in detectiong tomato pest *Tuta absoluta* damage.

In the final **Chapter 6**, we draw conclusions and recommendations based on previous Chapters that focused on the integration of ICT and artificial intelligence techniques to enhance tomato production based on a data driven emerging technological approach.

日本語要約

2050 年までの世界人口 97 億人に対応するためには、作物生産を 60%増やす必要があるとされている。野菜生産の増産の可能性は大きいが、いくつかの課題があげられ、特に気候条件は野菜の生産を大きく制限する。この研究では、特に経営規模の小さいトマト農家に着目し、労働制約・ICT 制約を抱えた日本およびサブサハラ・アフリカ（SSA）における小規模農家を対象とした。本研究は、生物的（トマト害虫・トマトキバガ：*Tuta absoluta*）および非生物的（微気象）要因による損失を減らすことで収量を上げ、食料安全保障の懸念を軽減することを目的に、データ駆動型の情報通信技術（ICT）と人工知能（AI）の新技術移転による小規模農家のトマト生産環境の改善につなげる課題に取り組んだ。

本論文は以下の 4 つの研究成果から成る：第 2 章）労働力制約のある小規模園芸農業におけるスマート農業の応用、第 3 章）ICT 制約のある小規模農家における新技術の研究、第 4 章）深層学習によるトマト害虫の早期発見、第 5 章）マルチスペクトル画像の機械学習によるトマト害虫の発見精度向上。

第 2 章：労働力に制約のある日本の小規模農家の微気象環境に着目し、これに対する解決策として、温室内のワイヤレスセンサーネットワークの開発と展開を行った。リアルタイムデータに基づく分析結果により、作物生育管理が信頼性の高い微気象環境調節で実装可能であることを示した。市販の安価なワイヤレスセンサーネットワークデバイスと、作物環境の温度センサーによる監視と管理によりトマトの収量向上が期待できることを示した。一方、本成果である微気象環境調節の SSA 小規模農家への適用に取り組む際に、事前に解決しなければならない生物的要因による損失の課題があることから、ICT 制約の SSA の小規模農家への ICT ベースの技術移転によるトマト害虫（*T. absoluta*）の損失軽減に着目した（第 3 章、第 4 章、第 5 章）。

第 3 章：この章では、トマト害虫の問題解決に取り組むため、タンザニアにおける *T. absoluta* 被害農家へのアンケート調査結果に基づき、深層学習ベースの手法を導入するための推奨プラットフォーム考案を行った。実験的研究の結果は、市場性のあるトマト市場の減少の高い相関は、*T. absoluta* の損傷によるものであることを示し、早期発見技術の開発が本課題の解決に必要であることが示された。

第 4 章：トマトの害虫 *T. absoluta* の圃場への侵入は、最大 100%の損失被害を引き起こす可能性がある。トマト生産の初期段階で効果的な管理オプションを得、経済的損失を回避するためには、害虫被害個体を早期に特定することが重要となる。本章の目標は、*T. absoluta* の早期識別および定量化ツールとしてのコンピュータービジョンに基づく深層学習技術を開発することである。具体的な目的は、*T. absoluta* 罹病トマト葉画像の畳み込みニューラルネットワーク（CNN）解析を用いた早期検出モデルを開発することである。SSA 国であるタンザニアにおいて 2018 年 8 月～2020 年 5 月の期間で、施設内実験（ネットハウス）を実施した。移植後 2 日目に、植えたトマトの苗に *T. absoluta*（4～8 匹の幼虫）をランダムな植物に接種し、トマト葉の高解像度 RGB 画像およびマルチスペクトル画像を定期的に撮影取得した。トマトの検出タスクでは、トマト葉の被害の有無および被害カテゴリ（被害なし，初期，重度）に分類する精度について、各モデル分類器（ResNet50，VGG16，VGG19，Inception-V3）のパフォーマンスを評価した。 結果として、被害有無検出器としては VGG16 モデルが他のモデルよりも優れていることを示した（精度 90%超）が、定量化（被害軽度・重度）の精度向上には課題を残した。

第 5 章： Sequoia（Parrot 社製）マルチスペクトルカメラを用いて撮影された画像は、Pix4D ソフトウェアを使用して前処理し、 4 つのスペクトルバンド（赤、緑、レッドエッジ、NIR）を用いた植生指数画像に変換し，植物体のみの範囲

に抽出した画像を用いた。個々のトマト植物体の植生指数画像を勾配ブースティング（Xgboost、LightGBoost、CatBoost）による機械学習分類を行った。結果として、植生指数 NDVI、GNDI、NRI、および MARI 画像のキャットブーストモデルが 79.4％の精度での罹病葉検出が可能であることを示しました。さらに、TreeExplainer アルゴリズムにより NDVI と GNDI がモデルへの寄与が最も高い指標であることが示され、トマト害虫被害の特定には近赤外線反射情報が有効であることが示された。

ACKNOWLEDGEMENT

First and foremost, I would like to praise and thank the God, the almighty, who has granted countless blessing, knowledge, and opportunity to finally be able to accomplish the thesis.

Apart from the efforts of me, the success of this thesis depends largely on the encouragement and guidelines of many others. I take this opportunity to express my gratitude to the people who have been instrumental in the successful completion of this thesis.

With immense pleasure and deep sense of gratitude, I wish to express my sincere thanks to the thesis committee chair **Kiyoshi TAJIMA**, Prof, of Faculty of Regional Environmental Science and to my supervisors **Sawahiko Shimada**, Prof, of Faculty of Regional Environmental Science, **Katsumori Hatanaka**, Prof, of Department of Agribusiness Management and **Ayako Sekiyama**, Associate Prof, Faculty of Regional Environmental Science, without their motivation and continuous encouragement, and also for providing me with infrastructural facilities and many other resources needed for my research, this research would not have been successfully completed

I would also like to acknowledge the support rendered by **my laboratory colleagues** in several ways throughout my research work.

I wish to extend my profound sense of gratitude to my **family members** for providing me with moral support and encouragement whenever required.

Last but not the least, I would like to thank my wife **Happy Benedict Magesa** for her constant encouragement and moral support along with patience and understanding for

the time that she needed me but I was undertaking the research works.

TABLE OF CONTENTS

ABSTRACT i

ACKNOWLEDGEMENT vi

LIST OF FIGURES xii

LIST OF TABLES xx

1 GENERAL INTRODUCTION **1**

1.1 Food Demand and Production 1

1.2 Importance of Vegetable production 3

1.3 Research scope and Focus 4

1.3.1 Challenges of vegetation production 4

1.3.2 Marginalized group low-resource farmers 4

1.3.3 Research objective 4

2 SMART AGRICULTURE APPLICATION IN LABOR CONSTRAINED SMALL SCALE HORTICULTURE FARMING. **6**

2.1 Introduction 6

2.2 Research objective 10

2.3 Materials and Methods 11

2.3.1 Smart agriculture system architecture 11

2.3.2 Sensors deployed 11

2.3.3 Data transmission 13
2.3.4 Data storage 14
2.3.5 Deployment in tomato greenhouse 15
2.3.6 Greenhouse microclimate monitoring approach 17
2.3.7 Greenhouse spatiotemporal distribution approach 19
2.4 Results and Discussion 19
2.4.1 Crop growth monitoring using microclimate 19
2.4.2 Spatiotemporal distribution 22
2.5 Conclusions 23

3 A STUDY OF EMERGING TECHNOLOGY IN ICT CONSTRAINED FARMERS 27

3.1 Introduction 27
3.2 Objectives 28
3.3 Study Site and Farmer Survey Data 28
3.4 Description of the study area 31
3.5 Results of farmer survey 32
3.5.1 Challenges farmers face 32
3.5.2 Information inflow 32
3.5.3 Description of farmer tranportation to farms 33
3.5.4 Awareness of *T. absoluta* early detection 34
3.6 Farmer survey discussion and conclusion 35
3.6.1 Experiment Study on *T. absoluta* impact on tomato yield 37
3.7 Results and Discussion of field experiments 38
3.8 Conclusions of field experiments 43

4 IMAGE RECOGNITION OF TOMATO PEST USING DEEP LEARNING TECHNIQUES 44

4.1 Introduction 44

4.2 Review of previous works 46

4.2.1 Computer vision in agriculture crops 46

4.2.2 Computer vision in tomato disease identification 48

4.3 Materials and Methods 50

4.3.1 The dataset 50

4.3.2 Definition of early stage 51

4.3.3 The dataset for classification 52

4.3.4 The dataset for quantification 53

4.3.5 Image pre-processing 53

4.3.6 The proposed CNN classification model 56

4.3.7 General CNN training algorithm 59

4.3.8 CNN Visual Explanation 62

4.3.9 Implementation 62

4.4 Results and discussions 65

4.4.1 Classification model 65

4.4.2 Training quantification classifier 66

4.4.3 Quantification model 70

4.5 Conclusion and Future Work 70

5 IMAGE RECOGNITION USING GRADIENT BOOSTING BASED ON MULTISPECTRAL IMAGING 75

5.1 Introduction 75

5.2 Materials and methods 80
5.2.1 Experiment setup 80
5.2.2 Multispectral image acquisition 81
5.2.3 Multispectral Image Preprocessing and Calculation of image indices 82
5.2.4 Classification of multispectral images using gradient boosting . . . 85
5.2.5 Determination of suitable image indices using TreeExplainer . . . 89
5.3 Results and Discussion 91
5.3.1 Gradient boosting results 91
5.3.2 Vegetation index based on SHAP summary plots 91
5.4 Conclusion 93

6 CONCLUSIONS AND RECOMMENDATION 95

6.1 Conclusion 95
6.2 Recommendation 98
REFERENCES 99
LIST OF PUBLICATIONS 109

Appendices

Appendix A Farm survey - Questionnaire 111

Appendix B Sample Dataset of Tomato Images 120

Appendix C EXIF Meta details of sample Images of cameras useds 123

LIST OF FIGURES

1.1 World food production demand and required threshold level to meet the food deficit shown as in horizontal dotted line 2

1.2 World Population Projection based on country income levels 2

1.3 Global production of selected top seven vegetables 3

2.1 A summary of 150 companies smart agriculture system categories in Japan. 9

2.2 An illustration of smart agriculture system architecture composed of Netatmo WSN devices for microclimate data collection, a Wi-Fi router for the Internet connectivity, a PC for data inputs and DB server for data storage and functions, like a crop calendar and so on. 12

2.3 Showing the deployed wireless sensors used, Netatmo. From left to right are; Outside model, Indoor model(Base station), Additional Module, wind gauge and rain gauge. All Outdoor modules are completely weatherproof. 13

2.4 Showing the deployed wireless sensors used, Netatmo mobile user interface dashboard 14

2.5 A web database used for collection of farm daily activities such as planting date, nursery planting dates, transplanting dates, harvest dates. NB. Japanese characters used since the system was designed for Japanese farmer. 15

2.6 A crop calender showing various complete crop growth cycle. Greeen represent nursery stage,blue represent the vegetative growth and fruiting before maturity and yellow represents the maturity stage as harvesting period. NB. Japanese characters used since the system was designed for Japanese farmer. 16

2.7 (a) WSN device in greenhouse, (b) block within greenhouse and (c) greenhouse layout showing the location of WSN devices. Blue, green and red points are WSN devices. Red points; base station modules that receive data from additional modules, green points and outdoor modules (blue points) connected via Bluetooth (blue dashed lines) to their respective base stations. Black dashed lines; block boundaries. Black solid lines; greenhouse boundaries. The black point with three curved lines; Wi-Fi router. Red boxes in (c); heating facilities. 17

2.8 Daily GDD within the greenhouse (Bottom). Accumulated GDD of selected crop cycle (Middle) Cumulative crop yield of selected crop cycle (Top). GDD denote cumulative GDD, Acc.crop yield denote cumulated daily crop yield. Crop cycle from CV11 to FV12, where first letters (C, D, E and F) denote block name, and appended V11 and V12 denote first crop cycle of normal tomato variety and second crop cycle of normal crop variety respectively 25

2.9 Spatiotemporal monthly GDD variations in tomato greenhouse for November 2017 and January 2018. Values on vertical and horizontal represent the greenhouse length and width in meters. 26

3.1 CLIMEX climatic suitability indices map of *T. absoluta* in Africa. Predictions are based on the eco-climatic index (EI), a measure of climatic suitability scaled from 1–100, for locations within CLIMEX's station database. EI = (0–5) location is not suitable; EI = (5–20) moderate level of suitability; EI = (20–50) high risk of establishment and EI > 50 very high likelihood of long-term survival. 29

3.2 Tanzania map showing the study sites. Green dot represents Arusha site, Red represent Morogoro site and Blue represent Iringa site. 30

3.3 Showing farmer interviewed in (a) the farm and (b) at farmers household during the farmer survey in Morogoro region in August 2020. 31

3.4 Disease Pest and wild animals Problem challenge during farmer survey in August and September 2020. 33

3.5 The usage of farmers Transport categories during farmer survey in August and September 2020. 34

3.6 Farmers awareness of *T.absoluta* damage at crop cycle for surveyed villages during farmer survey in August and September 2020. 35

3.7 Farmers farm visit tendency during crop growth stages. The visits determined by frequencies as 1;daily, 4; 4 days, 7; 7 days, 14; 14 days, 21; 21 days and 30; 30 days interval during farmer survey in August and September 2020. 36

3.8 Field experiment conducted in in-house screen house showing transplanting of tomato seedlings (a-Left) and *T. absoluta* larvae inoculation on the second day after transplanting ((a)-center image) and (a) -right is insert of *T. absoluta* larvae. Damage on plant parts (b) flower and (c) fruits. 38

3.9 Total Tomato per block that includes marketable fruits, non-marketable (affected by *T.absoluta* 39

3.10 Total Tomato yield for 6 irrigation types in each block 39

3.11 Showing Marketable and Non-marketable (affected by *T. absoluta*) yield of 2018 harvest season period 42

3.12 *T. absoluta* impact on crop yeild depicted as decreasing linear yield during farm experiment in between AIgust and September 2020. 42

4.1 In-house experiment set up screen houses. Arusha site (12M x 12M x 4.5M 0.1cm net size) (a) outside view (b) inside view, Morogoro site (15M x 12M x 5m, 0.1cm net size)(c) outside view (d) inside view, Morogoro farmers screen house (e) and (f) 51

4.2 Tomato crop cycle. Green dashed box show the early stage for this research 52

4.3 Tomato crop cycle of *T. absoluta* damage status within the early stage period. (b) Insert of elaborated *T. absoluta* mine damage progress. . . . 54

4.4 Damage status of *T. absoluta* as healthy (No *T. absoluta*), and two classes of affected plants defined as "Low Tuta" and "High Tuta". 54

4.5 *T. absoluta* mine infection progress. (a) is the health leaf before inoculation and red boxes are (b); 2^{nd}, (b); 4^{th}, (b); 6^{th}, and (e); 8^{th} days after inoculation with the *T. absoluta*. 55

4.6 The proposed deep CNN framework pretrained using ImageNet dataset. 57

4.7 Proposed binary classification for plants affected and non-affected *T. absoluta* using pretrained Deep CNN. 58

4.8 VGG16 Architecture. 58

4.9 VGG19 Architecture 58

4.10 Showing (a) Proposed binary classification for plants affected and non-affected *T. absoluta* using pretrained Deep CNN with a Grad-CAM used to visualize the model performance and (b) Shows the original images in the upper rows and the visualized image using Grad-CAM. . . 63

4.11 (a) Proposed Quantification model for plants Low Tuta, High Tuta and non-affected *T. absoluta* using pretrained Deep CNN with a Grad-CAM used to visualize the model performance.(b) Shows the original images in the upper rows and the visualized image using Grad-CAM. 64

4.12 Training and validation accuracy learning curves for the CNN model used in binary classification for plants affected and non-affected with *T. absoluta*. 67

4.13 Training and validation loss learning curves for the CNN model used in binary classification for plants affected and non-affected with *T. absoluta*. 68

4.14 The confusion matrix for the binary classification for plants affected and non-affected with *T. absoluta*. 69

4.15 Summary of F1-Score values of CNN quantification models for plants affected with *T. absoluta* as "No Tuta" and non-affected with *T. absoluta* as "Low Tuta" and "High Tuta". 71

4.16 Summary of Recall values of CNN quantification models for plants affected with *T. absoluta* as "No Tuta" and non-affected with *T. absoluta* as "Low Tuta" and "High Tuta". 71

4.17 Summary of Overall accuracy quantification values of CNN quantification models for plants affected with *T. absoluta* as "No Tuta" and non-affected with *T. absoluta* as "Low Tuta" and "High Tuta". . . . 72

4.18 Summary of accuracy and loss values of CNN quantification models for plants affected with *T. absoluta* as "No Tuta" and non-affected with *T. absoluta* as "Low Tuta" and "High Tuta". 72

4.19 The confusion matrix for the quantification models for plants affected and non-affected with *T. absoluta* as "No_Tuta" and non-affected with *T. absoluta* as "Low_Tuta" and "High_Tuta". 73

5.1 Multispectral image acquisition platform. (a) Zoom-in of sequoia camera image acquisition platform placed about 3m above plant crown in in-house experiment separated into three block with each plot of 1.2m^2. (b) captured, red, green, NIR and Red Edge bands. 82

5.2 Development of *T. absoluta* infection seen as mines on tomato leaves. (a) is the health leaf before *T. absoluta* inoculation, (b) is the *T. absoluta* infected plants shown as low Tuta damage on the 2nd day after inoculation and (c) is the *T. absoluta* infected plants shown as high Tuta damage on the 4th day after inoculation. 83

5.3 Multispectral image preprocessing preprocessing. (c) separately multispectral bands mosaicked using Pix4D software, (d) reflectance map of multispectral bands (e) image classification using ArcGIS, (f) using raster and shapefile, each plant canopy boundary extracted using ENVI software (g) a program for background removal based on threshold segmentation. 84

5.4 Summary of reflectance map spectrometer of tomato canopy affected and non-affected with *T. absoluta*. 84

5.5 Selected sample of preprocessed non-affected multispectral images. (a) Spectral bands with background not removed (b) are spectral bands with background removed, and (c) are selected sample vegetation indices of non-affected tomato plant canopy. 86

5.6 Selected sample of preprocessed affected multispectral images. (a) Spectral bands with background not removed (b) are spectral bands with background removed, and (c) are selected sample vegetation indices of affected tomato plant canopy. 87

5.7 Training and validation accuracies of Gradient Boosting Models. Xgboost and LightGBoost and CatBoost_model_1 used all the selected indices and bands. CatBoost_model_2 used GNDI, NDVI, NIR, RED, MARI, GREEN, NRI and RED indices. CatBoost_model_3 used NDVI, GNDI, NRI and MARI indices 92

5.8 Summary Plots of used metrics of vegetation indice and spectral bands of affected (herein Non-healthy) and non-affected (herein healthy)with *T. absoluta* for CatBoost models i.e CatBoost_model_1, CatBoost_model_3 and CatBoost_model_3. 94

B.1 Morogoro in-house experiment layout description. 121

B.2 Sample dataset of tomato Images 122

LIST OF TABLES

2.1 Summary of GDD for vegetative growth for eight complete tomato growth cycles 20

2.2 Summary of crop yield and GDD for harvest periods for eight complete tomato growth cycles. 20

2.3 Summary of crop yield and GDD for harvest periods for seven complete tomato growth cycles 21

3.1 Summary of age,farmers experience in tomato production and farm size for respective villages during farmer survey in August and September 2020 32

3.2 Summary of tomato yield of tomato fruits under three agronomic irrigation types during farmer experiment in September 2018. 40

3.3 Summary of Tukey multiple comparisons of means for tomato yield, loss and *T. absoluta* loss of tomato fruits under three agronomic irrigation types during farmer experiment in September 2018. 41

4.1 Data collection set-up and factors considered for each experiment 52

4.2 The hyper-parameters used during training 65

4.3 Classifier performance evaluation metrics on three dataset showing the overall accuracy. Words in curly brackets are the mean precision, mean recall and mean F1–score 66

4.4 Four pretrained model evaluation metrics accuracy precision (PRC), recall (RCL), F1–score (F1-S) accuracy and Overall average accuracy and loss on testing datasset. 70

5.1 Data collection set-up and factors considered including agronom for in-house experiment. 81

5.2 Statistics of Reflectance map of tomato canopy affected and non-affected with *T. absoluta*. 85

5.3 Summary of selected vegetation indices 88

C.1 Sample EXIF Meta data of Images taken using a PENTAX Camera during image data collection experiments in October to December 2019. 123

C.4 Sample EXIF Meta data of Images taken using a Parrot Sequoia multispectral camera during image data collection experiments in October to December 2019. 125

C.2 Sample EXIF Meta data of Images taken using a CANON Camera during image data collection experiments in October to December 2019. 127

C.3 Sample EXIF Meta data of Images taken using a Samsung Camera during image data collection experiments in October to December 2019. 128

CHAPTER 1

GENERAL INTRODUCTION

1.1 Food Demand and Production

A 60% increase (Figure 1.1) in agriculture production including vegetables is required to meet the projected 9.1 billion world population by 2050. Apparently 795 million lack adequate food supply, the majority from Sub-Saharan Africa (SSA) (FAO 2015). The Figure 1.2 clearly shows the gap in population projections amongst high income, low/middle income and high income countries [1]. We see a higher increase in the lowest income countries, therefore the majority low income countries could be negatively affected when the increased food demand isn't met.

Among foods, vegetables have the potential to contribute on the need to increase food demand to meet the required food shortage. FAO 2013 statistics show that, vegetation production increased from 0.9 billion Metric tonnes (Bt) in 2003 to 1.72 Bt in 2013. The European alone has 10% of total vegetable production output. A high income

[1] According to World Bank Atlas method, countries have been grouped as high-income, upper middle income, lower middle income and low-income based on per capita gross national income (GNI). In this research, upper middle and lower middle income are termed as Low/Middle income, high-income as high income and low-income as lowest income. Countries with less than $1,035 GNI per capita are classified as low-income countries, those with between $1,036 and $4,085 as lower middle income countries, those with between $4,086 and $12,615 as upper middle income countries, and those with incomes of more than $12,615 as high-income countries

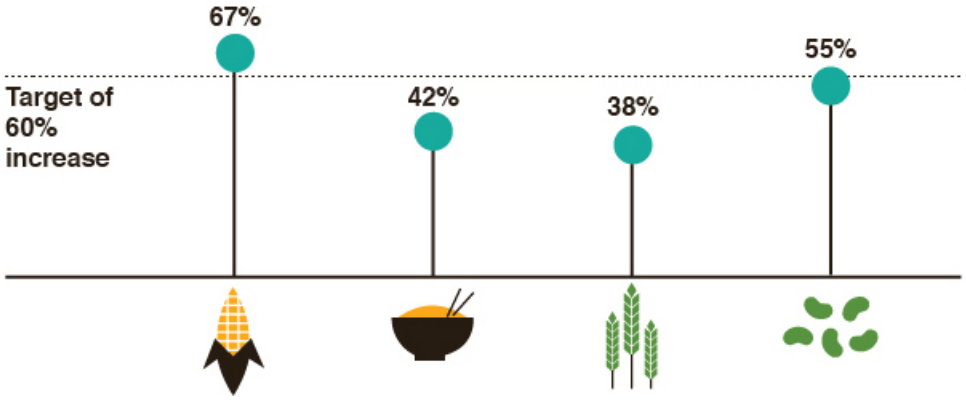

Figure. 1.1 World food production demand and required threshold level to meet the food deficit shown as in horizontal dotted line

Source: FAO 2015.

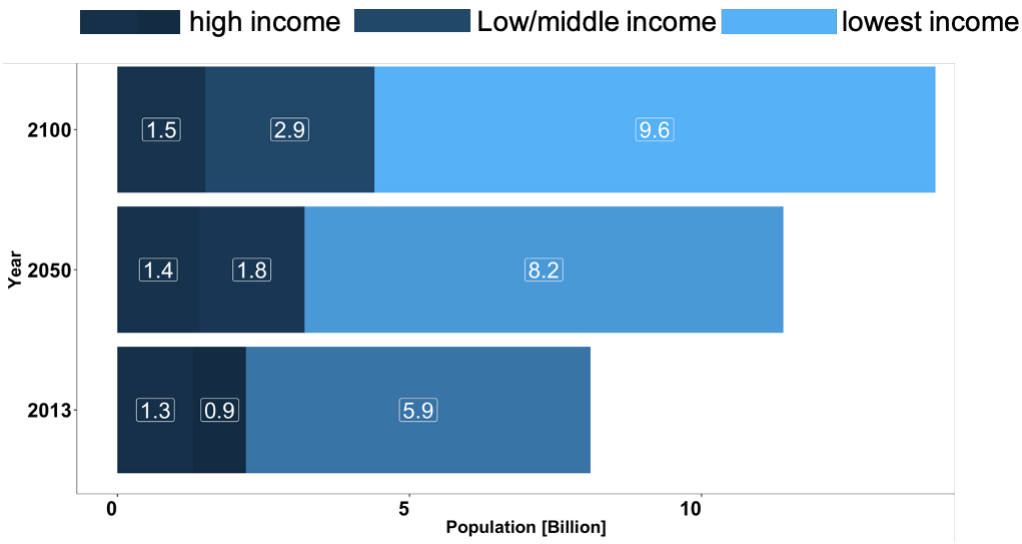

Figure. 1.2 World Population Projection based on country income levels

Source: United Nations.

country such as Japan, tomato production is about 730 MT, cucumber about 562 MT. Vegetation production being practiced on about 54n000 ha of land which is about 12% of total cultivated agriculture land. Contrarily, tomato production in African countries is about 19.1 MT, onions about 10.8 MT. Among, the vegetables, tomato are the highly produced vegetables which was a focus for this research (Figure 1.3).

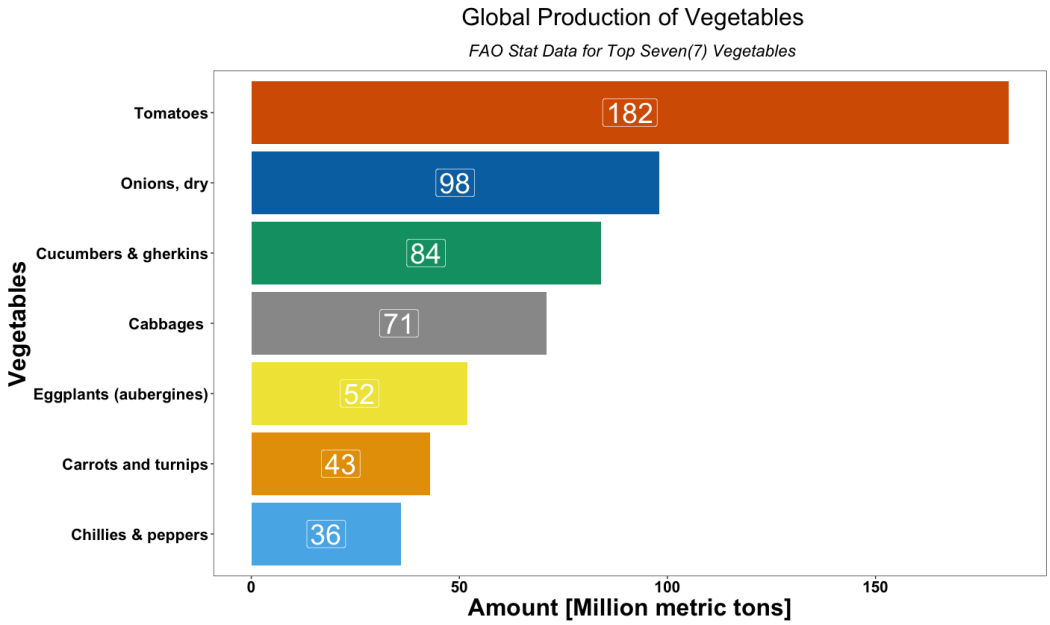

Figure. 1.3 Global production of selected top seven vegetables
Source: FAO.

1.2 Importance of Vegetable production

The World Health Organization (WHO) recommends a minimum vegetable intake of about 400g per day to prevent chronic diseases such as heart diseases, cancers and diabetes. Fruits and vegetables are essential sources for the micro-nutrients needed for human healthier diets. Some of the nutrients for instance Potassium in vegetables helps to maintain healthy blood pressure. The dietary fiber content also reduces blood cholesterol levels and may lower the risk of heart disease. Folate (folic acid) reduces the risks of birth defects, and vitamin A keeps eyes and skin healthy. Also vitamin C helps to keep, teeth and gums healthy and also aids in iron absorption.

Economically, vegetables also contribute to income and employment for small-scale farmers. Worldwide per capita consumption is estimated to be 20% -50% which is short of the minimum FAO standard (Dinham 2003, Matsane and Oyekale 2014).

1.3 Research scope and Focus

1.3.1 Challenges of vegetation production

The potentiality of vegatable to increase food demand is still subjected to challenges. Vegetables are highly vulnerable to crop failure owing to drought, adverse weather conditions (herein abiotic) and, pests, diseases and weeds (herein Biotic) (Nordey et al.,2017). The challenges greatly lead to negative economic impact thus loss of profit for small farmers and eventually higher cost to consumers (Matsane and Oyekale 2014).

1.3.2 Marginalized group low-resource farmers

In this research, we focused on marginalized group of low-resource small-scale farmers (small scale farmers here are farmers with average farm land size of 1.5ha). We further considered the labor constrained small-scale farmers. The target group of the labor constrained small-scale farmers in this study are the aged farmer, who are 64% of agriculture workers with average age of 65 years. The second target group was the ICT resource constrained in SSA. With a population of about 50 million who depend on agriculture.

1.3.3 Research objective

The core target of this study was the marginalized small- scale farmers, categorised as labor constrained and ICT constrained small-scale farmers in Japan and SSA respectively. The research goal was to approach the challenges using a data-driven emerging technological transfer to enhance tomato production with a focus to reduce losses due to biotic (herein tomato pests Tuta absoluta) and abiotic (herein

microclimate) factors, with a focus to increase yield and alleviate food security concerns using ICT and Artificial Intelligence techniques.

CHAPTER 2

SMART AGRICULTURE APPLICATION IN LABOR CONSTRAINED SMALL SCALE HORTICULTURE FARMING.

2.1 Introduction

The population of Japanese agricultural workers is decreasing, and aging is progressing at the same time. It should be noticed that the average age of farmers in Japan is 65.8 years old, and the ratio of workers aged 65 and above to the total agricultural population is 61.8%. We therefore could say that Japan is experiencing the arrival of a super-aged society and a full-fledged population-declining society, this then poses a concern of serious labor shortage in the near future. There are efforts to make agriculture a progressive industry, such efforts include full utilization of resources and the potential of rural areas through technological innovation (Kameoka and Hashimoto

2015, Nicolosi et al. 2017).

The initiative of the Ministry of Agriculture, Forestry, and Fisheries (MAFF) of Japan is to promote the introduction of smart agriculture aiming for labor-saving and efficiency improvement using state-of-the-art robot technology, and ICT and also to undertake research and development initiatives on-site by introducing cutting-edge technologies to realize smart agriculture (Singh et al. 2016).

Therefore, Wireless Sensor Network (WSN) as a smart agriculture technique was used in this study. WSN devices and various types of optical sensors are assumed to be a basic technology in smart agriculture which intends to achieve harmony with economic development and sustainable agro-ecosystem urges Fitz-Rodríguez et al. (2010). Bauer et al. (1984) urgue that WSN devices have been under rapid development and they have become a promising application in agriculture.

Previous studies on smart agriculture have been conducted, for instance Kameoka and Hashimoto (2015) conducted demonstration experiments using WSN in a mandarin orange orchard and in a vineyard to promote smart cultivation management. Bhatnagar et al. (n.d.) in their work, studied potato crop against phytophthora (a genus of water mold) by monitoring microclimate (humidity and temperature) using a large-scale WSN devices. The system had intentions of generating a policy to protect the crop against fungal disease based on the collected data. Kameoka et al. (2017) also developed a new WSN with a weather station and a soil water potential sensor that enabled long-range wireless communication, data acquired was standardized and used to create a web service that offered various kinds of phenological indices to farmers in the field (Kharel et al. 2020).

In fact, recent technologies in Japan have been initiated by large technological companies based on cloud computing service such as in the work of Fujino et al. (2016). Fujitsu's Akisai Food and Agriculture Cloud, the service is designed to provide comprehensive support to all aspects of agricultural management, such as administration, production, and sales in the open-field cultivation of rice and vegetables, horticulture, and animal husbandry (Suga and Okuyama 2016). Moreover, the Kubota Smart Agricultural System (KSAS) helps visualize agriculture business operations. The various data are collected from rice paddies and uploaded to the cloud server. The data is shared by the farmer, and the manager then the data can be analyzed to yield various information. The information can be easily accessed through a PC or a handheld device connected via a wireless Local Area Network (LAN). Data is collected in real time by agricultural machinery via the wireless LAN during operation (*KUBOTA REPORT, Business and CSR Activities 2016* n.d.).

We summarized Ministry of Agriculture Fishery and Forestry report of Japan (MAFF) smart agriculture catalog that contained 150 recognized types of smart agriculture systems. As shown in Figure 2.1, smart agriculture is subdivided into five categories i.e. data management (11%), cultivation management (16%), environmental management (7%), automatic and work mitigation (39%), and sensors for monitoring (28%). This research was an integration of all these categories (*MAFF: (Ministry of Agriculture Fishery and Forestry, Japan, 2018)* n.d.). It should be noted that, in Japan, smart agriculture application has been realized in farm management, plant growth diagnosis, land preparation, fertilizer application, pesticide application, water management, weed control, harvesting etc. Price of KSAS basic plan is from 35 USD per month. Cost of Akisai service is from 400 USD to 1000 USD per month. In addition to cost, it is

difficult to introduce smart agriculture in small scale horticultural facilities due to the lack of knowledge and understanding of advanced technologies of smart agriculture. Fitz-Rodríguez et al. (2010) claim that the fear that farmers cannot handle advanced technologies of smart agriculture when introduced is considered to be a barrier and the spread is delayed (*MAFF: (Ministry of Agriculture Fishery and Forestry, Japan, 2018)* n.d.).

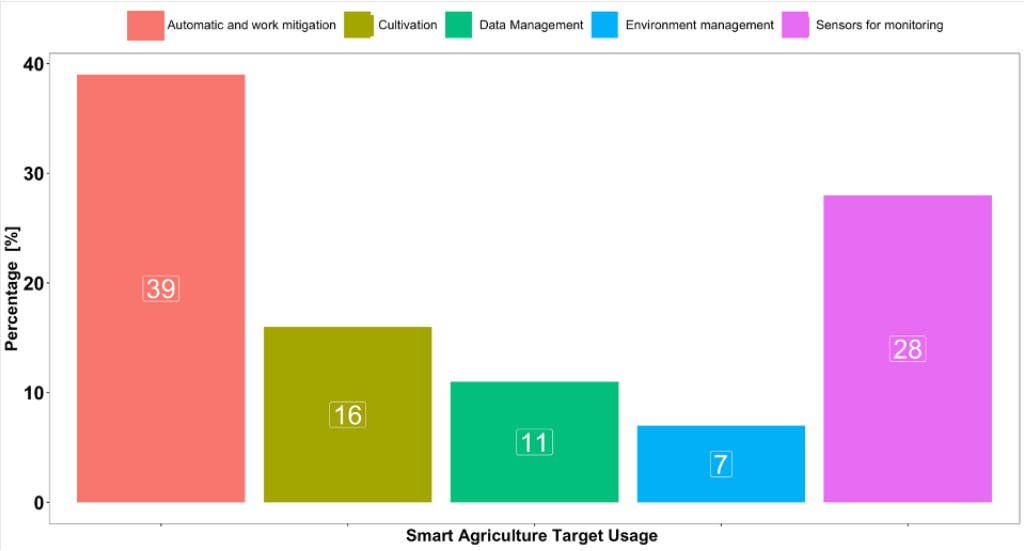

Figure. 2.1 A summary of 150 companies smart agriculture system categories in Japan. *Source:* MAFF.

This research therefore was in support of MAFF policies on research efforts to support cutting-edge technological ICT applications in agriculture and also to reduce the cost of expensive smart agriculture systems. The main aim of our research was to establish alternative approaches to ICT development and their applications in horticultural agriculture through the transfer of new advanced technologies to small-scale farmers in a collaborative support from research institutes to improve agriculture production management.

2.2 Research objective

In this study, we introduced and demonstrated a simplified smart agriculture system with real-time information capability that could be used for monitoring crop environment and crop management in a greenhouse at limited resource expense. We used inexpensive WSN devices and collaborated with tomato greenhouse farmers in Nara prefecture in Japan.

Real-time microclimate conditions were monitored using WSN devices and daily activities were collected during crop growth and stored data in the developed web DB. We used Growing Degree Days (growing degree units, GDD) technique to monitor crop growth (McMaster and Wilhelm 1997).

Nicolosi et al. (2017) showed the importance of crop microclimate in crop growth monitoring using cumulative GDD technique. Also, Miller et al. (2001) considered used GDD to monitor crop development, the assumption being that development is limited to a certain threshold. In addition, daily activity data were gathered and stored in a Google Drive spread sheet as explained in proceeding sections. Crop calendars were also embedded into the web DB for tomato farms (tomato cultivation is about ten crop growth cycles per year). We further showed microclimate spatiotemporal distributions within tomato greenhouse based on GDD. Conclusions of our study were drawn on how important the developed smart agriculture would be deployed by small-scale farmers such as the one discussed in this paper.

2.3 Materials and Methods

2.3.1 Smart agriculture system architecture

The smart agriculture system shown in Figure 2.2 was deployed on already existing tomato farmers existing greenhouse facility. The tomato greenhouse uses the soil-less cultivation technique called nutrient film technique (NFT) (Zekki et al. 1996). The system's architecture consisted of physical components for data collection i.e. WSN connection for microclimate data, PC for daily activity data. Microclimate data collected were stored in the WSN device cloud accessible by internet provided by installed Wi-Fi connection. PC installed with Google Drive spread sheet was accessible to a developed web DB for input of daily activities data such as fertilizer usage, harvest data and so on. Data collected were stored on rental server's database that was also used to host the web DB. WSN devices were distributed at and located in places for convenient accessibility due to the limitation of Wi-Fi connection between the base station and Wi-Fi router, and between the base station and connected indoor and outdoor modules. More details of deployed sensors, greenhouse layout, database is explained in proceeding sections

2.3.2 Sensors deployed

WSN devices used for the smart agriculture system was purchased from Netatmo (*Netatmo* n.d.). The WSN devices are equipped with sensors for air temperature, humidity, barometer, carbon dioxide meter, and sound meter. They are made of a single piece of durable aluminum shell and are UV resistant. The Netatmo modules are shown in Figure 2.3. Two main types of modules were used, indoor modules

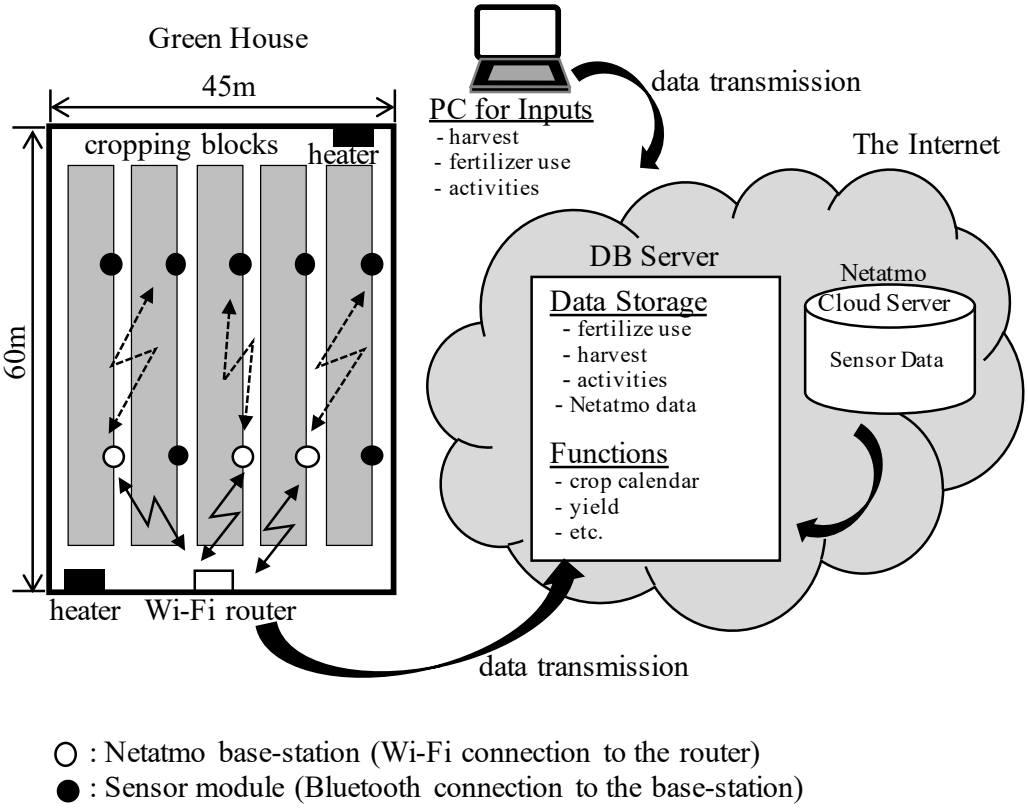

Figure. 2.2 An illustration of smart agriculture system architecture composed of Netatmo WSN devices for microclimate data collection, a Wi-Fi router for the Internet connectivity, a PC for data inputs and DB server for data storage and functions, like a crop calendar and so on.

Source: Author.

and outdoor modules. The indoor modules are of two categories i.e. base station and additional module. The base station is powered by a USB wall adapter while the outdoor modules and additional modules are powered by two triple-A batteries (up to 2 years lifespan). Wi-Fi router (Wi-Fi 802 b/g/n compatible (2.4 GHz) with supported security Open/WEP/WPA/WPA2) with internet access was required for the sensors to send data to Netatmo cloud server. The WSN devices are compatible with iOS, Android 4.0 minimum and windows 8.0 minimum operating systems. The additional modules and outdoor modules send their measurements to the base station via bluetooth. Using Wi-Fi access point, the indoor module then sends both its own measurements and other modules connected to it measurements to a registered netatmo account. The netatmo

data was viewed using netatmo user interface as shown by the mobile dashboard in figute 2.4.

Figure. 2.3 Showing the deployed wireless sensors used, Netatmo. From left to right are; Outside model, Indoor model(Base station), Additional Module, wind gauge and rain gauge. All Outdoor modules are completely weatherproof.

Source: Netatmo (*Netatmo* n.d.).

2.3.3 Data transmission

The system's data are categorized into two, microclimate data collected by the WSN devices and daily activities. The WSN devices collected data at a 5-minute interval (For analysis we used 30-minute interval data). Daily activities consisted of daily harvest such as fertilizer usage (calcium, nitrate solutions, Electrical Conductivity (EC) concentrations, pH). Data collected by the developed web DB consisted of planting and harvest duration dates, these data were collected and input manually using the PC installed with Google Drive spread sheet. The data input was managed by greenhouse employee who was ICT literate. The Wi-Fi router cost 70 USD and monthly running

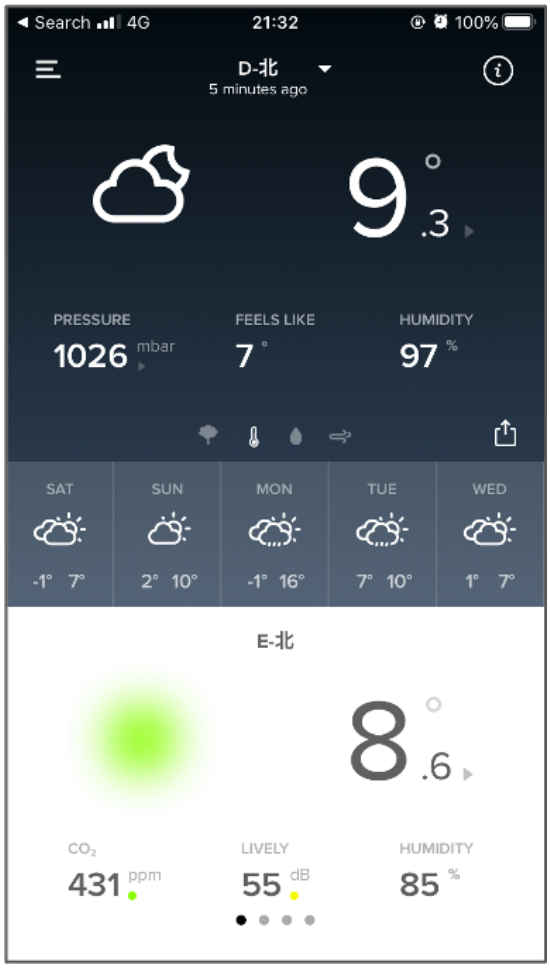

Figure. 2.4 Showing the deployed wireless sensors used, Netatmo mobile user interface dashboard

Source: Netatmo (*Netatmo* n.d.).

cost for 1GB was 4 USD. 0.3 MB of data is transmitted daily per module, thus 0.9 MB per month for each module. A total of 90 MB of data is transmitted from the 10 WSN devices per month.

2.3.4 Data storage

In our proposed smart agriculture system, as mentioned earlier, daily activities data was collected using a PC. A web DB as shown in Figure 2.5 hosted on a rental server was developed for daily activities data entry such as planting and harvest dates, number of transplanted seedlings and so on. The server composed of a rational MySQL

database for storage of data from Google Drive's spread sheet, daily activity data and microclimate data from netatmo cloud server. Using planting and harvesting dates data of individual greenhouse block that is stored in the database, a crop calendar 2.6, was created automatically and embedded into the web DB 2.5 .

Figure. 2.5 A web database used for collection of farm daily activities such as planting date, nursery planting dates, transplanting dates, harvest dates.
NB. Japanese characters used since the system was designed for Japanese farmer.

Source: Author.

2.3.5 Deployment in tomato greenhouse

The smart agriculture system was used on tomato greenhouse of six blocks as shown in Figure 2.7 (c) of greenhouse with an area of 2500 m^2, angle roof of 3.5 m high and an internal sheeting 3m high. Tomato production is done in a rotation cycle within one greenhouse. Using NFT wherein a very shallow stream of water containing all the dissolved nutrients required for tomato growth is re-circulated past roots of the plants in each row in soilless beds (a double row of 40 cm wide, 40 cm above floor and 80 cm apart each double row). Supplied nutrient solution consist of calcium solutions

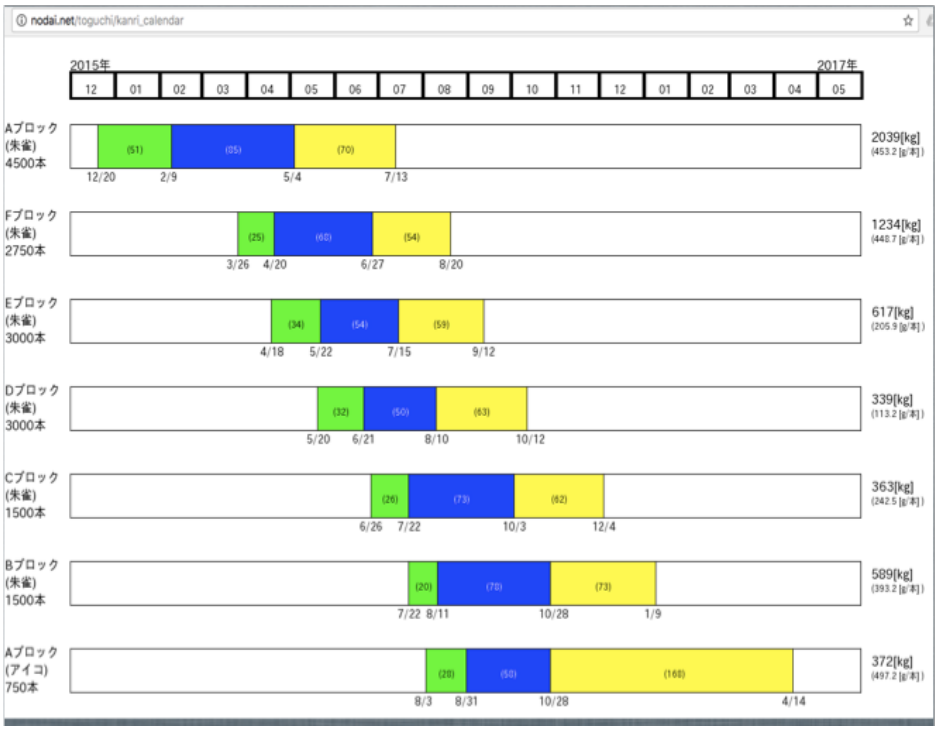

Figure. 2.6 A crop calender showing various complete crop growth cycle. Greeen represent nursery stage,blue represent the vegetative growth and fruiting before maturity and yellow represents the maturity stage as harvesting period.
NB. Japanese characters used since the system was designed for Japanese farmer.

Source: Author.

($CaCl_2$/$MgSO_4$) and nitrate solution. The nutrient solutions levels are controlled by determining their EC and pH. Tomato seedlings are grown in a separate nursery chamber before transplanted to the greenhouse. Blocks of the same size are F, E, and D and block A, B, and C. WSN devices were distributed in the tomato greenhouse as shown in greenhouse layout Figure 2.7. The WSN devices were installed 2 m above the floor as shown in Figure 2.7(a) to ensure that the microclimate near the tomato plants is measured. The tomato plants are supported by stakes to about 2.5 m high as shown in Figure 2.7 (b). In this research, microclimate parameters between July 2017 and December 2018 were considered for analysis. In the greenhouse layout, two WSN devices were used to collect data of blocks A, B and C. The WSN devices were installed at the boundaries since the block sizes were relatively smaller compared to block D, E

and F.

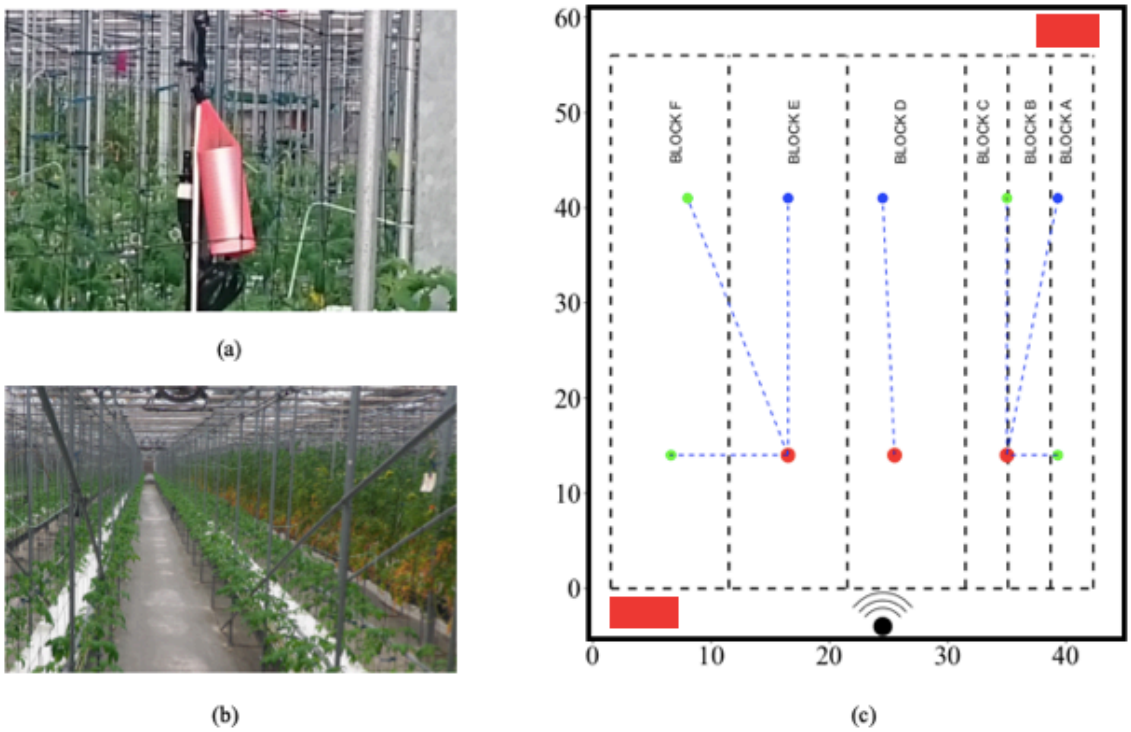

Figure. 2.7 (a) WSN device in greenhouse, (b) block within greenhouse and (c) greenhouse layout showing the location of WSN devices. Blue, green and red points are WSN devices. Red points; base station modules that receive data from additional modules, green points and outdoor modules (blue points) connected via Bluetooth (blue dashed lines) to their respective base stations. Black dashed lines; block boundaries. Black solid lines; greenhouse boundaries. The black point with three curved lines; Wi-Fi router. Red boxes in (c); heating facilities.

Source: Author.

2.3.6 Greenhouse microclimate monitoring approach

Monitoring of crop growth development was done within greenhouse blocks for different complete crop cycle. Snyder et al. (1999) urge that heat unit herein GDD, are often used to predict the rate of phenological development of plant species. Phenological developmental rate increase approximately linearly as a function of air temperature, and heat units are a measure of the time duration at various temperatures, this eventually makes GDD a good fit to quantify phenological development. However, development rates are assumed to be insignificant when the air temperature is below

the threshold termed as base temperature. When the temperature is more than the base temperature, then GDD is equal to observed air temperature minus the base temperature as shown in equation 2.1. Therefore, a bigger difference between the air temperature and base temperature implies more GDD and a faster development rate. Air temperature variables used were transformed to GDD using the following equation;

$$GDD = \begin{cases} T_{\text{mean}} - T_{\text{base}}, & \text{if } T_{\text{mean}} > T_{\text{base}} \\ 0, & \text{if } T_{\text{mean}} < T_{\text{base}} \\ T_{\text{mean}} = (T_{\max} + T_{\min})/2 & \\ T_{\text{base}} = 10^{\circ}\text{C}^{1} & \end{cases} \tag{2.1}$$

T_{mean} is the mean daily air temperature (average of daily maximum (T_{max}) and minimum temperature (T_{min}), T_{base} is the threshold or base temperature, we used 10^0 C (Snyder et al. 1999) as the base temperature. Whenever, the T_{mean} is less than the threshold (T_{mean}>T_{base}), GDD are set to zero ($GDD = 0$).

GDD within each respective block were used to monitor the vegetative growth period and harvest periods. For each block, the average of GDD for two WSN devices was used. GDD were then used in real-time monitoring of crop growth stages from the time tomato seedlings were transplanted to the end of crop cycle herein last harvest date. The collected crop harvest data and was manually input using a PC that was located in the greenhouse and eventually stored in web DB. Crop yield for each complete crop cycle was determined by dividing total daily harvests from each block by total plant numbers.

2.3.7 Greenhouse spatiotemporal distribution approach

The spatiotemporal distribution of the microclimate parameters in the greenhouse was determined by WSN device data interpolation. Assuming that microclimate variables are irregularly distributed in the greenhouse, we selected a linear method namely, a bivariate interpolation method, and a smooth surface fitting for values that are given at irregularly distributed points using akima method (Akima 1978). The linear method is based on a two-dimensional cartesian coordinate system with the length and width of the greenhouse layout considered as x-y plane and z (herein GDD) which represents a smooth surface of the z values at selected points irregularly distributed in the x-y plane. The selected points were the locations of the WSN. All the calculations were done using a statistical package R software installed with the akima package.

2.4 Results and Discussion

2.4.1 Crop growth monitoring using microclimate

Crop growth monitoring based on GDD was carried out. It is claimed by Bauer et al. that temperature and other factors such as photoperiod are important factors that affect the transition from vegetative to floral growth. In fact, Ito and Saito (1962) also evaluated the effects of air temperature on plant morphological development of other crops.(5,13) Therefore, for each block in a tomato greenhouse, the corresponding GDD was determined during the vegetative and harvest growth periods. As shown in Table 2.1, a summary of cumulative GDD (GDD) of eight selected blocks during vegetative growth and harvest periods. It can be seen that cumulative GDD was different for both vegetative and harvesting period of each block.

In order to evaluate the effect of microclimate parameters to tomato crop growth, we determined crop yield for eight selected complete crop cycles by dividing each block's total daily harvests by total number of plants in its block. We further determined the cumulative crop yield by summation of the daily crop yields. We also determined the daily means of carbon dioxide and humidity of each block using the average means of each specific WSN device.

Table 2.1 Summary of GDD for vegetative growth for eight complete tomato growth cycles

	Vegetative Growth		
Block	Transplanted	Just before harvest	* GDD
B	$2017-08-21$	$2017-09-29$	624.4
B	$2017-08-21$	$2017-10-13$	849.6
C	$2017-07-18$	$2017-09-18$	1187.0
C	$2017-12-24$	$2018-04-09$	875.9
D	$2017-10-26$	$2018-03-05$	1046.4
D	$2017-05-26$	$2017-07-25$	1030.5
E	$2017-10-05$	$2018-02-25$	1462.6
F	$2017-08-16$	$2017-10-23$	1121.0

Source: Author.

Table 2.2 Summary of crop yield and GDD for harvest periods for eight complete tomato growth cycles.

	Harvest Period					
Block	Harvest Start	Harvest End	$*$ GDD	Duration (Days)	Total Harvest(kg)	Crop Yield SD
B	$2017-09-29$	$2018-03-19$	1518.0	58	298.0	3.65
B	$2017-10-13$	$2018-03-19$	1288.5	56	220.2	3.85
C	$2017-09-18$	$2017-12-13$	890.3	38	576.0	5.59
C	$2018-04-09$	$2018-07-23$	1563.4	47	736.8	6.76
D	$2018-03-05$	$2018-07-03$	1460.2	52	1615.6	10.83
D	$2017-07-25$	$2017-10-16$	1194.5	37	1147.5	16.06
E	$2018-02-25$	$2018-05-07$	769.6	29	1214.9	12.04
F	$2017-10-23$	$2018-02-23$	1383.4	46	1398.3	7.08

Source: Author.

From Figure 2.8, we see that GDD are different throughout the year. GDD is seemingly high during July and September and between November and February GDD are low. The different microclimate conditions in the greenhouse as shown by GDD graph could imply that tomato plant growths are affected by microclimate. Cumulative crop yield sigmoid curves of the selected crop cycle were as well different throughout the

year.

In order to determine the response of tomato growth to microclimate conditions and nutrient parameters, analysis of variance of microclimate parameters and nutrient solution was carried out. The results indicated that all parameters were significantly different ($p < 0.001$) for nitrate, calcium solution and EC. Also, GDD, mean humidity and mean carbon dioxide concentration were significantly different ($p < 0.001$). For the selected complete crop cycles, a significance difference ($p < 0.05$) was observed for crop yield. This could suggest that crop yields are different amongst all the blocks. We further determined the linear relationships between microclimate, nutrient solution, and EC and tomato crop yield as summarized in table 2.3.

Table 2.3 Summary of crop yield and GDD for harvest periods for seven complete tomato growth cycles

model	variables	metric	CV11	CV12	DV11	DV12	EV12	FV11	FV12
Model 4	a	r^2	0.974	0.923	0.894	0.995	0.897	0.970	0.965
		p-value	***	***	***	***	***	***	***
		AIC	247.6	268.0	363.4	117.8	170.9	232.5	238.9
Model 3	a, carbon dioxide	r^2	0.982	0.993	0.978	0.996	0.931	0.973	0.996
		p-value	***	***	***	***	***	***	***
		AIC	240.2	213.5	321.5	117.0	167.2	232.4	195.3
Model 2	a	r^2	0.974	0.923	0.894	0.995	0.897	0.970	0.965
		p-value	***	***	***	***	***	***	***
		AIC	227.3	248.5	301.8	84.8	140.5	192.1	201.6
Model 1	nitrate solution	r^2		0.520	0.008	0.872	0.584	0.267	0.869
		p-value		***	0.56	***	***	***	***
		AIC		456.8	586.2	201.6	225.8	584.3	346.0
Model 1	EC	r^2		0.861	0.107	0.893	0.884	0.867	0.597
		p-value		***	0.028	***	***	***	***
		AIC		409.7	581.5	197.5	200.3	505.7	382.0
Model 1	calcium solution	r^2		0.520	0.934	0.872	0.584	0.463	0.869
		p-value		***	***	***	***	***	***
		AIC		456.8	464.3	201.6	225.8	570.0	346.0
Model 1	humidity,	r^2		0.273	0.168	0.237	0.218	0.209	0.236
		p-value		***	**	0.018	0.038	***	**
		AIC		472.6	578.3	242.6	238.5	587.8	402.5

* significant at $p < 0.05$; ** significant at $p < 0.005$; *** significant at $p < 0.001$.

From table 2.3, model 1,2 and 3 are linear regression models using dependent variable as cumulative crop yield and independent variables for 4-day daily moving averages of

humidity, carbon dioxide, nitrate solution, calcium solution and EC. Model 3 is multiple linear regression model using GDD (denoted as a) as independent variable and 4-day moving average of carbon dioxide. Model 4 is linear regression model using GDD as independent variable.

Results of the analysis indicated that a strong linear relationship ($r^2 > 0.89$; Model 2,3,4) between GDD, and carbon dioxide and cumulative crop yield for all the seven selected crop cycles. Results of four crop cycles indicated a linear relationship between nitrate solution, calcium, and EC and crop yield. There wasn't any observed linear relationship between humidity and crop yield. Results of the linear relationships between microclimate and crop yield indicate that tomato growth is affected by microclimate. On the basis of the hypothesis that the microclimate within the greenhouse is not equally distributed, we determined microclimate spatiotemporal distribution using only temperature parameters as discussed in proceeding section 2.4.2.

2.4.2 Spatiotemporal distribution

In order to understand the factors for varying tomato crop yields, it was important to determine the spatiotemporal microclimate distribution in the greenhouse. Prior to determining the spatiotemporal distribution of GDD, analysis of variance of WSN device parameters was carried out. Results showed significance differences ($p < 0.001$) for temperature and humidity. There were significant differences ($p < 0.001$) in carbon dioxide among the WSN devices (only three WSN devices had significant difference with $p - value$ more than 0.05).

Results showed that there were significant spatial and temporal variations within the greenhouse especially in the winter season. As shown in Figure 2.9, the spatiotemporal

distributions of monthly averages of GDD in November and January are showing distinct variations and this clearly shows how microclimate conditions within the greenhouse could be different in winter season.

From the spatiotemporal variation graphs, it is observed that hotter area at specific spatial locations in the greenhouse depicted the location of the heating facility (heating facility are located in the two corners of greenhouse).

2.5 Conclusions

In this study on the development of a simplified smart agriculture system for small-scale greenhouse farming, we draw conclusions on how important smart agriculture could be used effectively with a deepened understanding of smart agriculture application in small-scale horticultural farming a case of tomato production. We discussed the application of smart agriculture system with a real-time capability and for reliable monitoring within the greenhouse. We should note that tomato production is done in a rotation cycle within one greenhouse. This study shows the necessity to monitor specific block microclimate conditions in real-time. We were able to extract knowledge from the WSN device data in order to make intelligent decisions to help in farm decision making.

We also selected a simple algorithm such as GDD and showed how it could be used for crop growth monitoring. The use of only temperature in a simplified algorithm is a dimensionality reduction of many parameters collected by WSN devices. We used only GDD data in determining the spatiotemporal variations in the greenhouse and showed how important it was to maintain a well-balanced microclimate environment in the greenhouse. Therefore, to ensure a well-controlled microclimate within the greenhouse,

farmers could regulate heating and cooling facilities for optimum growing environment during plant growth stage, leading to a reduction of energy required for greenhouse heating and cooling.

As it was stated earlier, the challenge of shortage of agricultural labor would therefore imply using such a simplified smart agricultural system in a labor demanding situation. Taking into account the initial and running costs as mentioned in sections 2.2 and 2.3, the developed system is cost-effective relative to functionality in limited resource small-scale horticultural farm. The reliability of WSN device data makes it efficient, and consequently, it could be used for accurate crop production planning and decision making of cultivation activities. This was achieved by using the crop calendar that was integrated in the web DB. The crop calendar helps farmers visualize farm activities and therefore reschedule farm activity to enhance efficient farm management. The results of this research imply that by using a simplified smart agriculture system, the application could be transferred to other tomato greenhouses.

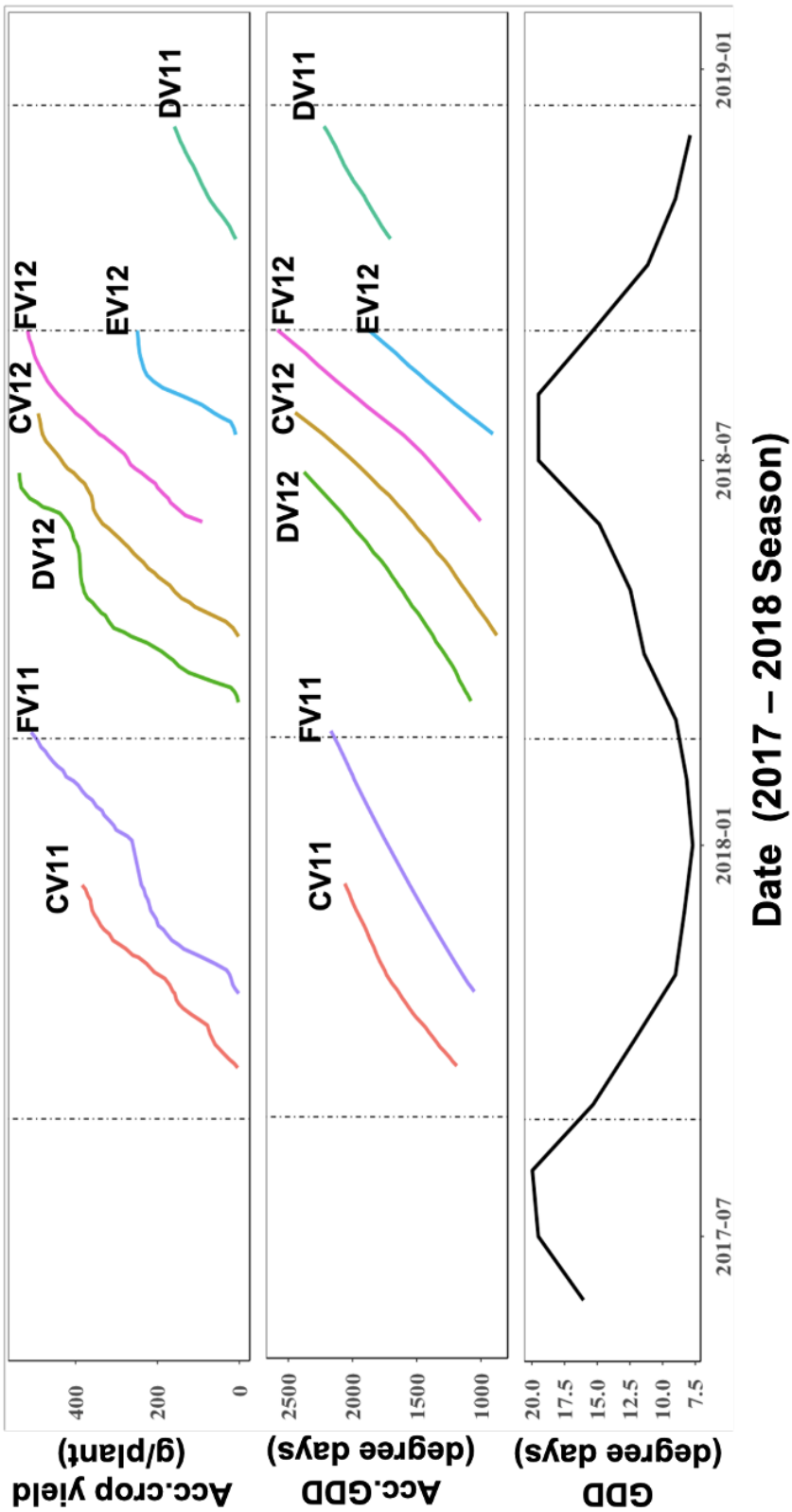

Figure. 2.8 Daily GDD within the greenhouse (Bottom). Accumulated GDD of selected crop cycle (Middle) Cumulative crop yield of selected crop cycle (Top). GDD denote cumulative GDD, Acc.crop yield denote cumulated daily crop yield. Crop cycle from CV11 to FV12, where first letters (C, D, E and F) denote block name, and appended V11 and V12 denote first crop cycle of normal tomato variety and second crop cycle of normal crop variety respectively

Source: Author.

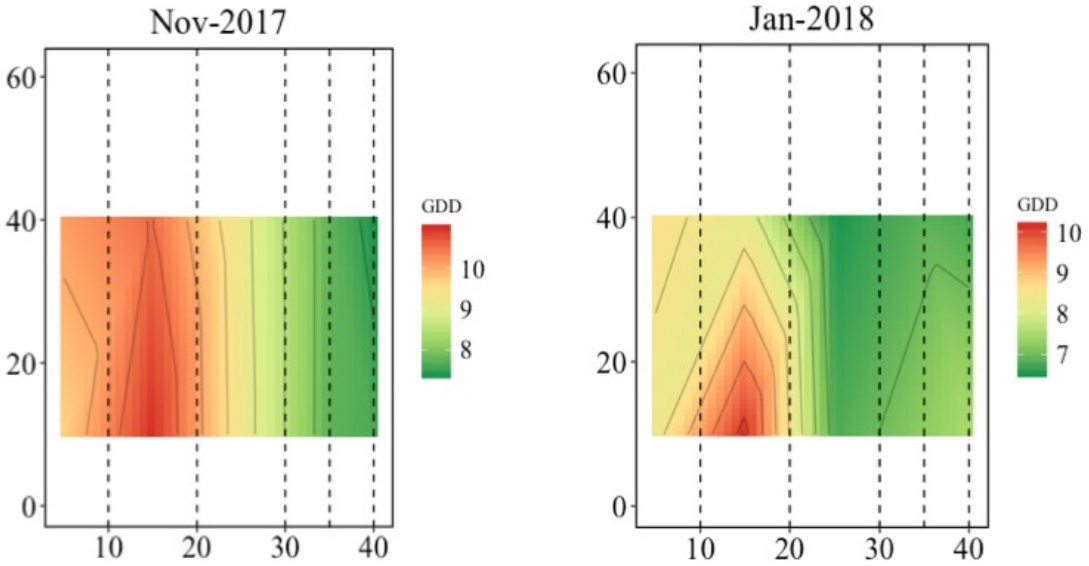

Figure. 2.9 Spatiotemporal monthly GDD variations in tomato greenhouse for November 2017 and January 2018. Values on vertical and horizontal represent the greenhouse length and width in meters.

CHAPTER 3

A STUDY OF EMERGING TECHNOLOGY IN ICT CONSTRAINED FARMERS

3.1 Introduction

This research was part of the aforementioned research focus, a deep learning and machine learning approach based on images. Out earlier research work, an ICT based approach was taken to tackle the challenge of micro-climate in horticultural tomato farmers, and as a technological transfer to small-scale farmers of SSA, the challenge of ICT constrained farmers was raised that become the basis of this work. Therefore, the key research question were to understand what available information and platforms could enhance adoption of emerging technologies in order to tackle the most dominant and destructive tomato pest in SSA.

Owing to the success of improved technological transfer that have resulted to increased use of mobile based technologies in agriculture. Several applications have laid upon

such technologies. The need to use such related platforms would be a better way to tackle prevailing tomato pest challenges. Therefore, it was adequately required to design a method of introducing some of the artificial intelligence techniques in such a manner. The research further focused on artificial intelligence approach to tackle tomato pest *Tuta absoluta*. In direction to the artificial intelligence approach, it raised a need to first understand information flow and adoption of a technology in ICT constrained resource countries such as in SSA. *T. absoluta* has become a threat to small scale farmers in SSA, all due to the favorable climate conditions. The impact of the tomato pest raised and spread in most African countries as shown in Figure 3.1.

3.2 Objectives

This research was done to first understand the demography and information flow for tomato farmers in SSA. Further, examination of tomato farmers understanding on Tomato pests *T. absoluta* damage and how damage could be controlled and later devise a recommended platform for introduction of a artificial intelligence based approach to tackle *T. absoluta*.

3.3 Study Site and Farmer Survey Data

This study was conducted in Tanzania regions of Arusha, Morogoro and Iringa between 15th August 2020 to 30th September 2020, as shown in the Figure 3.2. The study included a questionnaire survey of small scale tomato farmers (Figure 3.3a). 332 farmers were picked at random. The study was conducted in the major tomato growing regions. We used agriculture experts to collect the questionnaires (Detailed of the questionnaires are in Figure B.1).

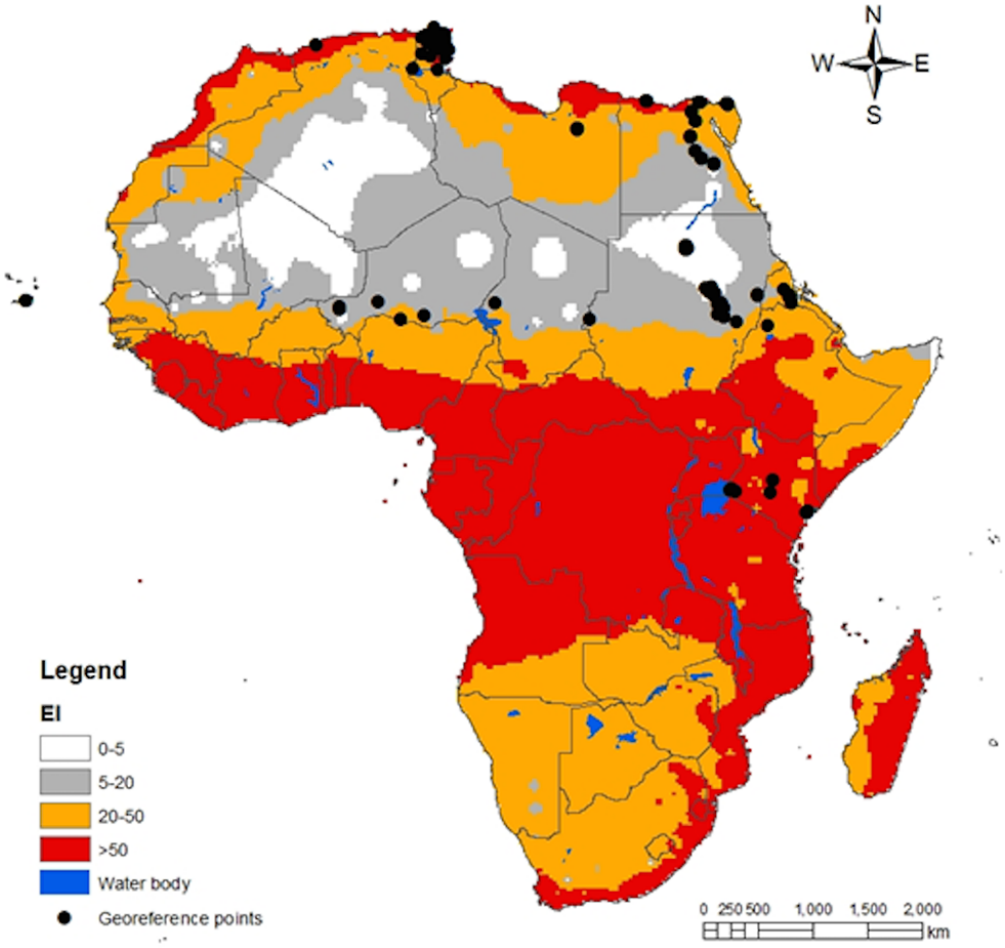

Figure. 3.1 CLIMEX climatic suitability indices map of *T. absoluta* in Africa. Predictions are based on the eco-climatic index (EI), a measure of climatic suitability scaled from 1–100, for locations within CLIMEX's station database. EI = (0–5) location is not suitable; EI = (5–20) moderate level of suitability; EI = (20–50) high risk of establishment and EI > 50 very high likelihood of long-term survival.

Source: Tonnang et al. (2015)

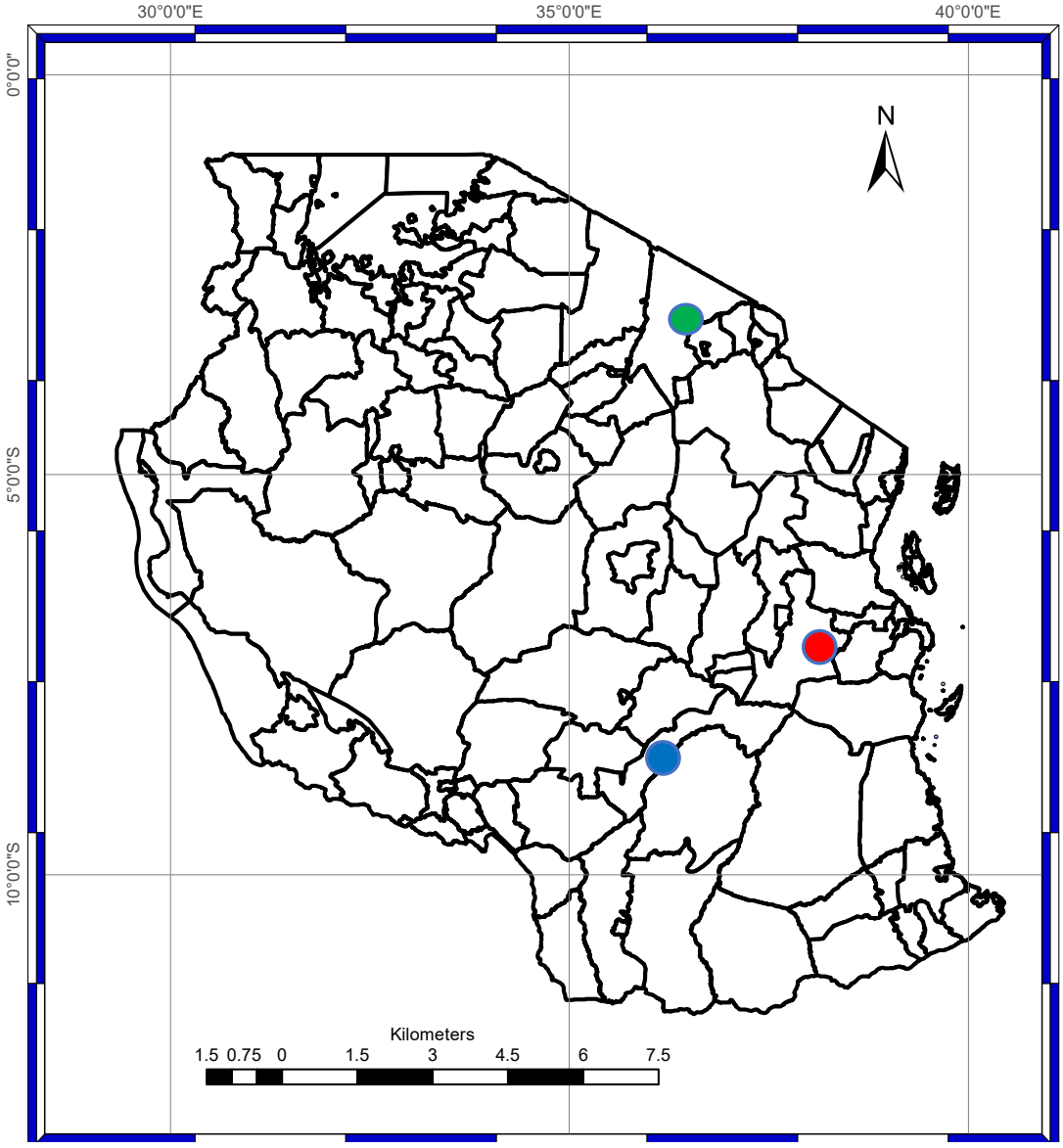

Figure. 3.2 Tanzania map showing the study sites. Green dot represents Arusha site, Red represent Morogoro site and Blue represent Iringa site.

Source: Author.

(a) **(b)**

Figure. 3.3 Showing farmer interviewed in (a) the farm and (b) at farmers household during the farmer survey in Morogoro region in August 2020.

Source: Author.

3.4 Description of the study area

In this study, the average age of the farmers was 47.6 years in Arusha with villages of Ngarenanyuki (Ng/nyuki) and Ngabobo, 49.1 years in Morogoro with villages of Doma, Kalenga and Mlali, and 44.2 years in Iringa with villages of Ilula, Mbuyuni and Kipera. This could suggest that farmers who practise tomato farming are generally middle-aged (Table 3.1). We can also see that Iringa region villages have the lowest average age. Most respondents surveyed in three regions (8 villages) were male 65% of the respondant. In terms of farmers experience in tomato production, 34.3% had experience of about 5 years, 25.3% had experience of about 10 years, 22.6% had experience of about 20 years, 10.2% had experience of more than 20 years and only 7.5% had experience of less that a year (new tomato farmers). In terms of land holding, farmers in Arusha owned more land, compared to the farmers in Morogoro and Iringa.

Table 3.1 Summary of age,farmers experience in tomato production and farm size for respective villages during farmer survey in August and September 2020

	Age				Experience				Farm Size				
Village	Mean	SD	Min	Max	Mean	SD	Min	Max	Mean	SD	Min	Max	n
Doma	46.4	13.0	24	60	11.7	6.4	5	20	1.9	1.4	0.5	7	41
Ilula	40.8	16.6	24	75	9.3	7.0	1	20	1.2	0.8	0.25	5	38
Kalenga	44.4	14.3	24	75	12.1	10.2	1	40	1.0	0.7	0.25	4	41
kipera	53.6	13.2	30	75	16.7	14.5	1	40	1.0	0.5	0.5	3	39
Mbuyuni	38.2	11.6	24	70	6.7	5.6	1	20	1.2	0.8	0.25	3	41
Mlali	47.3	16.0	24	75	13.7	11.6	1	40	1.1	1.2	0.5	8	47
Ng/nyuki	47.9	13.2	24	70	12.5	10.3	5	40	1.5	0.8	0.5	5	42
ngabobo	47.3	14.0	24	75	21.3	13.5	5	40	2.6	1.6	1	10	40

SD; Standard Deviation, Min; Minimum, Max; Maximum, n: sample size

3.5 Results of farmer survey

3.5.1 Challenges farmers face

The most common challenge farmers faces was tomato disease (82% of total respondants) followed by tomato pests (68.1% of total respondants) and wild animals (11.1% of total respondants). From Figure 3.4, we can clearly see the distribution of major challenges farmers face amongst the villages. Doma, Ng/nyuki and Ilula had the same number of cases for both disease and pest. Other villages, disease and pest had the most commonly challenges compared to wild animal cases. Mlali, Doma and Ng/nyuki didn't report any wild animal cases.

3.5.2 Information inflow

We studied the way information flows amongst farmers. The term of information referred to how farmers get to hear about solutions to challenges they face and how they share the information amongst others farmers. Regarding using information to tackle farmers challenges, results of the survey showed that 19% of respondants rely on past experience to tackle the challenges, about 50% relied on advise from agriculture experts

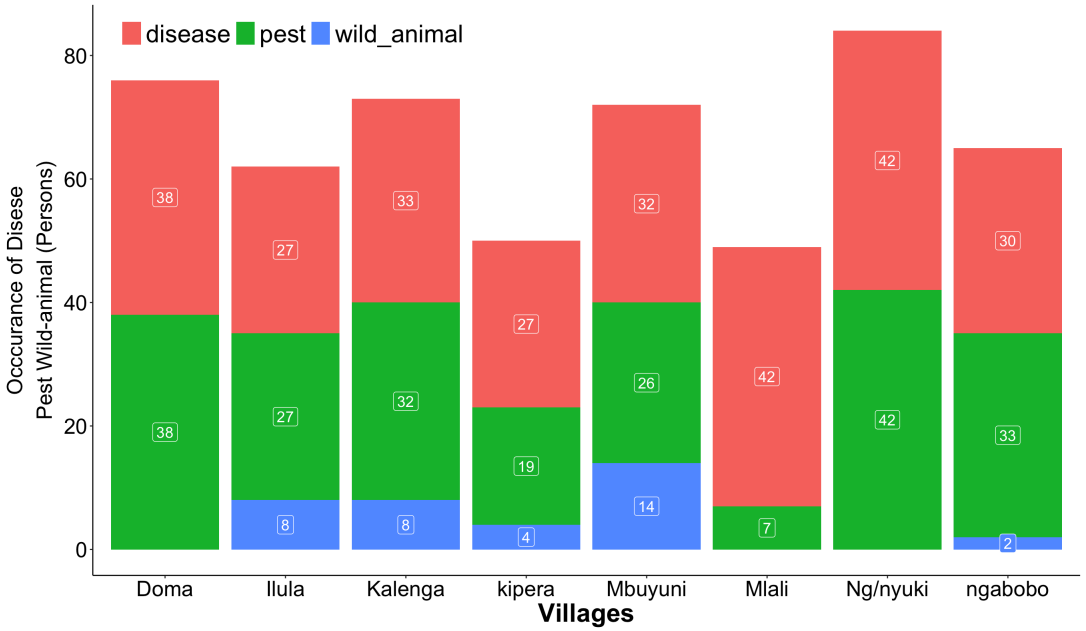

Figure. 3.4 Disease Pest and wild animals Problem challenge during farmer survey in August and September 2020.

information and about 30% of farmers rely on other farmers source of information to tackle the challenges they face. This information flow medium included mouth to mouth, using cellular phones and agriculture experts.

3.5.3 Description of farmer tranportation to farms

In this survey, we also studied farmers transportation between their farms and household places. Results showed that majority of farmers travel by foot to their farms followed by motorcycle and bicycle. A simple statistical analysis was done to compare the transport usage amongst the villages. Results showed that no significant (*p-value* 0.963) difference amongst the village transport types but there was significant difference within transport (*p-value* of 5.25^{-05} at 1% significant level) across villages means of transport.

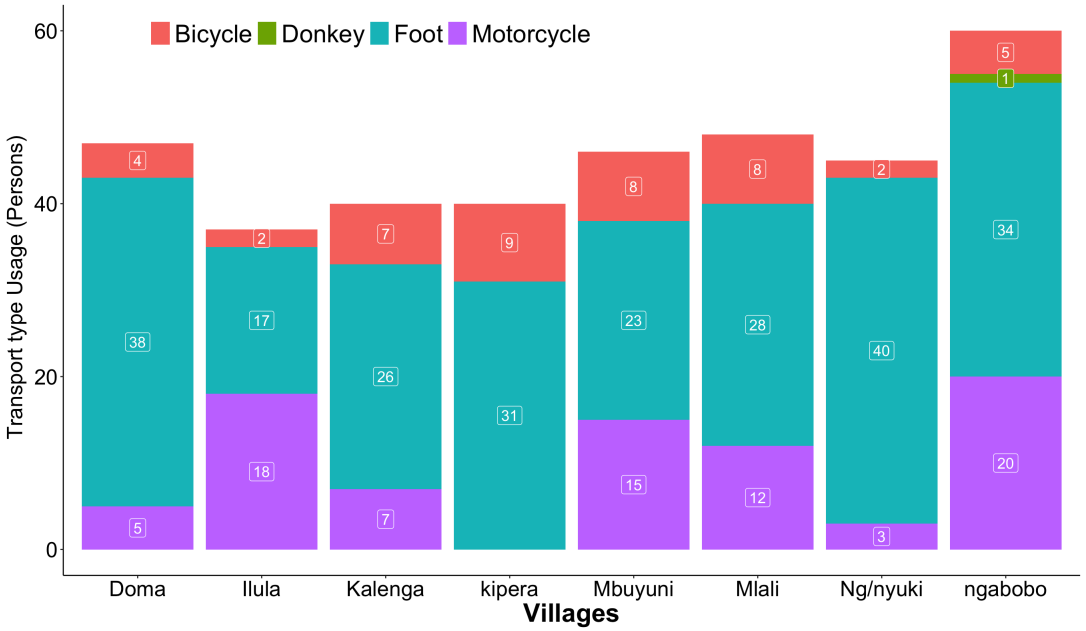

Figure. 3.5 The usage of farmers Transport categories during farmer survey in August and September 2020.

3.5.4 Awareness of *T. absoluta* early detection

Part of the survey was to understand the relationship of farmers activities that symbolize methods towards early detection of invasive tomato pest *T. absoluta*. Therefore, we studied farmers awareness of how they define *T. absoluta* damage, crop growth stage farm visits and current measures taken to control pests.

Figure 3.6 shows the results of farmers awareness of *T. absoluta* damage. Five main parts of the plant are affected by *T. absoluta*. *T. absoluta* damage can be recognised by dry leaves, flower abortion, leaves fold, fruit performation and last fruit rot. In this study, we categorised the damages as early stage and, fruiting and maturity. The response to damage awareness amongst the villages varied between dry leaves and leave folds. This indicated that atleast the farmers could identity and recognize *T. absoluta* damage at early stage of crop cycle. Another significant awareness was the fruit perforation and rot at fruiting and maturiy stages. Fruit perforation and rot is

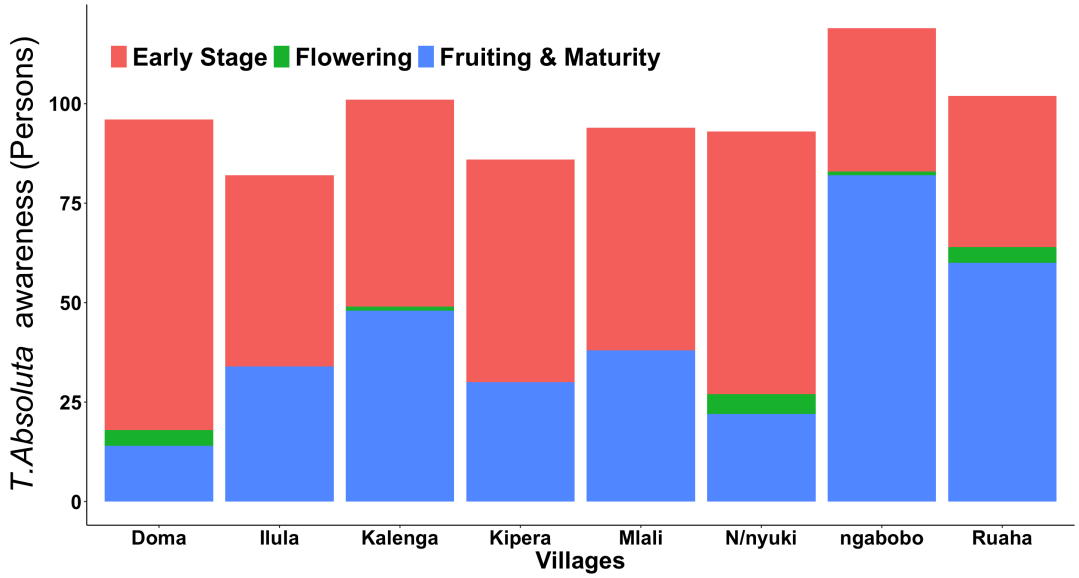

Figure. 3.6 Farmers awareness of *T.absoluta* damage at crop cycle for surveyed villages during farmer survey in August and September 2020.

usually during harvest stage. This could be referred to as late stage damage during crop growth cycle. It was also noted that, the farmers are less aware of *T. absoluta* damage as flower abortion.

Farm visit was studied based on the frequency intervals of farmers visiting farm during crop growth cycle (Figure 3.7). The interval were daily basis, 4-day interval, 7-day interval, 14-day interval, 21-day interval and 30-day interval. Results showed that, farmers visit farms often at early planting stages and less often during vegetative growth stage. Further, farmers tendency to visit farm reduces toward the late crop growth cycle (flowering, fruiting),however, during harvesting, the farm visit frequency tends to increase.

3.6 Farmer survey discussion and conclusion

Understanding farmers comprehension and awareness level of *T. absoluta* damage is critical.Farmers were aware about the dry leaves as symptoms to identify *T. absoluta*

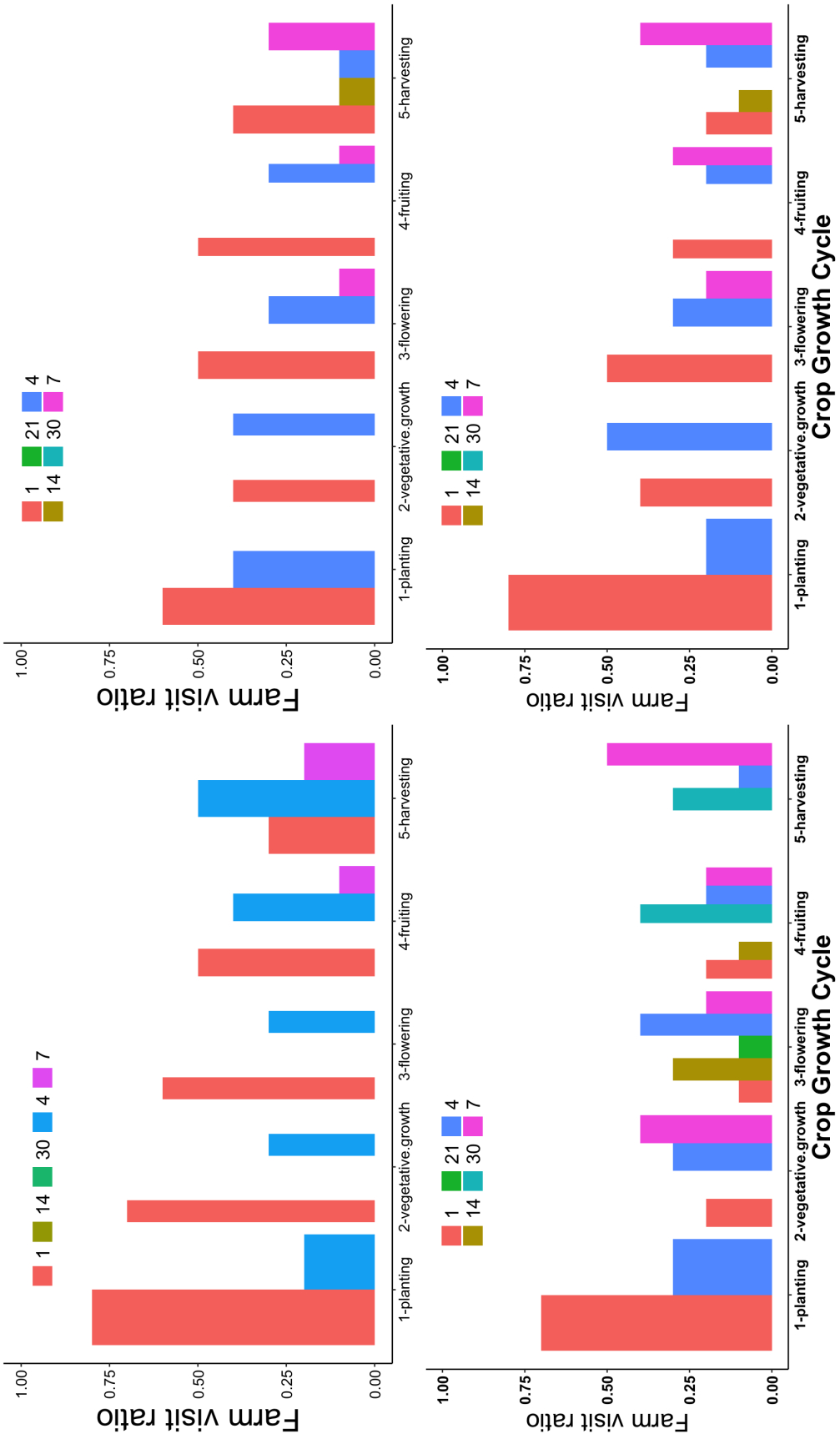

Figure. 3.7 Farmers farm visit tendency during crop growth stages. The visits determined by frequencies as 1;daily, 4; 4 days, 7; 7 days, 14; 14 days, 21; 21 days and 30; 30 days interval during farmer survey in August and September 2020.

Crop Growth cycle	Average visit
Planting	6
Vegetative growth	9
Flowering	10
Fruiting	12
Harvesting	10

damage in tomato plants, this was the basis for a need to focus on early detection methods that could eventually aid in the faster and efficient detection of *T. absoluta* damage. In addition, farmers visits show how an accomplishment of early detection procedure would be made effective, the fact that it was necessary for the farmers to visit the farm in order to use the devised method that could help in early detection of *T. absoluta* symptoms. Furthermore, information flow within the farmers community was a basis to be considered in the nearby future in case an artificial intelligence based approach is to be deployed and practically used by farmers. Therefore, a farmers platform would be effective in technological transfer.

3.6.1 Experiment Study on *T. absoluta* impact on tomato yield

In this study, an experimental study was carried to determine the impact of *T. absoluta* on tomato yield. The In-house experiments were conducted on one of the major areas prone to *T. absoluta* infestation Arusha in Tanzania. Figure 3.8 (a) show the in-house experiments used with controlled pests from outside. Commonly practiced agronomic practice for the experiments. Plants were inoculated a range of 2 to 8 *T. absoluta* larvae per plant on the second day after transplanting. At fruiting and maturing stages, we collected all the tomato fruits from start of fruiting to end of mature growth stage.

(a)

(b)

(c)

Figure. 3.8 Field experiment conducted in in-house screen house showing transplanting of tomato seedlings (a-Left) and *T. absoluta* larvae inoculation on the second day after transplanting ((a)-center image) and (a) -right is insert of *T. absoluta* larvae. Damage on plant parts (b) flower and (c) fruits.

3.7 Results and Discussion of field experiments

The results of the in-house experiment revealed that *T. absoluta* effects differently in agronomic fields as shown in Figure 3.10.

The mean yield for total harvest (marketable fruits), total loss relative to total loss due to *T. absoluta* as shown in Figure 3.9, show how greatly yield is impacted.

We can also see that, marketable yield during the tomato harvest decrease drastically as

depicted in Figure 3.12

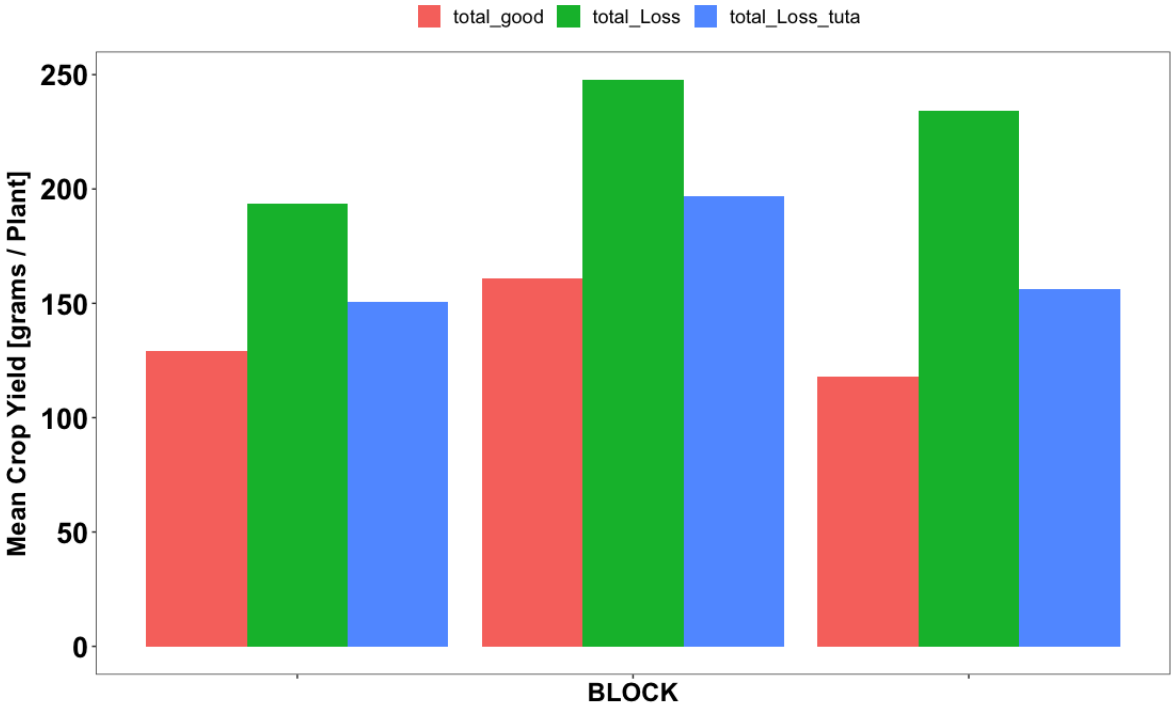

Figure. 3.9 Total Tomato per block that includes marketable fruits, non-marketable (affected by *T.absoluta*

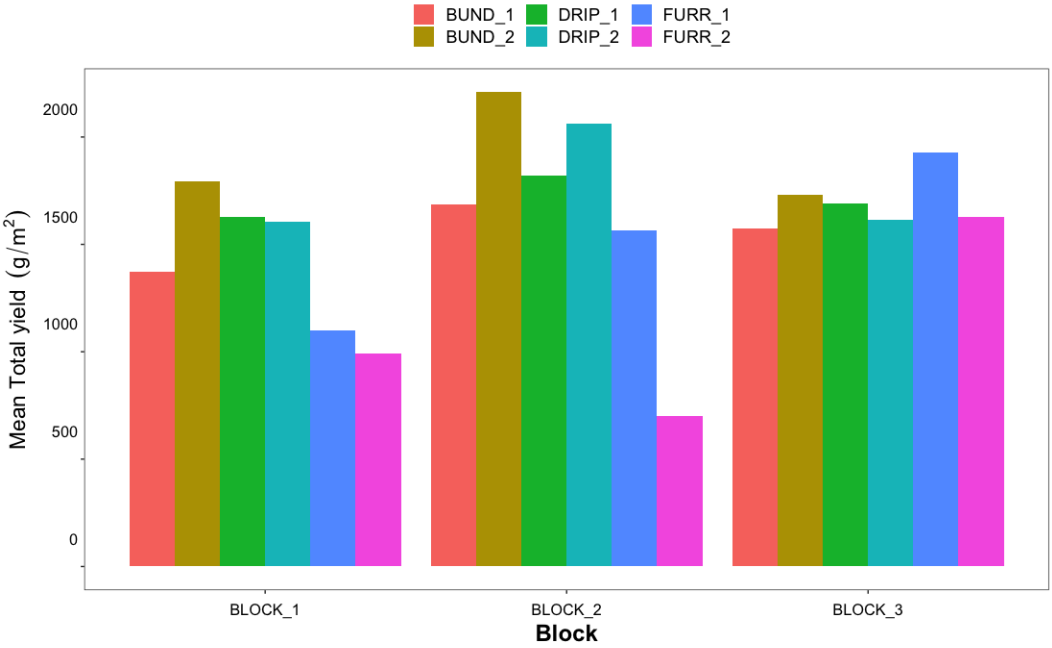

Figure. 3.10 Total Tomato yield for 6 irrigation types in each block

ANOVA test was conducted, results showed Signigicant differences exist within plots for total yield with *p-value* of 0.0943, for total loss yield the *p-value* was 0.405 and

Table 3.2 Summary of tomato yield of tomato fruits under three agronomic irrigation types during farmer experiment in September 2018.

Block	Plot	Marketable Yield (g/m^2)	Non-marketable loss (g/m^2)	Tuta Loss (g/m^2)	Total loss ratio	*T. absoluta* loss ratio
BLOCK_1	BUND_1	565.43	806.94	605.99	0.59	0.75
BLOCK_1	BUND_2	716.74	1074.62	836.4	0.6	0.78
BLOCK_1	DRIP_1	686.97	942.56	566.08	0.58	0.6
BLOCK_1	DRIP_2	583.47	1022.94	674.69	0.64	0.66
BLOCK_1	FURR_1	574.19	524.9	336.1	0.48	0.64
BLOCK_1	FURR_2	282.15	710.82	457.35	0.72	0.64
BLOCK_2	BUND_1	564.42	1120.75	851.44	0.67	0.76
BLOCK_2	BUND_2	893..15	1315.67	999.79	0.6	0.76
BLOCK_2	DRIP_1	765.11	1057.21	699.06	0.58	0.66
BLOCK_2	DRIP_2	683.89	1376.11	1093.22	0.67	0.79
BLOCK_2	FURR_1	494.43	1068.61	704.93	0.68	0.66
BLOCK_2	FURR_2	188.03	511.07	312.39	0.73	0.61
BLOCK_3	BUND_1	471.90	1102.51	753.96	0.7	0.68
BLOCK_3	BUND_2	532.26	1200.26	704.75	0.69	0.59
BLOCK_3	DRIP_1	421.75	1268.88	588.83	0.75	0.46
BLOCK_3	DRIP_2	547.81	1068.03	820.07	0.66	0.77
BLOCK_3	FURR_1	656.01	1272.01	867.61	0.66	0.68
BLOCK_3	FURR_2	487.44	1140.96	827.31	0.7	0.73

BLOCK_1, BLOCK_2 and BLOCK_3; represent the in-house blocks partitioned into three respective block shown by _1,_2,and _3. BUND_1 and BUND_2; represent plots of bund irrigation of first and second plot of in a block. DRIP_1 and DRIP_2; represent plots of drip irrigation of first and second plot of in a block. FURR_1 and FURR_2; represent plots of furrow irrigation of first and second plot of in a block.
Source: Author.

Table 3.3 Summary of Tukey multiple comparisons of means for tomato yield, loss and *T. absoluta* loss of tomato fruits under three agronomic irrigation types during farmer experiment in September 2018.

Plots	Total yield *p-adj*	Total loss yield *p adj*	*T. absoluta* loss *p adj*
BUND_2 - BUND_1	0.693	0.931	0.980
DRIP_1 - BUND_1	0.981	0.998	0.972
DRIP_2 - BUND_1	0.948	0.975	0.966
FURR_1 - BUND_1	1.000	1.000	0.986
FURR_2 - BUND_1	0.533	0.869	0.792
DRIP_1 - BUND_2	0.965	0.993	0.712
DRIP_2 - BUND_2	0.989	1.000	1.000
FURR_1 - BUND_2	0.661	0.827	0.773
FURR_2 - BUND_2	0.065	0.377	0.416
DRIP_2 - DRIP_1	1.000	0.999	0.657
FURR_1 - DRIP_1	0.974	0.982	1.000
FURR_2 - DRIP_1	0.224	0.668	0.994
FURR_1 - DRIP_2	0.934	0.910	0.721
FURR_2 - DRIP_2	0.170	0.482	0.368
FURR_2 - FURR_1	0.565	0.955	0.985

BUND_1 and BUND_2; represent plots of bund irrigation of first and second plot of in a block. DRIP_1 and DRIP_2; represent plots of drip irrigation of first and second plot of in a block. FURR_1 and FURR_2; represent plots of furrow irrigation of first and second plot of in a block.
Source: Author.

loss due to *T. absoluta* the *p-value* was 0.303. Further a Tukey multiple comparisons of means between the plots showed significant differences within the plots as shown in Table 3.3.

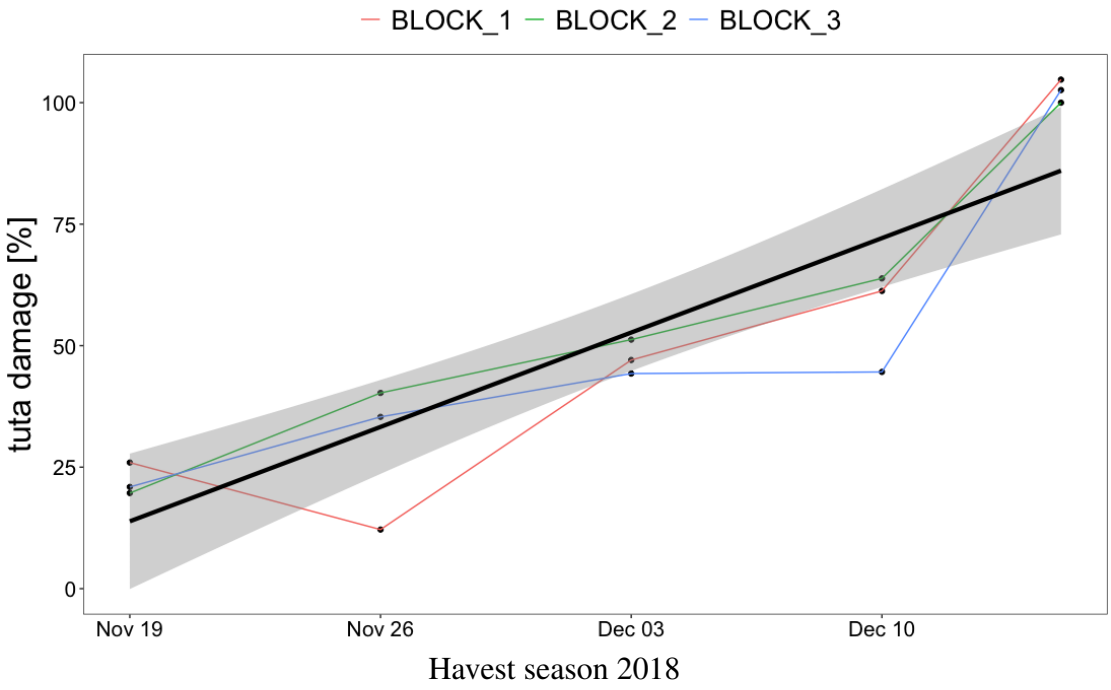

Figure. 3.11 Showing Marketable and Non-marketable (affected by *T. absoluta*) yield of 2018 harvest season period

.

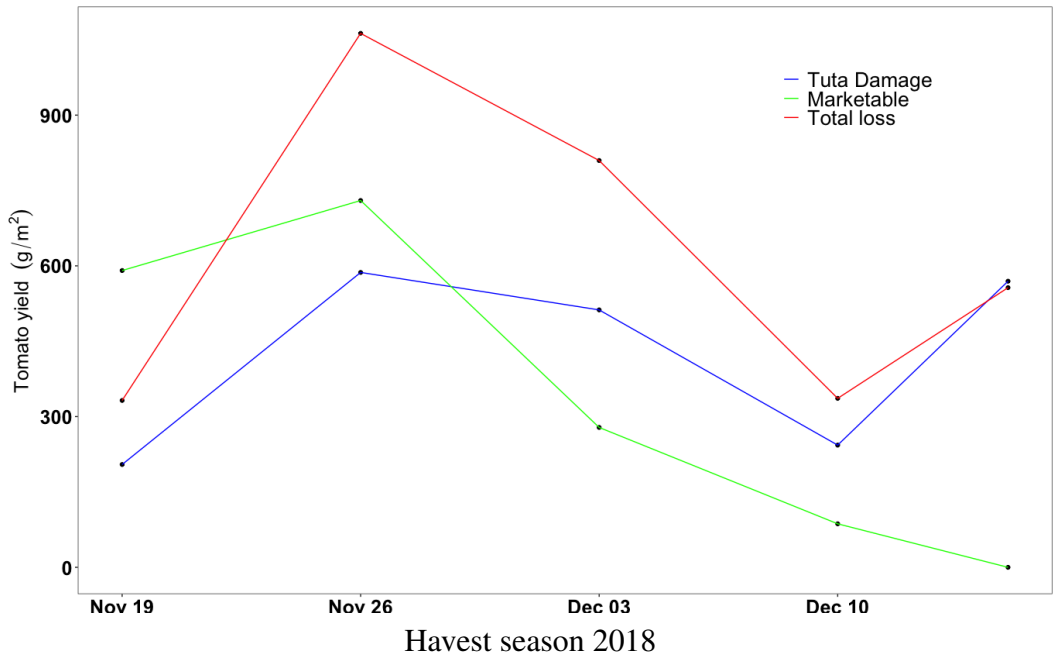

Figure. 3.12 *T. absoluta* impact on crop yeild depicted as decreasing linear yield during farm experiment in between AIgust and September 2020.

3.8 Conclusions of field experiments

The in-house experiments carried out showed that *T. absoluta* has great loss tomato yield. With the different agronomic practices carried out as irrigation types, it also showed that, the agronomic practices might hinder *T. absoluta* damage. Therefore, there was a need to further investigate on how different agronomic factors could impact *T. absoluta* damage. Also a need to monitor irrigation practices and provide recommendation for efficient use of water to control *T. absoluta*.

In this research, it was necessary to determine and understand the impacts of *T. absoluta* to yield such that proper machine learning solutions could be implementated. Therefore, a basis of applied machine learning techniques were devised as discussed in the next Chapters.

CHAPTER 4

IMAGE RECOGNITION OF TOMATO PEST USING DEEP LEARNING TECHNIQUES

4.1 Introduction

Tomato *Lycopersicon esculentum* is a nutrition-rich and an edible plant that is widely grown throughout the world (Schreinemachers et al. 2018). Globally, approximately 160 million tons of tomato are produced each year. In 2016, more than 247,135 t of tomatoes were harvested in Tanzania within an area of 54,520 ha. This production is equivalent to 64% of all fruits and vegetables in the country (Ministry of Agriculture 2016/17). Tomato is considered to be a cash crop to small-scale farmers, and, therefore, the plant contributes largely to poverty reduction. Given the economic importance of tomato, we should consider the factors affecting its production and find more appropriate technological solutions to maximize its productivity.

The production of tomato is threatened by an invasive pest called tomato leafminer (*T.*

absoluta), which tends to attack the plant and weaken its growth and yield capacity. Tomato leafminer was originated from South America and later spread to the rest of the world. The mature female can lay between 250 and 300 eggs at once, and has a life cycle with four development stages: egg, larva, pupa, and adult. It has reproductive rate of around 12 generations per year (Guimapi et al. 2016). The second stage (larva) is the most dangerous one because the pest at this stage can mine, develop, and feed on leaves, stems, and fruits of the tomato plant (Guimapi et al. 2016). Therefore, if the larva is left uncontrolled at the early stages of its growth, it may consume all plants in the farm (Zekeya et al . 2017). Management of tomato leafminer has continued to be a great constraint in the industry of tomato production, hence calling for scholars to devise approaches of identifying and combating it before causing great losses to farmers. Recent statistics show that farmers of tomato, the main host for the pest, have continued to incur heavy yield loss, ranging from 80%-100%, due to the invasion (Zekeya et al . 2017).

Of the available approaches to address the issue, deep learning has demonstrated successful results (LeCun et al. 2015, 1995). Various deep learning techniques have been applied to identify, classify, and quantify diseases, pests, and stress on different crops. Among these techniques, Convolutional Neural Network (CNN) techniques provides sophisticated ways of image analysis, and thus facilitates diagnosis of plant diseases. It is required to apply these advanced techniques to develop more effective approaches for identifying early invasion of *T. absoluta* in tomato.

Invasion of *T. absoluta* has for years, been causing great production and economic loses in the world. And, to date, no suitable solution is available to control its spread. Despite existence of various ways of controlling the pest (using chemical

pesticides and pheromone traps, and cultivation of resistant tomato varieties), early identification of the pest remains an open-ended research question (Zekeya et al. 2017). In Tanzania, for instance, the agricultural system depends on extension officers as key facilitators in providing farmers with appropriate knowledge on pest and disease management. However, the extension service system is currently conducted locally by limited extension officers' visits to provide training and workshop to meet demands of all farmers in the given area (Maginga et al. 2018). This challenge calls for a need to integrate sophisticated technologies, including those based on deep learning, into agriculture to identify pest and to maximize productivity (Zahedi et al. 2012).

This research introduces transfer learning, a deep learning approach, for identifying the invasion of *T. absoluta* at early stages. The approach reinforces classification of leaf images collected from a field setup in a controlled environment (controlled environment refers to preventing the spread of *T. absoluta* to other neighboring tomato fields using net house). Transfer learning was selected because of its ability of improving the performance of a neural network by speeding up the time taken to train models through reuse of models that were trained on similar tasks. Transfer learning allows the use of few data in training a neural network as compared to training from scratch that requires large amount of data.

4.2 Review of previous works

4.2.1 Computer vision in agriculture crops

Various studies have revealed that image-based plant diagnosis methods generate more accurate results compared with human visual diagnosis.

Ramcharan et al. used a pretrained InceptionV3 to detect incidence of three cassava diseases and two pests on the image dataset with 11,670 images collected from a field in Tanzania (Ramcharan et al. 2017). The model could correctly identify the diseases and pest damages with various accuracies: 98%, brown leaf spot; 96%, red mite damage; 95%, green mite damage; 98%, cassava brown streak disease; and, 96%, cassava mosaic disease. The study recommended transfer learning as a powerful deep learning technique for developing highly performing classifiers.

Maize, the source of starch crop grown worldwide, is also affected by diseases and pests that have devastating effects on its productivity – a consequence that threatens food security. DeChant et al. (2017) used convolutional neural network to detect a disease called Northern leaf blight (NLB) in maize. The study involved inoculation of maize leaves with fungal, a causal agent of NLB, for acquiring dataset from the infected plant. The analysis was carried out on 1,796 images composed of health and infested images, and the authors' model yielded an accuracy of 96.7% on the dataset.

The authors in Ouppaphan (2017) used a pretrained deep learning model to identify three corn leaf diseases. They used PlantVillage dataset containing 8,506 healthy and unhealthy corn leaf images; the unhealthy ones had the following diseases: common rust, northern blight, and gray spot. The results obtained after training the model were 98.95%, 98.25%, and 98.79% for the ResNet50, Inception V3, and MobileNet, respectively. The study revealed that the pretrained deep learning models perform well and can be widely adopted in other agricultural crops.

Another work by Liu et al. (2017) proposed a deep learning model to classify four diseases from apple leaves dataset containing 1,053 images of diseased and healthy

leaves. The author used AlexNet architecture (Krizhevsky et al. 2012) to classify apple mosaic, rust, brown spot, and Alternaria leaf spot. The approach attained an overall accuracy of 97.62%.

Furthermore, Lu et al. successfully identified 10 rice diseases from a dataset of 500 images containing health, and infected leaves of rice and stems Lu et al. (2017). The study used CNN to more accurately classify the images into their respective classes. The authors concluded that CNN yields better results compared with the traditional machine learning techniques of identifying diseases on rice.

4.2.2 Computer vision in tomato disease identification

Several studies have proposed deep learning as an effective approach of diagnosing various tomato stress. Consequently, we have witnessed great revolution in agriculture, including substantial increase in crop production. The study by Zhang et al., for instance, used CNN architectures, pretrained on 5,550 images (from an open access repository), to identify eight tomato diseases: early blight, yellow leaf curl, corynespora leaf spot, leaf mold, virus, late blight, septoria leaf spot, and two-spotted spider mite Zhang et al. (2018). All the authors' models could clearly and correctly classify the diseases at the following performances: 95.83%, AlexNet; 95.66%, GoogleNet; and, 96.51%, ResNet50.

Brahimi et al. compared the performances of shallow models (Simple Vector Machine and Random Forest) against pretrained deep models (AlexNet and GoogleNet) in the identification of nine tomato diseases Brahimi et al. (2017). The pretrained deep models outperformed the shallow models by identifying the diseases with high accuracies of 98.66% and 98.53% for AlexNet and GoogleNet, respectively; Simple Vector Machine

and Random Forest generated accuracies of 94.53% and 95.46%, respectively, much lower than those depicted deep models.

Rangarajan et al. (2018) used two pretrained deep learning models, VGG16 (Simonyan and Zisserman 2014) and AlexNet to classify six tomato diseases. They used images from PlantVillage dataset containing healthy leaves and unhealthy ones with six tomato diseases: late blight, leaf mold, two-spotted spider might, target spot, mosaic virus, and yellow leaf curl virus. The models attained classification accuracies of 99.24% and 96.51% for VGG16 and AlexNet, respectively.

Ferentinos used deep learning, specifically the VGG model, to recognize eight tomato plant diseases and two tomato pests from a dataset of 87,848 tomato leaves images Ferentinos (2018). The model exhibited a great performance of 99.53% in plant disease detection. This high-level performance suggests that Convolutional Neural Networks are suitable for the automatic detection of plant pest and diseases through the analysis of leaf images.

Several research have used deep learning techniques and have applied them for plant disease detection. These techniques have exhibited good performance; however, no technique has been developed to detect tomato leaf miner invasion. In addition, there has been no publicly available dataset with images of tomatoes infected by *T. absoluta*. This lack of dataset hinders progress of research on early detection of *T. absoluta* in tomatoes. Therefore, using images we captured from the field, the current study presents a deep learning approach for *T. absoluta* identification at early stages of the tomato plant growth. Our dataset was deposited in a public repository and can be accessible at Denis et al. (2020). This dataset also help to facilitate further research

in *T. absoluta* identification from diseased tomato plants.

4.3 Materials and Methods

4.3.1 The dataset

Four in-house data collection experiments (Figure 4.1) were conducted in two of the major areas prone to *T. absoluta* infestation, Arusha region located at $3°22'31''$ S, $36°52'25''$ E, in Northern part of Tanzania, which is a sub tropical area that experience an annual average temperature of 25°C and Morogoro located at $6°53'28''$ S, $37°37'45''$ E, in Easter part of Tanzania (Details of the layout are in Appendix C). Table 4.1 summarizes experiments for the period between August 2018 and April 2020. Figure 4.1 show the in-house experiments used with controlled pests from outside. We followed commonly practiced agronomic practice for the experiments. The table also shows factors that were put into consideration to have a vast diverse dataset of the real field situations i.e regions of the country that are highly infestated with *T. absoluta*, crop cycle season, mainly grown tomato varieties and mainly practiced farming systems. We planted healthy tomato seedlings (free from other diseases and pests) and inoculated some plants on a range of 2 to 8 *T. absoluta* larvae per plant on the second day after transplanting and on a daily basis took pictures of every plant between 08:00 and 10:00 A.M consecutively for two weeks. A total of 11236 Images (more images are shown in Figure B.2 of tomato plants were collected using Canon EOS Kiss X7 camera with a resolution of 5184 $\times$ 3456 pixels (details shown in Appendix C.2)and low resolution mobile camera (details shown in Appendix C.3). We focused on capturing the upper part of the plant at nadir, approximately 40 cm away from the plant, specifically the plant crown (plant canopy because this part is always affected at early growth stages of

the plant.

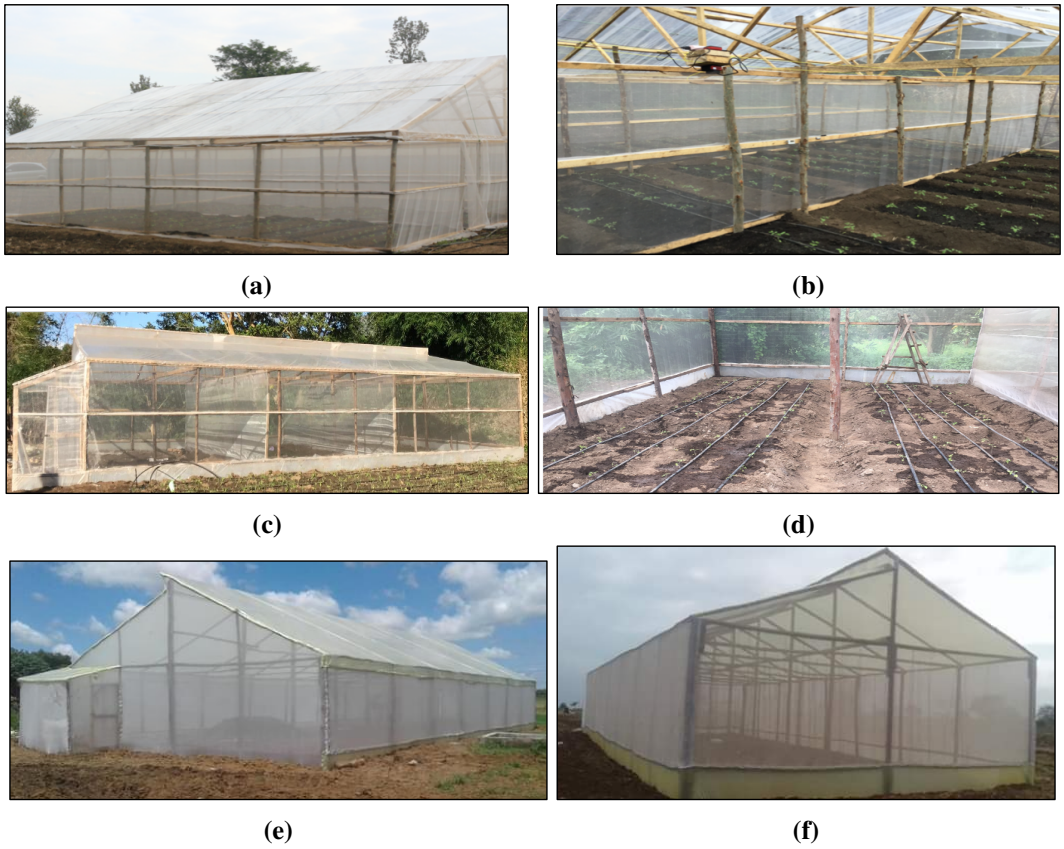

Figure. 4.1 In-house experiment set up screen houses. Arusha site (12M x 12M x 4.5M 0.1cm net size) (a) outside view (b) inside view, Morogoro site (15M x 12M x 5m, 0.1cm net size)(c) outside view (d) inside view, Morogoro farmers screen house (e) and (f)

4.3.2 Definition of early stage

Tomato crop cycle typically consists of early growth stage of about 21 days since sowing, followed by vegetative growth stage in the range of 20 days to 25 days, followed by flowering stage of about 20 days to 30 days and lastly fruiting and maturing of about 15 days to 28 days as described by Jones (2013).

In this research, we define early growth stages (herein, early stage) of the tomato crop cycle as the growth cycle between day of transplanting and the next 15 days after transplanting (Figure 4.2). The early stage is when *T. absoluta* is mostly realized and detected in plants. Normally during nursery stage, the seedlings are grown

Table 4.1 Data collection set-up and factors considered for each experiment

Duration	Season	Region	Variety	Farming system	Images
Aug - Nov 2018	dry	north	1	drip, furrow, bund	2248
Jan - May 2018	dry	north	3	drip	2012
Oct - Dec 2019	dry/wet	north	3	drip	4060
Jan - Apr 2020	wet	east	2	drip, furrow, bund	2916

under controlled conditions free from *T. absoluta* attack in small green houses. After transplanting, is when the plants are first subjected to *T. absoluta* attack.

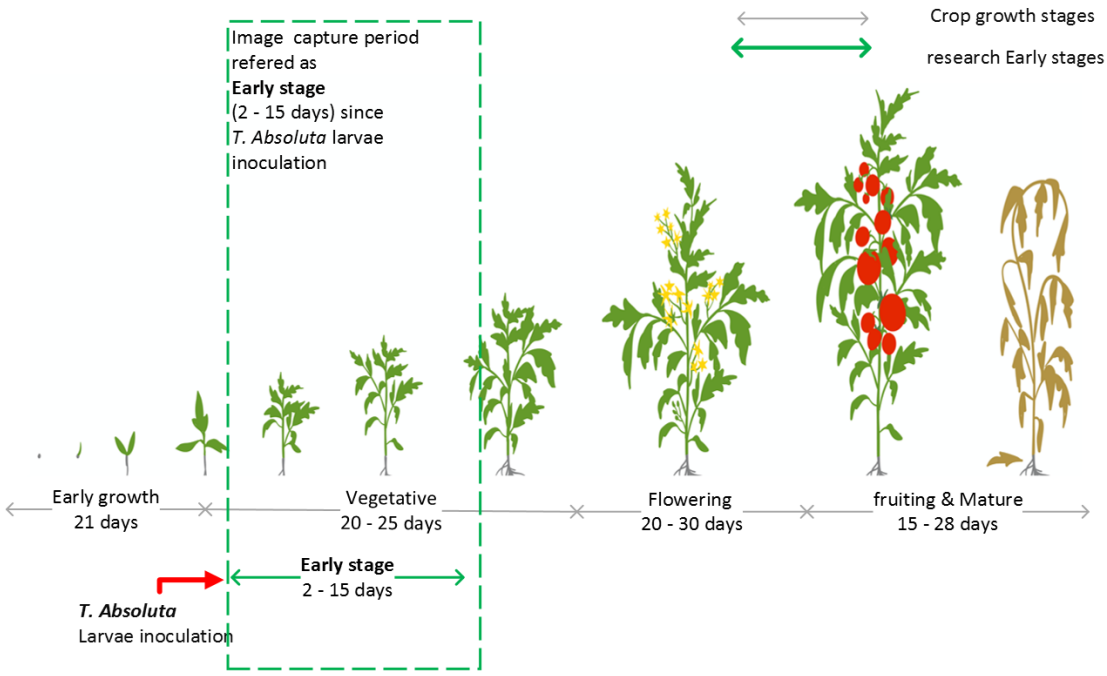

Figure. 4.2 Tomato crop cycle. Green dashed box show the early stage for this research *Source:* Jones (2013).

4.3.3 The dataset for classification

The dataset used for classification task consisted of two classes, images of healthy plants (non-affected with *T. absoluta* and images of plants affected with *T. absoluta* . Non-affected with *T. absoluta* images were more than images affected with *T. absoluta* , therefore, to reduce the bias due to imbalance data, 10% of the images were held as

test set, and the remaining 90% were sub-divided into training and validation sets in the ratio of 85:15. Also, non-affected *T. absoluta* images were divided into 4 clusters of images while retaining 10% for testing. Therefore making four datasets each with a total of 1623 for training, we used 230 images for validation and 218 images for testing.

4.3.4 The dataset for quantification

T. absoluta can cause progressive damage in short time, it is important to identify and quantify the damage status at early stage of tomato growth. Therefore, the main target of quantification task was to be able to identify and quantify *T. absoluta* damaged tomato plant severity status that could help to make clear distinction between the predefined three classes. The dataset used for quantification task, consisted of three classes. Using the *T. absoluta* infested plant, images were separated into two categories of *T. absoluta* damage severity status examined by agricultural expert as low *Tuta* (we define low *Tuta* as plants that were inoculated with less than 3 *T. absoluta* larvae) and High *Tuta* (we define high *Tuta* as plants that were inoculated with more than 3 *T. absoluta* larvae). A total of 692 images of low *Tuta*, 692 of high *Tuta* images and 2768 images of No *Tuta* from the whole dataset was used, finally making three classes. We refer to the three classes as; No *Tuta* (implying the plants that were not infested with *T. absoluta*), low *Tuta* and high *Tuta* as shown in Figure 4.4 and elaborated further in tomato crop growth cycle of figure 4.3.

4.3.5 Image pre-processing

Image pre-processing refers to the manipulation of raw image data before being processed by the deep learning algorithm, the purpose being to enhance data quality.

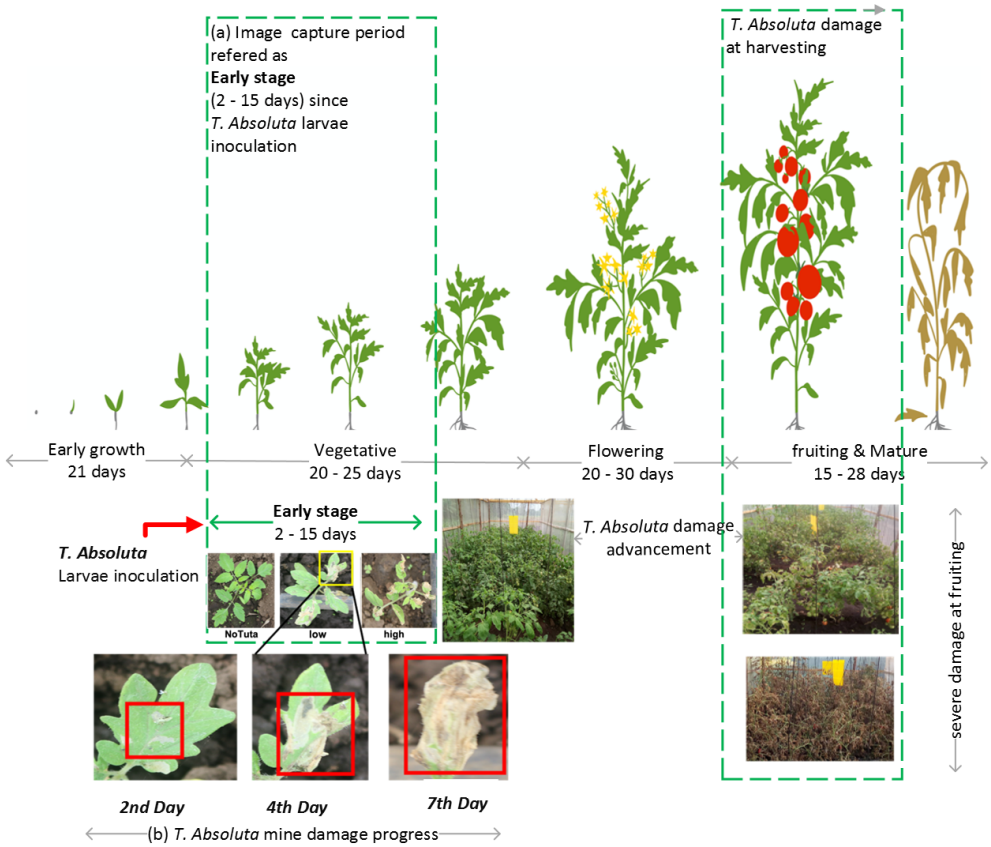

Figure. 4.3 Tomato crop cycle of *T. absoluta* damage status within the early stage period. (b) Insert of elaborated *T. absoluta* mine damage progress.

Source: Jones (2013).

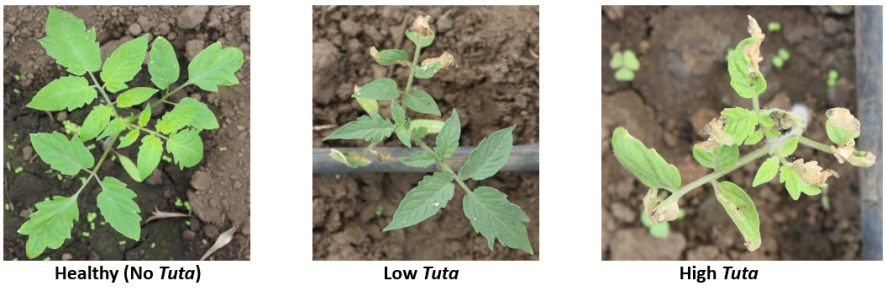

Figure. 4.4 Damage status of *T. absoluta* as healthy (No *T. absoluta*), and two classes of affected plants defined as "Low Tuta" and "High Tuta".

Source: Author.

Building a well-performing model requires careful consideration of the network architecture as well as the input data format. We pre-processed our dataset to allow the proposed model to undertake intelligent diagnosis of extracting appropriate features from the images (Jeong et al. 2018).

(a) (b) (c) (d) (e)

Figure. 4.5 *T. absoluta* mine infection progress. (a) is the health leaf before inoculation and red boxes are (b); 2^{nd}, (b); 4^{th}, (b); 6^{th}, and (e); 8^{th} days after inoculation with the *T. absoluta*.

Source: Author.

The pre-processing involved three stages: Manually labelling the images. We resized the images with the goal to generate 224 $\times$ 224 images required by VGG16 , VGG19, (Simonyan and Zisserman 2014) and ResNet50 (He et al. 2016) and 299 $\times$ 299 for InceptionV3 (Szegedy et al. 2016). The standard *resize* function in Keras (Ketkar 2017) can, by default, resample an input image to a target size. We resized all images to uniform sizes of 256 $\times$ 256 for the *resize* function to resample such resized images according to the proposed architecture requirements. The last pre-processing we did was image augmentation. Augmentation ensures the availability of a large amount of training data to clearly learn features contained in the training data and to attain high classification accuracy on the unseen data. Because of insufficient data in our research, a challenge that could promote overfitting and generalization (on test data) issues, we performed several random augmentations, including rescaling, shearing, flipping, zooming, rotation, and channel shifting. This approach increased the size of our dataset and enabled our classifier to learn more features while achieving the outstanding performance (Perez and Wang 2017).

4.3.6 The proposed CNN classification model

Deep learning consists of multiple processing layers that allow representation learning of multiple level data abstraction. The strength of deep learning emanates from its capacity to create and extrapolate new features from raw representations of input data without being instructed explicitly on which features to use and on how such features can be extracted (LeCun et al. 2015, Lee et al. 2017). This technique has been applied in various fields, including computer vision, natural language processing, speech recognition, and bioinformatics. More specifically, in computer vision, deep learning have demonstrated high accuracy in image classification and object detection. This category of deep learning uses CNN that takes in an input image, processes it, and classifies it under certain categories. CNN models can be built from scratch or from transfer learning. Using transfer learning is advantageous the fact that using pretrained models through transfer learning wouldn't require a lot of well-labelled data, compared to building a model from scratch that would require well-labelled data and many computational resources.

In this work, we have proposed a transfer learning approach based on CNN models pretrained on ImageNet dataset as shown in Figure 4.6 framework. This approach was preferred because of insufficient number of images available as inputs to our work. Transfer learning can be the best approach for building powerful classifiers, especially under conditions of limited data, through fine-tuning the parameters of network trained on a larger dataset (Ghazi et al. 2017). Consequently, we have explored three CNN architectures, namely VGGNet (VGG16 and VGG19) Simonyan and Zisserman (2014) and ResNet50 He et al. (2016), and have evaluated their performances on our dataset

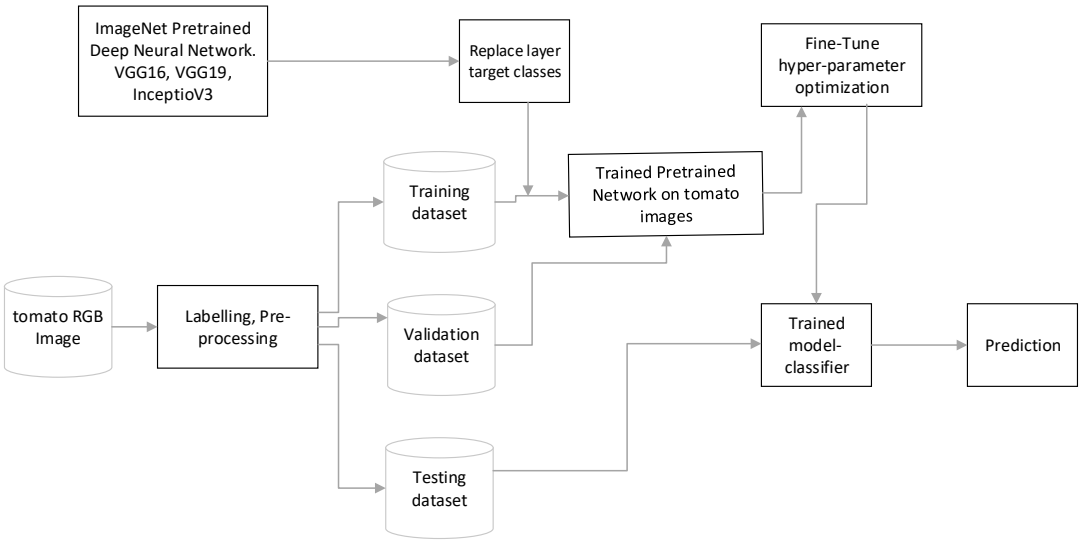

Figure. 4.6 The proposed deep CNN framework pretrained using ImageNet dataset.
Source: Author.

to classify images into correct categories of plants affected and non-affected with *T. absoluta* as elaborated in Figure 4.7.

VGGNet is the widely used architecture for ImageNet, and composes of VGG16 (Figure 4.8 and VGG19 (figure 4.9)with 16 and 19 weight layers, respectively. The architecture takes 224 $\times$ 224 input images and generates multiple outputs with probabilities corresponding to each class. VGG16 contains thirteen convolution layers, three fully connected layers, and five pooling layers. Furthermore, VGG19 contains sixteen convolution layers, three fully connected layers, and five pooling layers. Convolutional layers are used for extracting features from an image; each layer contains a 3x3 filter with a one-pixel stride and a ReLU activation function. The output layer contains a sigmoid activation function, which is used for classification.

ResNet50 is a convolutional neural network trained on more than a million images from the ImageNet database. This network takes a 224 $\times$ 224 image and produces an output with a probability of a specific class. ResNet50 contains 50 layers deep, and can classify images into 1000 object categories, including keyboard, mouse, pencil, and

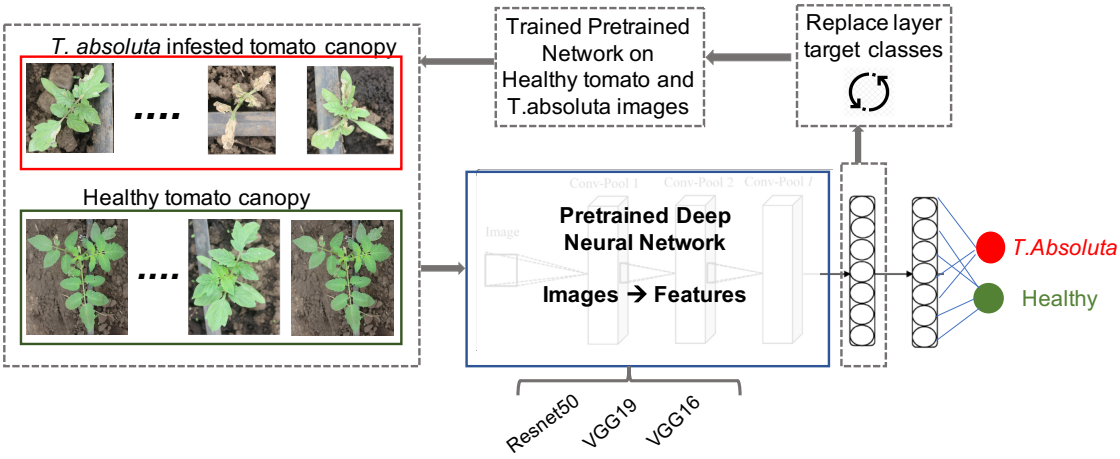

Figure. 4.7 Proposed binary classification for plants affected and non-affected *T. absoluta* using pretrained Deep CNN.

Source: Author.

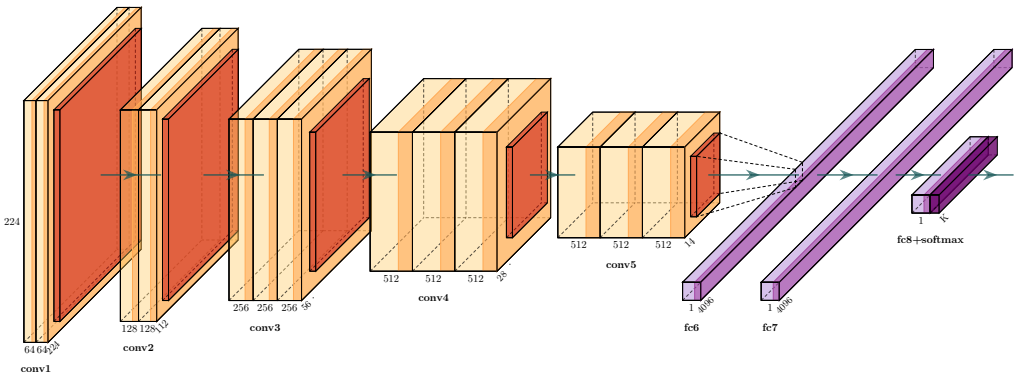

Figure. 4.8 VGG16 Architecture.

Source: Simonyan and Zisserman (2014).

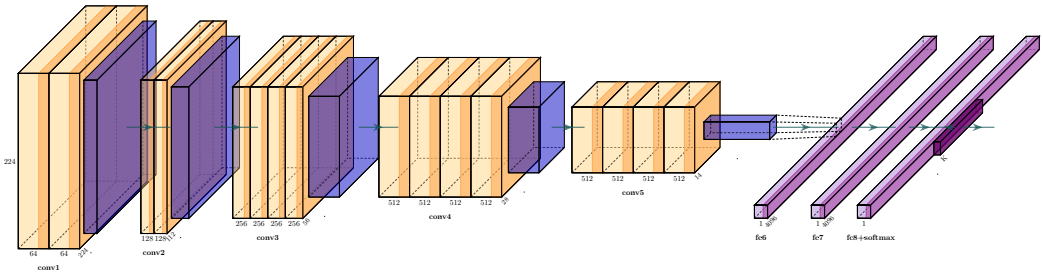

Figure. 4.9 VGG19 Architecture

Source: Simonyan and Zisserman (2014).

animals. In 2015, ResNet emerged as the first winner of the ImageNet Large Scale Visual Recognition Challenge (ILSVRC) classification task.

We expect that CNN can learn feature contained in our training data automatically and use them to classify unseen data. Hence we will no longer rely on experts in identifying the features associated with *T. absoluta* infection. The approach would improve the method of *T. absoluta* identification as farmers will be able to detect the invasion earlier and take appropriate measures to rescue the farms and hence improve production.

4.3.7 General CNN training algorithm

The basic architecture in the CNN begins with several convolutional layers and pooling layers, followed by fully connected layers. For an input x of the ith convolutional layer, it computes

$$x_{ic} = \mathrm{ReLU}\left(W_i * x\right), \tag{4.1}$$

where $*$ represents the convolution operation and W_i represents the convolution kernels of the layer. $W_i = [W_i^1, W_i^2 \ \ldots, W_i^K]$, and K is the number of convolution kernels of the layer. Each kernel W_i^K is an $M \times M \times N$ weight matrix with M being the window size and N being the number of input channels (Agarap 2018, Dahl et al. 2013, Agarap 2018, Arora et al. 2016).

ReLU represents the rectified linear function $\mathrm{ReLU}(x) = \max(0, x)$, ReLU function returns 0 if it receives any negative input, but for any positive value x it returns that value back. We used ReLU as the activation function in our models, as deep CNN with ReLUs train several times faster than their equivalents with saturating non-linearities.

Fully connected layers are added on top of the final convolutional layer. Each fully

connected layer computes $\mathrm{ReLU}\left(W_{\mathrm{fc}}X\right)$, where X is the input and W_{fc} is the weight matrix for the fully connected layer.

The loss function measures the discrepancy between the predicted result and the label of the input, which is defined as the sum of cross entropy (Aurelio et al. 2019):

$$E(W) = -\frac{1}{n}\sum_{x_i=1}^{n}\sum_{k=1}^{K}\left[y_{ik}\log P\left(x_i = k\right) + (1 - y_{ik})\log\left(1 - P\left(x_i = k\right)\right)\right] \quad (4.2)$$

where W indicates the weight matrixes of convolutional and fully connected layers, n indicates the number of training samples, i is the index of training samples, and k is the index of classes. $y_{ik} = 1$ if the i th sample belongs to the k th class; else $y_{ik} = 0$.$P\left(x_i = k\right)$ is the probability of input x_i belonging to the k th class that the model predicts, which is a function of parameters W. So the loss function takes W as its parameters. Network training aims to find the value of W that minimizes the loss function E. We use gradient descent algorithm (Mandic 2004, Ruder 2016) where W is iteratively updated as,

$$W_k = W_{k-1} - \alpha\frac{\partial E(W)}{\partial W}, \quad (4.3)$$

where α is the learning rate, which is a very important parameter that determines the step size of the learning. We use early stopping as the training stop strategy to stop training when the network begins to overfit the data. The performance of the network is evaluated at the end of each epoch using the test set. If the loss value of the test set stops improving, the network will stop training.

To prevent overfitting, the transfer learning is conducted as follows: fully connected layers are replaced with a new one and only fine-tune the top convolutional block for

VGG16 and VGG19 and the top residual block for ResNet50, along with the new fully connected layers. To avoid triggering large gradient updates to destroy the pretrained weights, the new fully connected network should be initialized with proper values rather than with random values. So firstly we freeze all layers except the new fully connected network. The new fully connected network is trained on the output features of the final convolutional layer. The weights learned from training are initial values for fine-tuning. After that, the top convolutional block for VGG16 and VGG19 and the top residual block for ResNet50 are unfreezed and then trained along with the new fully connected network with a small learning rate (Wang et al. 2017, Shao et al. 2018).

The parameters that reached optimal performance for training shallow networks and finetuning pretrained models are presented in table 4.2. Besides, a learning rate schedule is employed. The initial learning rate is dropped by a factor of 0.1 every 48 epochs during training the deep networks. Because the network goes deeper, it needs more training steps to converge. Training the classifiers was done for 1000 epochs with a batch size of thirty two and a Stochastic Gradient Descent (SGD) optimizer of a learning rate of 1×10^{-5} (Bottou 2012, 2010).

We used three pretrained architectures (VGG16, VGG19, and ResNet50) as classifiers that were fine-tuned through transfer learning. The fully connected layer for each pretrained architecture was replaced by the new layer, and then we fine–tuned the convolutional blocks for the VGGnet and fine–tuned the top residual block for ResNet50. Firstly, we freezed all layers, except the new added fully connected layer, such that this layer could be trained on the output of the final convolutional layer, generating the learned weights that could be used as the initial values in fine tuning. Thereafter, the top convolutional layers for VGG16 and VGG19, and the top

residual block for ResNet50, were unfreezed and trained with the new fully connected layer.

4.3.8 CNN Visual Explanation

To better understand our pretrained model on the selected architectures, we used a visual explanations technique called Gradient-weighted Class Activation Mapping (Grad-CAM) (Selvaraju et al. 2019). Grad-CAM are more transparent and explainable. Grad-CAM uses the gradients of any target concept such as tomato image for our classification task. This follows the final convolutional layer to produce a coarse localization map highlighting the important regions in the image for predicting the concept. We chose to use Grad-CAM claimed since the authors of Grad-CAM claim that it is applicable to a wide variety of CNN model-families, such as CNNs with fully-connected layers. In this study, visual explanation was applied on only VGG and VGG19. The advantage being that no architectural changes or re-training is required for our model as explained in Figure 4.10a for classification task.

4.3.9 Implementation

The experiments were performed on Ubuntu workstation, pre-installed with Ubuntu 18.04 equipped with one Intel Core i9-9900K 3.6 GHz CPU (64 Gb RAM) accelerated by one GeForce RTX 2080Ti Graphical Processing Unit (GPU) (12 GB memory). We trained 1000 epoch for each model and it took an average of 41 minute on a complete model training powered by Keras deep learning library using Tensorflow (Abadi 2016) as backend. In total, about 13 hours were required to run training on the 16 runs of the models i.e 4 runs for each of the 4 CNN architecture.

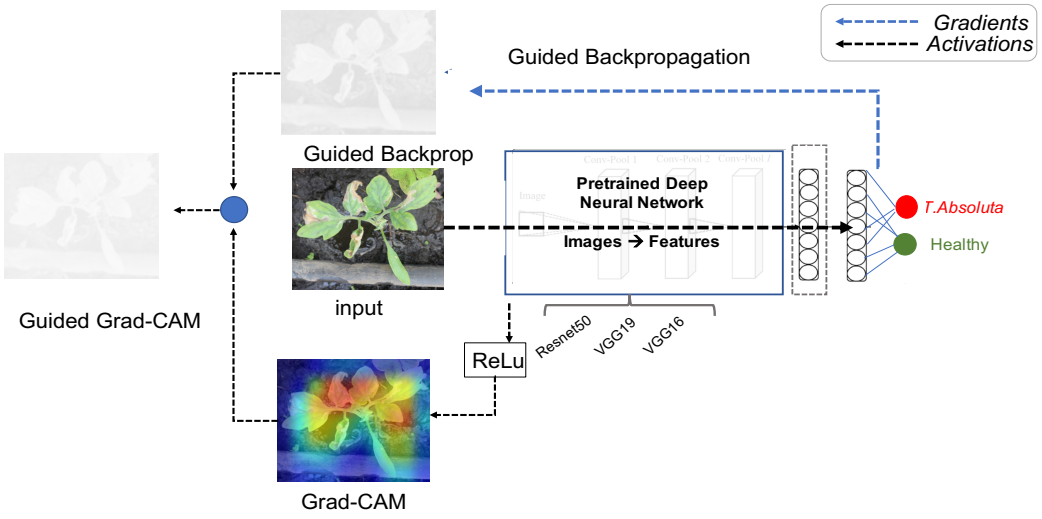

(a)

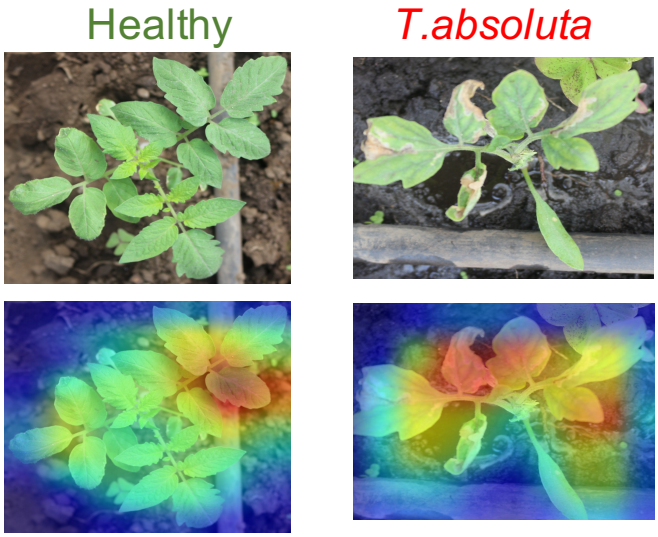

(b)

Figure. 4.10 Showing (a) Proposed binary classification for plants affected and non-affected *T. absoluta* using pretrained Deep CNN with a Grad-CAM used to visualize the model performance and (b) Shows the original images in the upper rows and the visualized image using Grad-CAM.

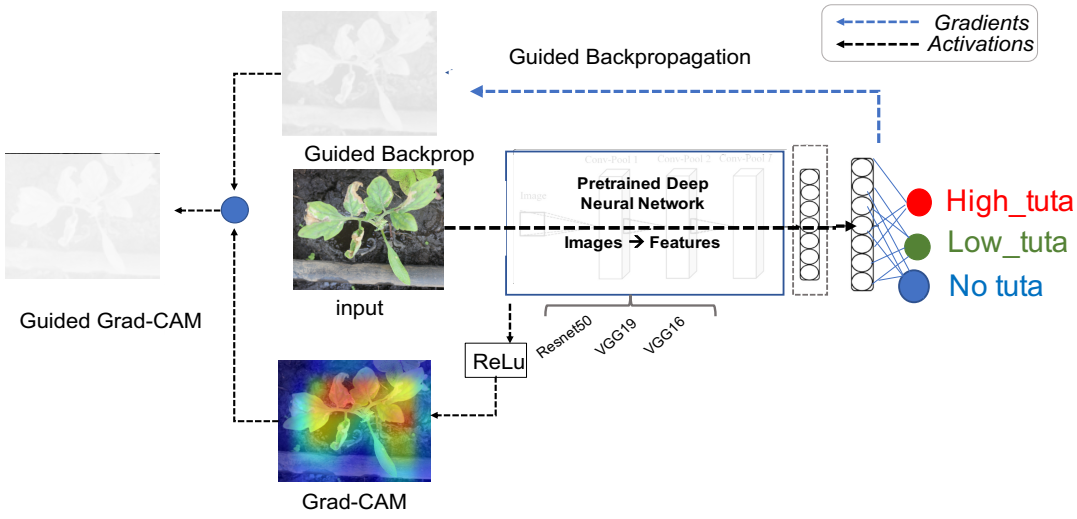

(a)

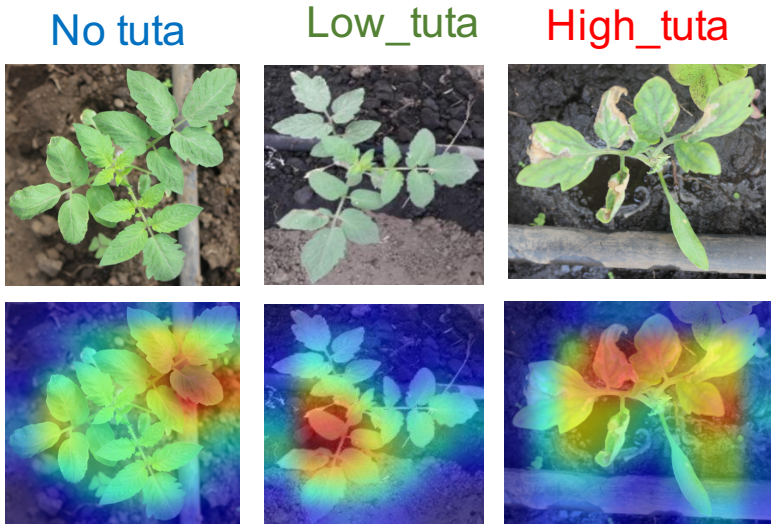

(b)

Figure. 4.11 (a) Proposed Quantification model for plants Low Tuta, High Tuta and non-affected *T. absoluta* using pretrained Deep CNN with a Grad-CAM used to visualize the model performance.(b) Shows the original images in the upper rows and the visualized image using Grad-CAM.

Table 4.2 The hyper-parameters used during training

Parameter	Value
Epochs	1000
Batch size	32
Optimizer	SGD
Learning rate	1e-5
Dropout	0.5
Momentum	0.9
Early stopping	50 epochs

4.4 Results and discussions

4.4.1 Classification model

All the CNN architectures were trained on the dataset by using the hyper-parameters as shown in Table 4.2. Such architectures were compared based on their performances on the test dataset, and based on various metrics, such as accuracy, precision, recall, and F1-score. Performance evaluation was done by averaging the metrics over four runs for each dataset division

Table 4.3 reports F1-score, mean precision, mean recall, and overall accuracy of the classifiers trained on each dataset, as calculated by using equations (4.4) through to equation (4.7):

$$\text{Accuracy} = \frac{TP + TN}{TP + TN + FP + FN}, \tag{4.4}$$

$$\text{Precision} = \frac{TP}{TP + FP}, \tag{4.5}$$

$$\text{Recall} = \frac{TP}{TP + FN}, \tag{4.6}$$

$$\text{F1-score} = 2 \times \frac{\text{Precision} \times \text{Recall}}{\text{Precision} + \text{Recall},} \tag{4.7}$$

where TP = "True Positive", number of images with *T. absoluta* and classified as having

T. absoluta; TN ="True negative", number of images with no *T. absoluta* and classified as not having *T. absoluta*; FP = "False Positive", number of images with no *T. absoluta* and classified as having *T. absoluta*; and, FN = "False Negative", number of images with *T. absoluta* and classified as not having *T. absoluta*.

The overall accuracy was considered as the evaluation metric for our experiments. The best performance accuracy was 91.9% attained using VGG16 on 85:15 dataset.

Table 4.3 Classifier performance evaluation metrics on three dataset showing the overall accuracy. Words in curly brackets are the mean precision, mean recall and mean F1−score

Dataset	VGG16	ResNet50	VGG19
75:25	$0.901_{\{0.909, 0.901, 0.901\}}$	$0.852_{\{0.856, 0.853, 0.853\}}$	$0.839_{\{0.852, 0.841, 0.841\}}$
80:20	$0.906_{\{0.915, 0.915, 0.905\}}$	$0.854_{\{0.867, 0.856, 0.856\}}$	$0.831_{\{0.853, 0.841, 0.836\}}$
85:15	$0.919_{\{0.922, 0.919, 0.919\}}$	$0.868_{\{0.871, 0.868, 0.868\}}$	$0.831_{\{0.851, 0.833, 0.833\}}$

Figure 4.12 and Figure 4.13 show the learning curves of the average accuracy and the average loss across the six clusters versus the number of epochs during training process, respectively. As seen in Figure 4.12, it shows that the validation accuracy rises fast at the early training stages and rises slowly at the later stages. In Figure 4.13, the losses fell rapidly at the early stages and slowly afterwards. This observation implies that our model learns well the features contained in our dataset at initial and later stages.

To evaluate the ability of our classifier to generalize the unseen images, we performed the prediction on 66 images that were unused during the training process. The confusion matrix in Figure 4.19 shows how well the classifier could classify the images into correct categories.

4.4.2 Training quantification classifier

We used four ImageNet (Deng et al. 2009) pretrained architectures VGG16, VGG19, ResNet50 and InceptionV3 as classifiers. The fully connected layer for each pretrained

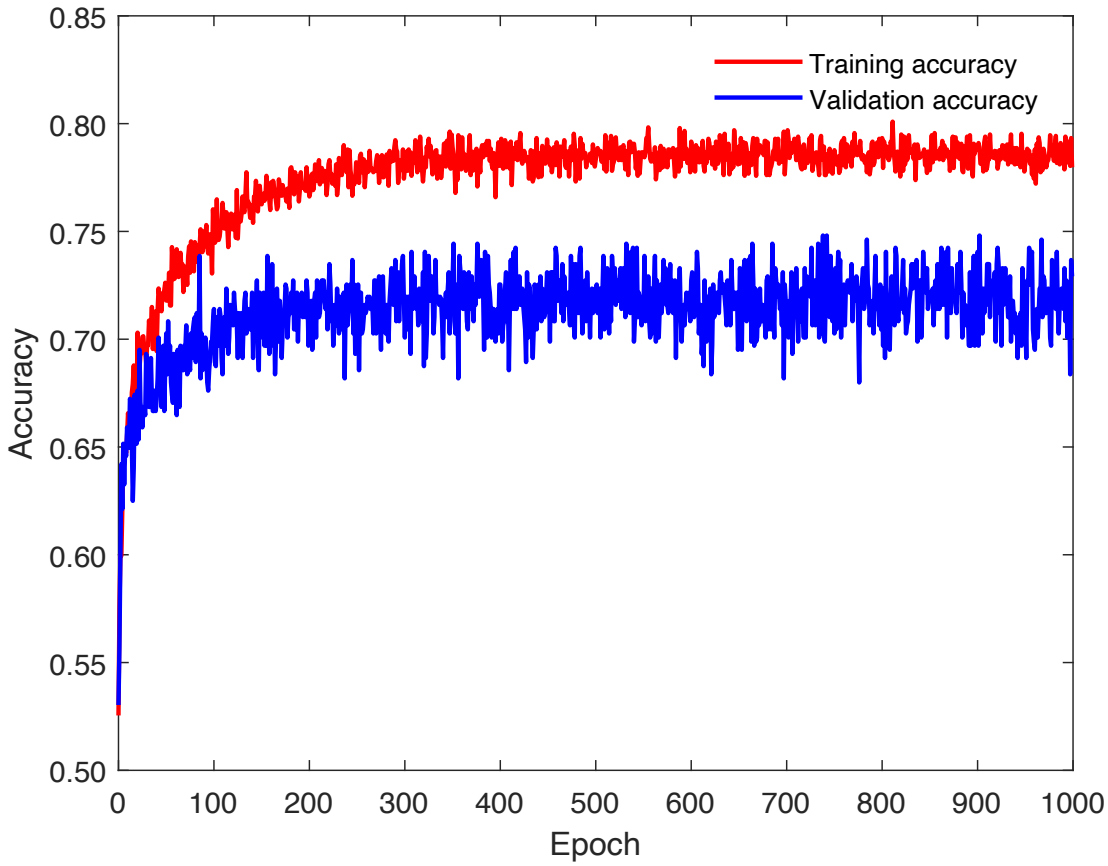

Figure. 4.12 Training and validation accuracy learning curves for the CNN model used in binary classification for plants affected and non-affected with *T. absoluta*.

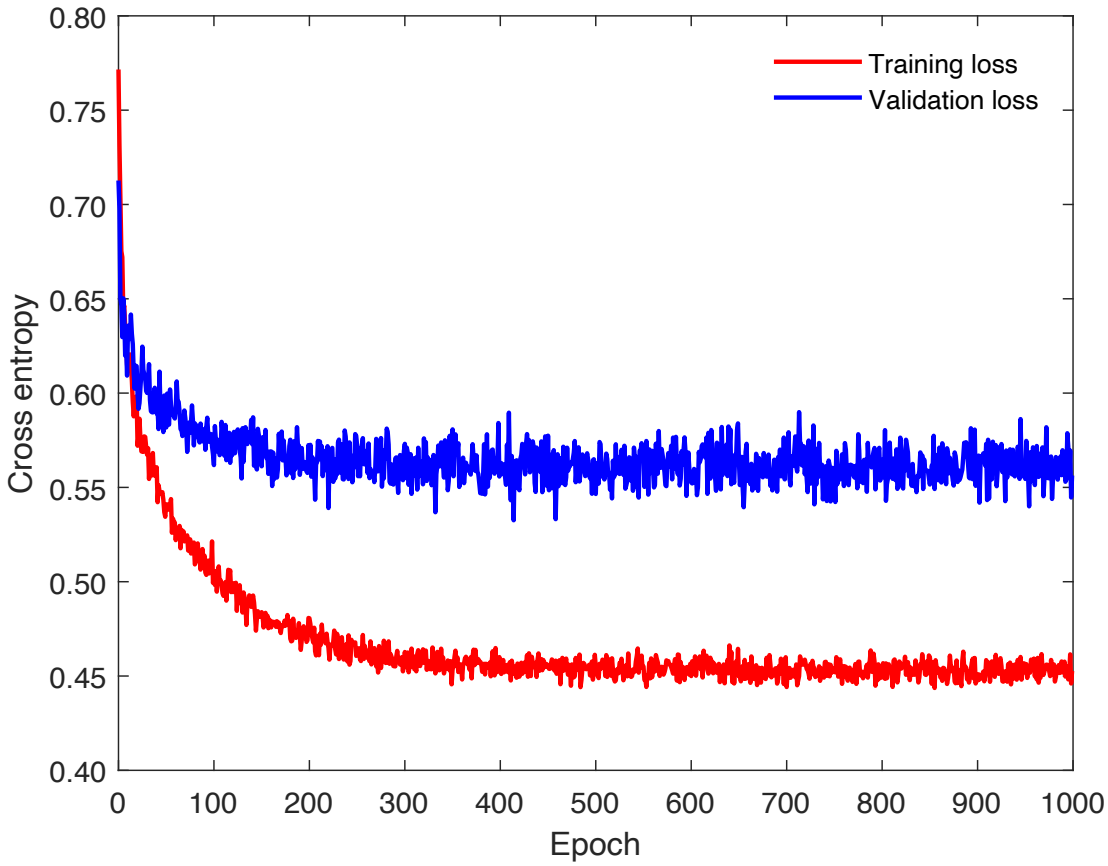

Figure. 4.13 Training and validation loss learning curves for the CNN model used in binary classification for plants affected and non-affected with *T. absoluta*.

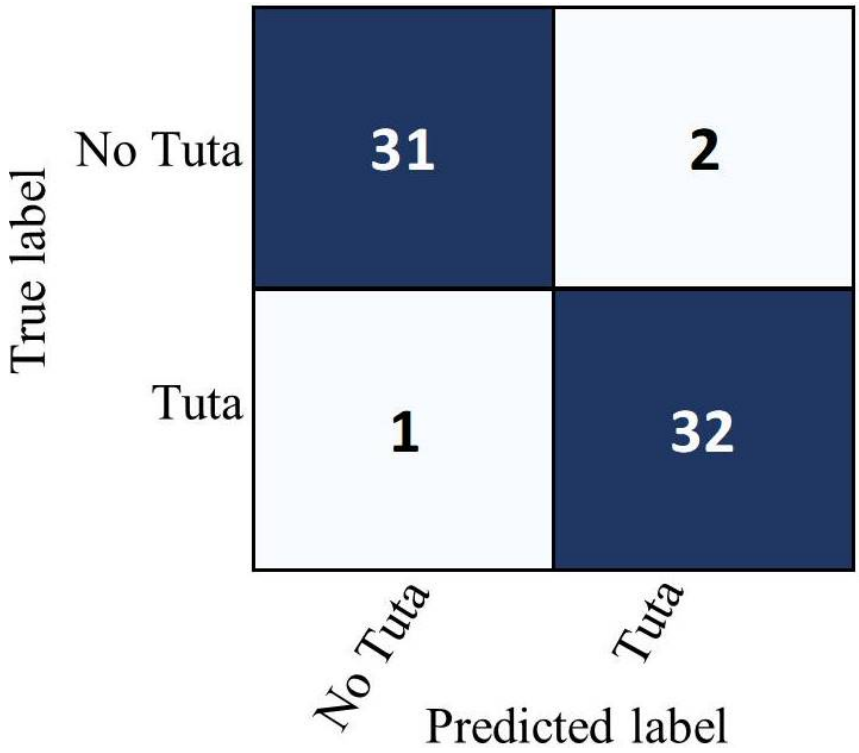

Figure. 4.14 The confusion matrix for the binary classification for plants affected and non-affected with *T. absoluta*.

architecture was replaced by the new layer (3-class classifier for our dataset). We trained our classifiers using 50 epochs with a batch size of 16 and using Keras (Ketkar 2017) implementation of Adam (Zou and Shen 2018), a first-order gradient-based method for stochastic optimization. The initial learning-rate (lr) was set to lr=$1x10^{-4}$, and was halved every time the validation loss did not decrease after 32 epochs in batches of 16 images, and aborted if the validation loss did not decrease after 32 epochs. The model with the smallest running validation loss was continuously saved, in order to re-start the training after an abortion. In such cases, training was repeated with the initial learning rate lr=$0.5x10^{-4}$. With the four subset dataset, we run all the four models on each of the subsets.

4.4.3 Quantification model

We used evaluation metrics F1–score, precision and recall accuracy and the overall evaluation metrics was a result of averaging over the 4 runs on each dataset of each CNN architecture as summarized in table 4.4

The main goal was severity status of *T. absoluta* determination. In term determining the severity status images, all models precision accuracy was highest in identifying High Tuta images i.e 90.5%, 90.5%, 90.3% and 91.5%. VGG16 and Inception-V3 had the highest recall accuracy i.e 96.5% on No Tuta images. Also all models had F1-score highest for High Tuta images. All the four models had the lowest evaluation metrics accuracy in determining Low Tuta images. Among the trained models, Inception-V3 model had the highest accuracy of 87.2% on the test set.

Table 4.4 Four pretrained model evaluation metrics accuracy precision (PRC), recall (RCL), F1–score (F1-S) accuracy and Overall average accuracy and loss on testing datasset.

	VGG16			**VGG19**			**ResNet50**			**Inception-V3**		
Severity	PRC	RCL	FI-S	PRC	RCL	FI-S	PRC	RCL	FI-S	PRC	RCL	FI-S
No Tuta	0.877	**0.965**	0.918	0.883	0.918	0.918	0.878	0.900	0.890	0.895	**0.933**	0.915
Low Tuta	0.760	0.355	0.448	0.708	0.538	0.595	0.500	0.445	0.470	0.660	0.518	0.575
High Tuta	**0.905**	0.940	**0.920**	**0.905**	**0.948**	**0.920**	**0.903**	**0.910**	**0.905**	**0.915**	0.930	**0.923**
Average Accuracy	0.871			0.783			0.837			**0.872**		
Loss	**0.152**			**0.258**			**0.334**			0.205		

4.5 Conclusion and Future Work

This research proposes pretrained deep learning models for determining severity status of *T. absoluta* tomato damages plants. For the accomplishment of this work, we used images containing health and *T. absoluta* infested tomato plant images collected from in-house experiments. Among the pretrained models, we showed that Inception-V3 model performed best, achieving an averaged accuracy of 87.2% on the test set compared to other models.

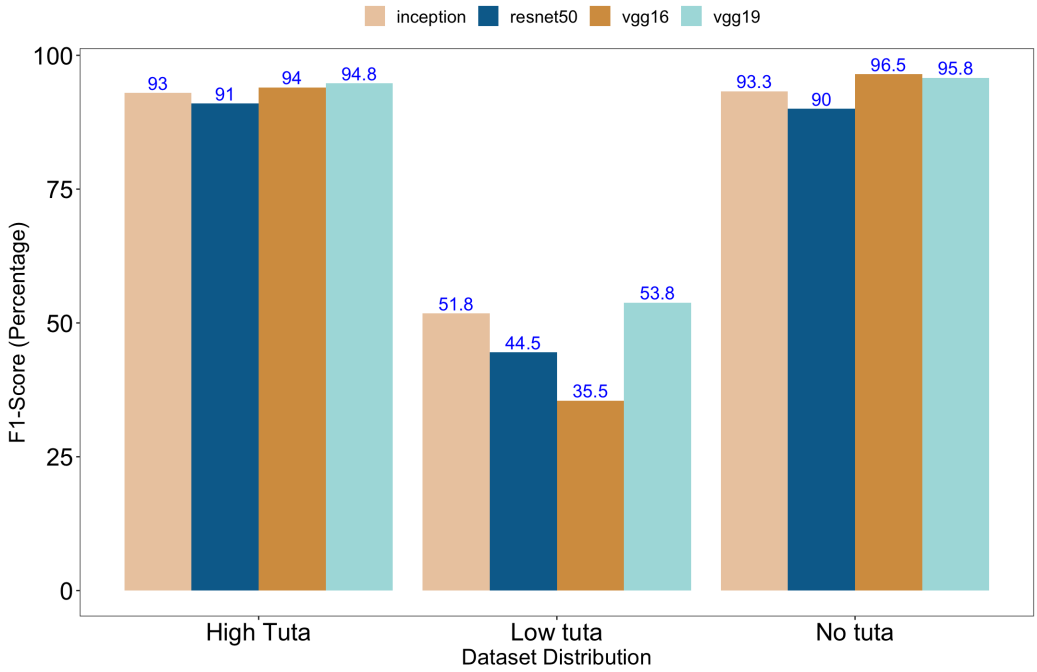

Figure. 4.15 Summary of F1-Score values of CNN quantification models for plants affected with *T. absoluta* as "No Tuta" and non-affected with *T. absoluta* as "Low Tuta" and "High Tuta".

Source: Author.

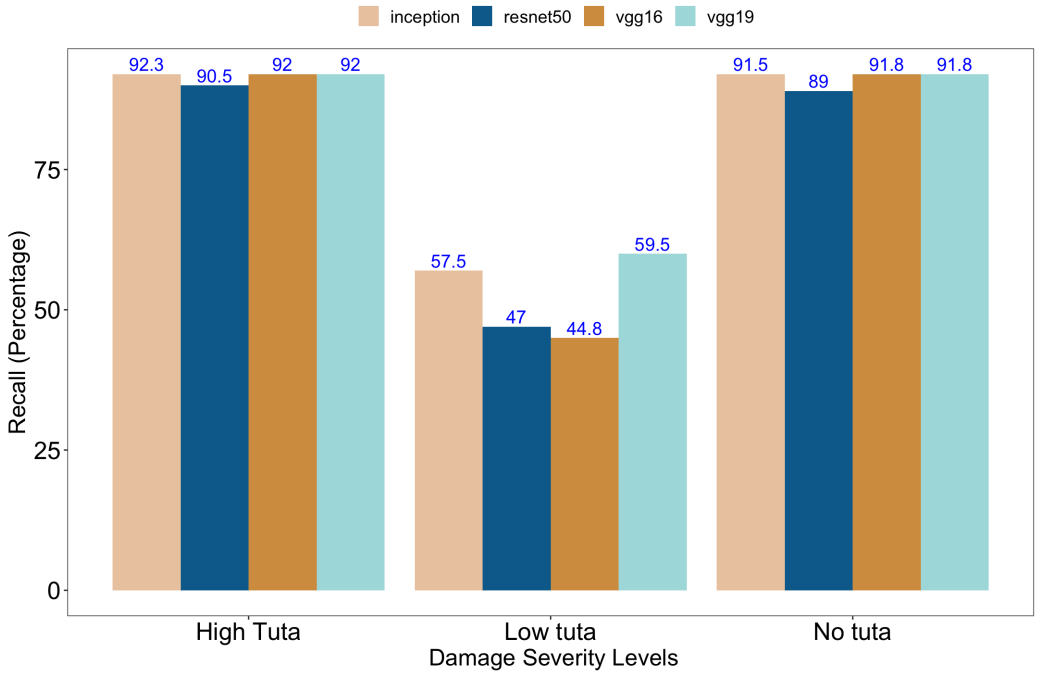

Figure. 4.16 Summary of Recall values of CNN quantification models for plants affected with *T. absoluta* as "No Tuta" and non-affected with *T. absoluta* as "Low Tuta" and "High Tuta".

Source: Author.

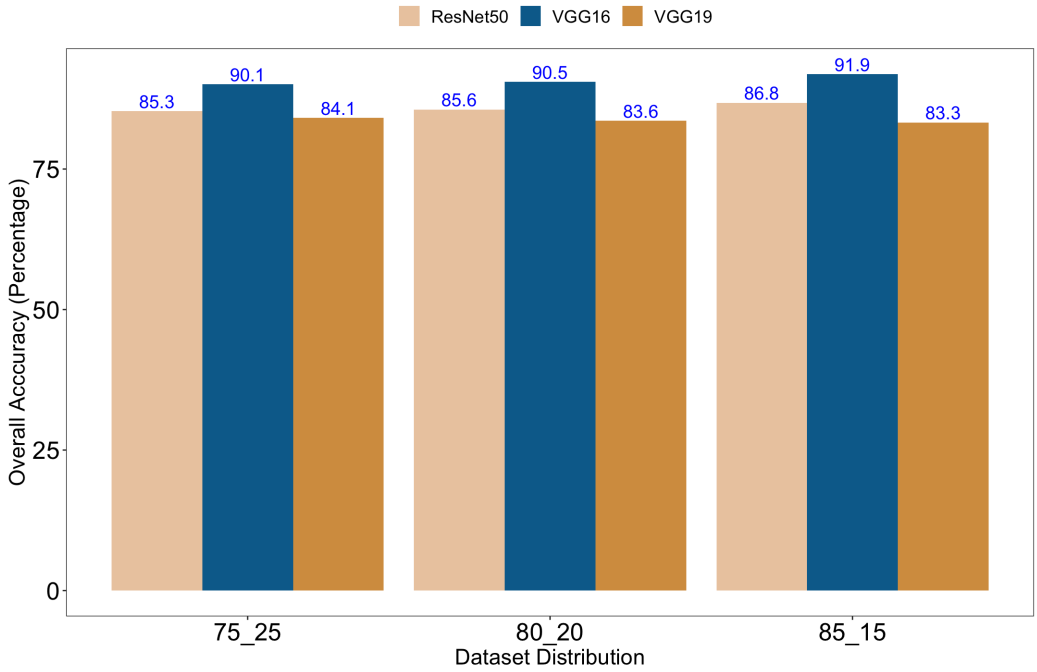

Figure. 4.17 Summary of Overall accuracy quantification values of CNN quantification models for plants affected with *T. absoluta* as "No Tuta" and non-affected with *T. absoluta* as "Low Tuta" and "High Tuta".

Source: Author.

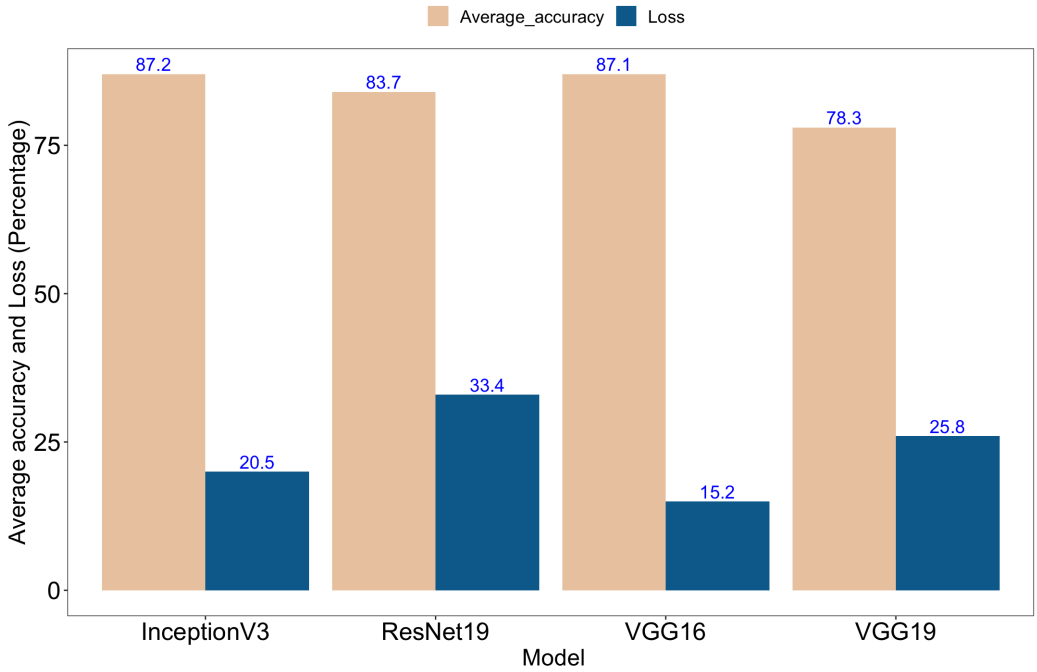

Figure. 4.18 Summary of accuracy and loss values of CNN quantification models for plants affected with *T. absoluta* as "No Tuta" and non-affected with *T. absoluta* as "Low Tuta" and "High Tuta".

Source: Author.

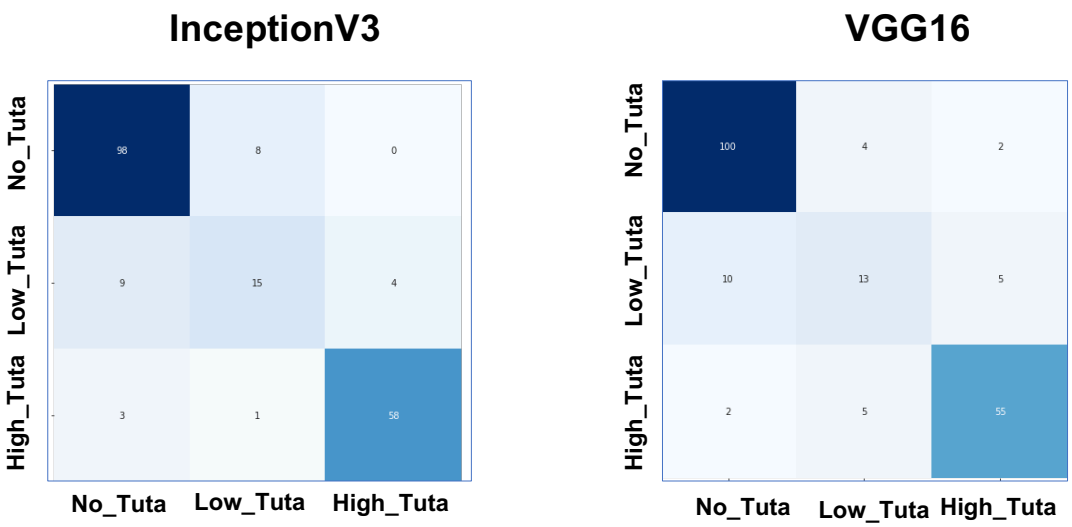

Figure. 4.19 The confusion matrix for the quantification models for plants affected and non-affected with *T. absoluta* as "No_Tuta" and non-affected with *T. absoluta* as "Low_Tuta" and "High_Tuta".

Source: Author.

Among, the three severity status, all models could more easily identify High tuta images than other severity status based on the evaluation metrics. The comparison of the evaluation metrics on each of the severity status reveals that it is a bit harder to detect Low Tuta than High Tuta and No Tuta images. With the goal of early identification of *T. absoluta* severity status in tomato plants, we clearly show the success of using deploying CNN models in such tasks. High Tuta severity status being determined as early as the first two weeks of plant growth cycle is important to reduce severe loss that are accounted when no preventive and management practices are not available.

In this research, we have proposed a deep learning model for identifying *T. absoluta* pest in tomato plants. We have used transfer learning through VGG16, VGG19, and ResNet50 models, pretrained on the ImageNet, to train classifiers on our dataset. The training of the models was performed using a dataset with 2145 images with healthy and infected leaf images collected from an in-house experiment. The highly performing model was VGG16, which achieved an overall accuracy of 91.9% in the classification

of the previously unseen 66 images from the test set. The results suggest that transfer learning is a powerful method that can achieve high accuracy in the identification of *T. absoluta* pest from tomato plant leaf images. Our method performs automatic feature extraction, thereby serving experts from the labor-intensive task of feature extraction that usually generates erroneous results.

In future, scholars may collect more dataset to increase the performance of our model to classify the unseen images. Consequently, the model will be enhanced with the capability of quantifying the severity of *T. absoluta* invasion in the farm. Therefore, we may have a decision support system to enable farmers take appropriate measures of rescuing the farm after detecting invasion at an early stage of tomato plant growth.

In future work, we intend to experiment on other CNN based models for task such as instance segmentation for localization of *T. absoluta* images. Infact, ongoing work includes, annotation of images at infested plant based and localised *T. absoluta* patches on the plant leaves for instance segmentation tasks.

Quantification task main focus was to develop early detection and quantification CNN models for tomato infested by *T. absoluta* damage characteristics and quantification to enhance early detection, the work proposes approaches in determining severity status of *T. absoluta*'s effects on tomato plants.*T. absoluta* at early stages of tomato plant's growth. The study will help farmers and extension officers to make intelligently informed decisions that could improve tomato productivity and rescue farmers from the losses they incur every year.

CHAPTER 5

IMAGE RECOGNITION USING GRADIENT BOOSTING BASED ON MULTISPECTRAL IMAGING

5.1 Introduction

Tomato *Lycopersicon esculentum* is a nutrition-rich and edible plant that is widely grown throughout the world (Schreinemachers et al. 2018)and could contribute to feeding the projected 9.6 billion people by 2050, (DESA 2018). Globally, approximately 160 Mt of tomato are produced each year Tomatonews (2019 (accessed July 9, 2019). Tomato is considered to be a source of income to small-scale farmers, and, therefore, the plant contributes largely to poverty reduction. Given the economic importance of tomato, a need to consider the factors affecting its production and find more appropriate technological solutions to maximize its productivity.

The production of tomato is threatened by an invasive pest called tomato leafminer *T. absoluta*, which attack the plant leaves, flower and fruits and interfears its growth and

yield capacity. *T. absoluta* originated from South America and later spread to the rest of the world. The pest has reproductive rate of around 12 generations per year depending on environmental conditions. Adult lifespan ranges between 10 and 15 days for females and 6–7 days for males (Estay 2000).

During its lifetime, a single female may produce up to 260 eggs (Uchoa-Fernandes et al. 1995). The eggs are laid singly or in small groups, mainly on young leaves (73%) and secondly on stems (21%), sepals (5%) and green fruits (1%) (Estay 2000). and has a life cycle with four development stages: egg, larvae, pupa, and adult. The second stage (larvae) is the most dangerous one because the larvae at this stage can mine leaves, develop, and feed on leaves, stems, and fruits of the tomato plant (Gebremariam 2015, Guimapi et al. 2016).

Therefore, if the larvae is left uncontrolled at the early stages of its growth, it may destroy all plants in the farm (Zekeya et al . 2017). Control and management of *T. absoluta* has continued to be a great constraint in tomato production, hence the need for research to devise approaches of identifying and combating it before causing great economic losses to farmers. Infact, small farmers have incured yield loss, ranging from 80%-100%, due to *T. absoluta* invasion (Zekeya et al . 2017). A study by Shiberu and Getu (2015), farmers conditions in Ethiopia, yield loss encountered were in the range of 60.08% to 82.31%. Mohamed et al. (2012) reported the first damage in Sudan with fruit damage ranging between 80% and 100%. Also in Tunisia, Chermiti et al. (2009) reported losses ranging from 11% to 43%. In another study of Moussa et al. (2013), losses were estimated up to 100% in Egypt. In tanzania where this study was conducted, Chidege et al. (2016) reported the first case, with loss between 90% and 100%.

Invasion of *T. absoluta* has, for years, been causing economic loses in the world. And, to date, no suitable solution is available to effectively control its spread. Despite existence of various ways of controlling the pest (using chemical pesticides and pheromone traps, and cultivation of resistant tomato varieties), early identification of the pest is important and therefore requires more research solutions (Zekeya et al. 2017, Tonnang et al. 2015, Bhadane et al. 2013).

In Sub-Saharan Africa, Tanzania, for instance, the agricultural system depends on extension officers as key facilitators in providing farmers with appropriate knowledge on pest and disease management. However, the extension service system is currently conducted locally by limited extension officers ' visits to provide training and workshop to meet demands of all farmers in the given area (Maginga et al. 2018). This challenge calls for a need to integrate sophisticated technologies, including those based on machine learning, into agriculture to identify pest and to maximize productivity (Zahedi et al. 2012, Bhadane et al. 2013).

This research introduces machine learning based on gradient boosting method, for classifying infected and non-infected *T. absoluta* tomato plant at early stages. The approach reinforces classification of plant canopy images collected from a field setup in a controlled environment (controlled environment refers to preventing the spread of *T. absoluta* to other neighboring tomato fields using net house).

Prior studies have showed that image-based plant pest analysis using machine learning algorithms result to more accurate results compared with human visual diagnosis. For instance, studies of detecting insect infestations in fruits and vegetable using visible color cameras such as the research of Blasco et al. (2007), summaries the application

of NIR, UV and fluorescence computer vision systems in the identification of the most common defects of citrus fruits. They proposed a fruit sorting algorithm that combines different spectral information (including visible) to classify fruit according to the type of defect. Results showed that the contribution of non-visible information can improve the detection and identification of some defects. Compared with the results from colour images, the detection accuracy of anthracnose increased upto 86% by using NIR images and the accuracy of green mould was increased from 65% to 94% by using images of fluorescence.

In addition, a computer vision system was developed for the recognition and classification of 11 most common external defects in citrus using images acquired in five spectral areas, including the study of NIR reflectance and ultraviolet induced fluorescence (Kameoka et al. 2017). The proposed fruit-sorting algorithm to identify defects in more than 2000 citrus fruits that included mandarins and oranges with overall success rate of 86%.

Further, another study on monitoring crop health status using sensing techniques. Their study aimed at characterising the spectral properties of Chinese cabbage (*Brassica Rapa L. subspecies Chinensis*) grown under varying fertilizer treatments of nitrogen, phosphorus and potassium. Using visible and infrared spectral measurements taken from 60 samples inside a laboratory. Contiguous spectral regions were plotted to show spectral profiles of the different fertilizer treatments and then classified using gradient boosting model and random forest classifiers. Gradient boosting model yielded higher classification accuracies than random forest (Mokoatsi et al. 2017).

Further more, a research done by Pathy et al. (2020), the study was about prediction

of algal biochar yield along with its composition with the extreme gradient boosting (XGB) machine learning method. In this study, an extensive grid search method was implemented in the XGB model to explore all the possible considered input parameter combinations for predicting the biochar yield using 13 different pyrolytically important input parameter combinations. They used feature importance plots that helped to reveal temperature amongst other parameters as the most influential factor. They further used shapley Additive explanations (SHAP) (Lundberg and Lee 2017) dependence plots that depicted the interactive effect of temperature and other input parameters on the algal biochar yield. Summary plots showed the combined features of importance through feature and SHAP values. Infact the developed XGB model provided new insights on comprehending the influence of input parameters on predicting the algal biochar yield.

The above examples of machine learning techniques showed good performance; however, few of research was done using techniques to classify tomato pest *T. absoluta* invasion based on vegetation indices and using multispectral images in a machine learning based on gradient boosting methods. In addition, there has been no publicly available dataset with images of tomatoes infected by *T. absoluta*. This lack of dataset hinders progress of research on early detection of *T. absoluta* in tomatoes. Therefore, in our previous reseach, we captured both regular colored images and multispectral images from our set up fields. We used the color images deep learning based methods (Rubanga et al. 2020, Mkonyi et al. 2020), results showed the potential uses of images for classification of tomato affected and non-affected. The color image dataset (Denis et al. 2020) is deposited in a public repository to facilitate further research in *T. absoluta* identification from diseased tomato plants. This current study presents a machine

learning approach for *T. absoluta* identification at early stages of the tomato plant growth using gradient boosting method bases on multispectral images.

5.2 Materials and methods

5.2.1 Experiment setup

Four in-house experiments as shown in Table 5.1 were conducted between two seasons (dry and wet) of tomato growth from August 2018 to April 2020. The in-house experiment plots with dimensions 12m x 12m x 4.5m (LWH) with 0.1 mm net size . The in-house screen house was subdivided into 3 block, each block had 12 sub-plots of 1.2 m^2 planted with 16-18 plants in two rows at a spacing of 0.3 m between plants and 0.5 m between rows as shown in Figure 5.1. The screen house were first fumigated to eliminate any other pests or diseases which may happen to be there and at the end of the experiment all the plants were destroyed so that *T. absoluta* does not migrate to neighboring areas. The *T. absoluta* larvae for inoculation of tomato plants were be obtained from the World Vegetable Centre in Arusha, Tanzania where they are reared under chemical-free greenhouse environment.

The location of the study area was in Arusha regions, located in Northern part of Tanzania, which is a sub tropical area that experience an annual average temperature of 25^oC, annual total sunshine hours of 2500 h and annual total rainfall of 900 mm. Soil type for the experiment site are of the following composition for the top soil (0 to 20 cm). Soil pH 6.43 slightly acid, total nitrogen (N) content percentage 0.23 adequate, total organic carbon percentage 2.33 moderate, total phosphorus (P) ppm 140, total potassium me percentage 3.6, total calcium me percentage 18.5, total magnesium percentage 1.02, total manganese percentage 0.37 , total copper ppm 4.48, total iron

ppm 23.8, total zinc ppm 12.5 and total sodium percentage 2.47.

Guided by the agricultural expert and entomologist experts, the tomatoes were inoculated with *T. absoluta* in the in-house experiment divided into three blocks of 12 plots each that was controlled from other pests. The experiments was under commonly practiced agronomic practice at the early growth stage i.e on the second day after transplanting. The in-house subdivided into three (3) blocks, each block had 12 small sub plots.

Table 5.1 Data collection set-up and factors considered including agronom for in-house experiment.

Duration	Season	Region	Varieties	farming system	Multispectral Scenes
Aug - Nov 2018	dry	North	1	drip, furrow, bund	3 block-season
Jan - May 2019	dry	North	3	drip	4 block-season
Sep - Dec 2019	wet	North	3	drip	3 block seasons
Jan - Apr 2020	wet	East	2	drip, furrow, bund	3 block-seasons

5.2.2 Multispectral image acquisition

Multispectral image of tomato plants canopy were collected with a 1.2 megapixel Sequoia Parrot camera that was mounted on an image acquisition platform as shown in Figure 5.1. Parrot Sequoia camera captures upto 40 nm wide bands in the Green (550 nm), Red (660nm), Red edge (735nm) and Near infrared (790nm) regions using camera of sensor of dimensions 4.8mm x 3.6mm . The Sequoia also captures simultaneous true-colour imagery with a 16 megapixel sensor (RGB Sequoia). Multispectral Sequoia images were acquired from 3 m above the tomato plant canopy with about 80 % longitudinal overlap and 70 % lateral overlap, yielding an average Ground Sampling Distance (GSD) of 0.1 cm. The captured dataset contained images of healthy (non-affected) and unhealthy (affected) tomato plants (the unhealthy ones were inoculated with *T. absoluta* larvae). The images were collected within 14 days from the

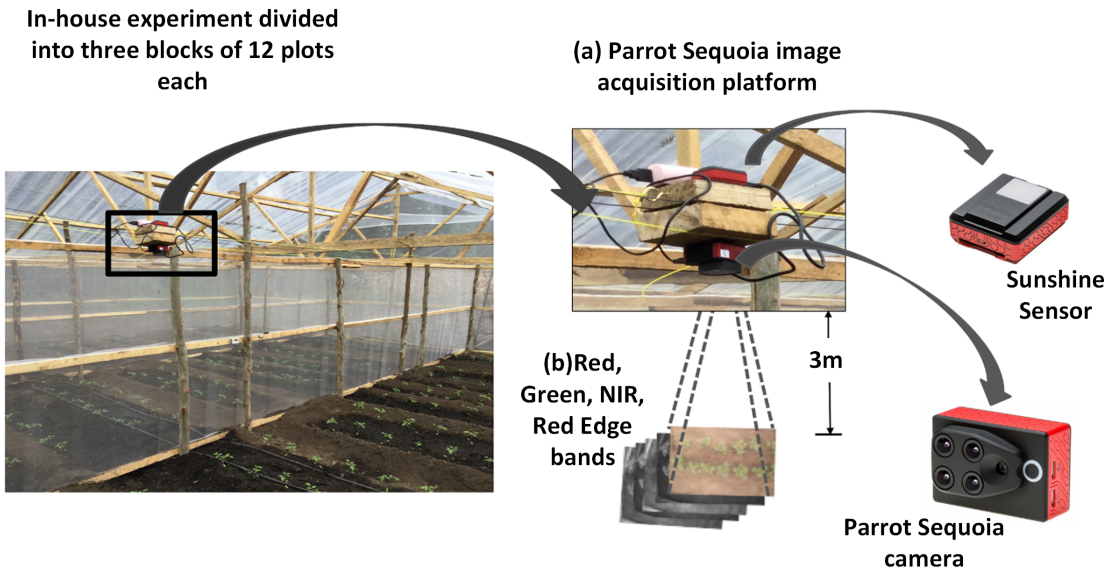

Figure. 5.1 Multispectral image acquisition platform. (a) Zoom-in of sequoia camera image acquisition platform placed about 3m above plant crown in in-house experiment separated into three block with each plot of 1.2m^2. (b) captured, red, green, NIR and Red Edge bands.

day of inoculation in each experiment. Specifically the plant canopy since the leaves are the ones affected at early growth stages of the plant. Figure 5.2 shows sample plant canopy color images collected from the field showing three stages of damages status (stages characterised as the extent of *T. absoluta* mine density as explained in previous subsection 4.3.4.

5.2.3 Multispectral Image Preprocessing and Calculation of image indices

After the multispectral image acquisition, images were analyzed by using Photogrammetric processing software Pix4Dmapper Pro 4.6.1.(Sequoia Inc) as elaborated in Figure 5.3 (c). The preprocessing was done using Windows 10 (64-bit) O.S with CPU: Intel(R) Core (TM) i7-4790 CPU 3.6GHz, RAM 16GB with a GPU Intel(R) HD Graphics 4600. Images were calibrated and geolocated during the processing using the GPS data initially geo-tagged based on data from the Sequoia GPS (located in the Sequoia Sunshine Sensor Figure 5.1).

(a) Healthy plant **(b)** Low Tuta damage **(c)** High Tuta damage

Figure. 5.2 Development of *T. absoluta* infection seen as mines on tomato leaves. (a) is the health leaf before *T. absoluta* inoculation, (b) is the *T. absoluta* infected plants shown as low Tuta damage on the 2nd day after inoculation and (c) is the *T. absoluta* infected plants shown as high Tuta damage on the 4th day after inoculation.

Multispectral images were radiometrically calibrated based on a reference tile with known albedo values imaged with the Sequoia camera on the ground prior to each flight. Some of the geospatial products results during processing derived are true-colour imagery that included orthomosaics, point clouds and digital surface models, while those derived from multispectral imagery included colour-balanced orthomosaics, non-balanced 'raw' reflectance maps and normalized difference vegetation index (NDVI) maps. For this study we used reflectance maps as shown in Figure 5.1 (d). The mosaicked calibrated reflectance map of respective spectral bands (red, green, red Edge and NIR) were further used in ArcGIS Figure 5.3 (e). Figure 5.4 and Table 5.2 shows typical reflectance spectrometer of healthy and *T. absoluta* infected tomato.

Results of reflectance map tomato canopy images contained canopy portions (i.e., tomato plant) and non-canopy portions (i.e., soil background) as shown in Figure 5.3 (f). Using ArcGIS software, the NDVI thresholding method was used to segment and extract the canopy portion of the canopy images based on the difference of the reflectance spectrum between the NDVI values of plant canopy and non-canopy as shown in Figure 5.4 (e) and statistics of reflectance summarized as shown in 5.2.

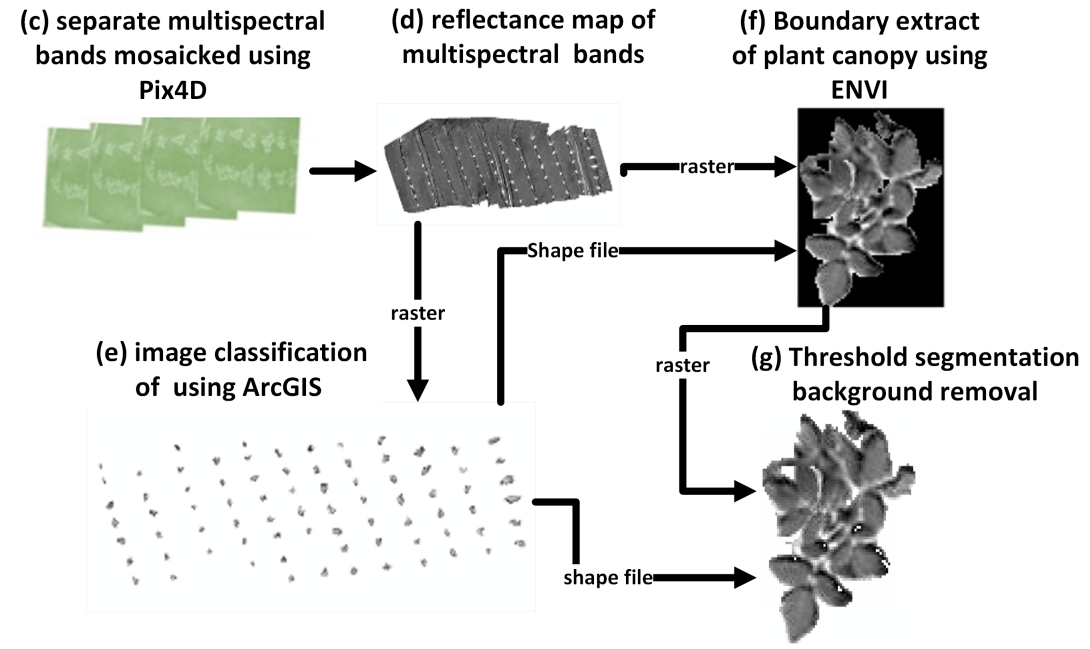

Figure. 5.3 Multispectral image preprocessing preprocessing. (c) separately multispectral bands mosaicked using Pix4D software, (d) reflectance map of multispectral bands (e) image classification using ArcGIS, (f) using raster and shapefile, each plant canopy boundary extracted using ENVI software (g) a program for background removal based on threshold segmentation.

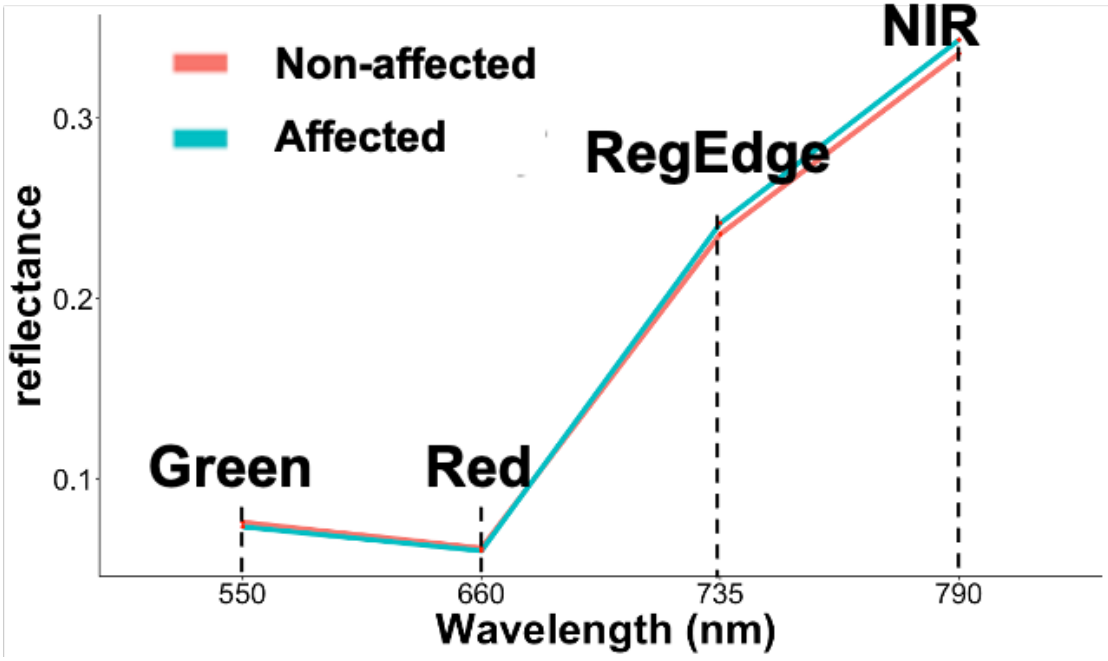

Figure. 5.4 Summary of reflectance map spectrometer of tomato canopy affected and non-affected with *T. absoluta*.

Table 5.2 Statistics of Reflectance map of tomato canopy affected and non-affected with *T. absoluta*.

Status	Band	Min	Max	Mean	Standard Deviation
Affected	green	0.029	0.153	0.076	0.027
Affected	nir	0.158	0.539	0.336	0.104
Affected	red	0.025	0.147	0.062	0.025
Affected	reg	0.071	0.401	0.236	0.075
Non-affected	green	0.038	0.118	0.073	0.023
Non-affected	nir	0.167	0.478	0.343	0.096
Non-affected	red	0.032	0.130	0.060	0.020
Non-affected	reg	0.118	0.411	0.242	0.075

Results of the NDVI segmentation Figure 5.3 (e) were used for segmentation the reflectance maps red, green, Red Edge and NIR. The generated canopy reflectance maps were converted to polygon shape. Using ENVI software as shown in Figure 5.3 (f), separate plant canopy reflectance map was generated based on the DICE method which required input as reflectance map (as raster file) and shape file that were created in ArcGIS.

Then, a python program was made for segmentation of canopy and non-canopy pixels from the reflectance map using the above results of NDVI canopy segmentation as shown in Figure 5.3 (g). After reflectance map segmentation, 14 image indices for canopy were calculated using equations in Table 5.3, Figure Figure 5.5 (b):Non-affected plant without background and Figure Figure 5.5 (b):Affected plant without background, elaborates the results of threshold segmentation background removal.

5.2.4 Classification of multispectral images using gradient boosting

The previous section described the preprocessing and the results of the threshold segmentation background removal, was eventually converted to tabular. Then gradient boosting classification analysis was carried out to analyze the relationship between

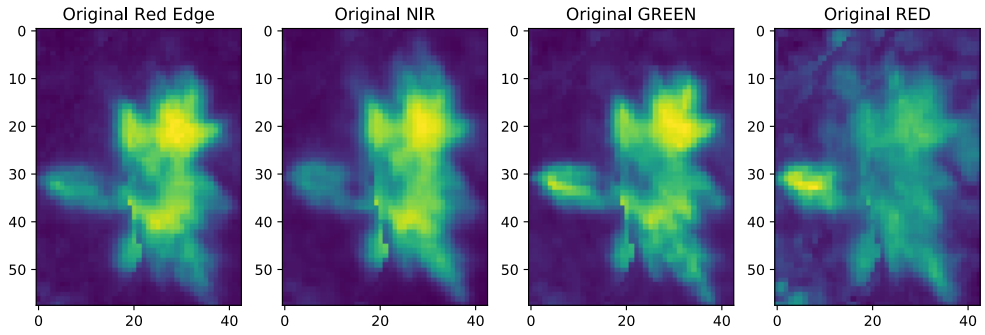

(a) Non-affected plant canopy with background

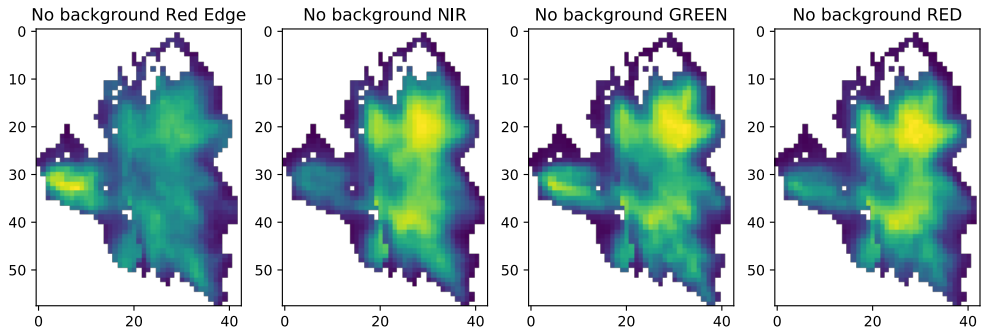

(b) Non-affected plant without background

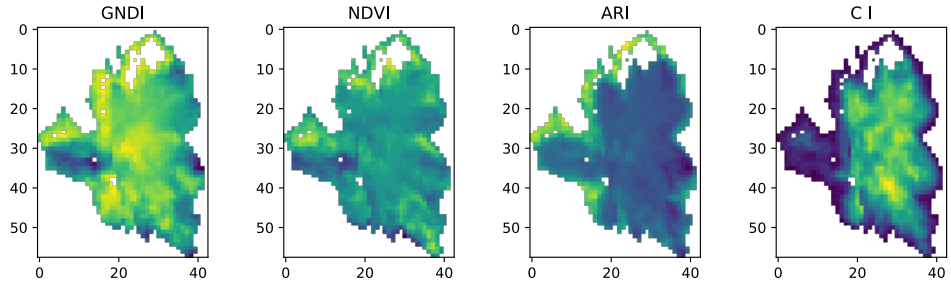

(c) Non-affected plant vegetation indice

Figure. 5.5 Selected sample of preprocessed non-affected multispectral images. (a) Spectral bands with background not removed (b) are spectral bands with background removed, and (c) are selected sample vegetation indices of non-affected tomato plant canopy.

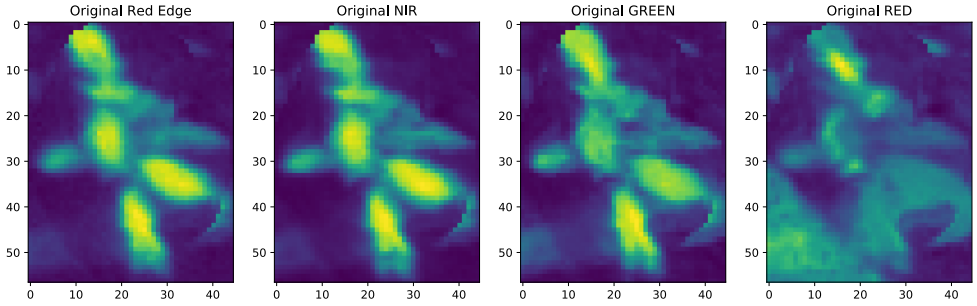

(a) Affected plant canopy plant with background

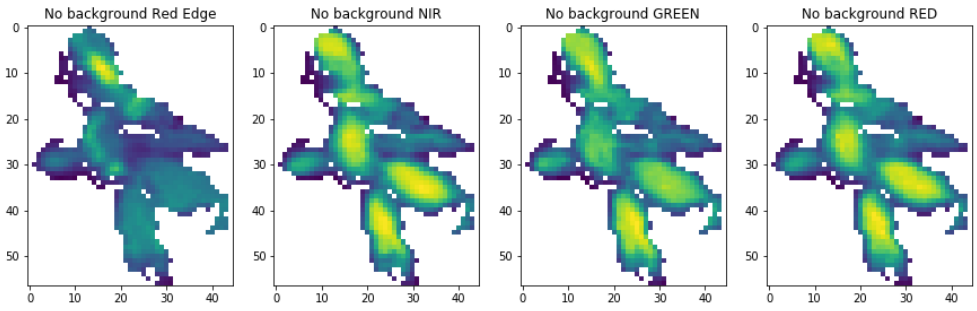

(b) Affected plant canopy plant without background

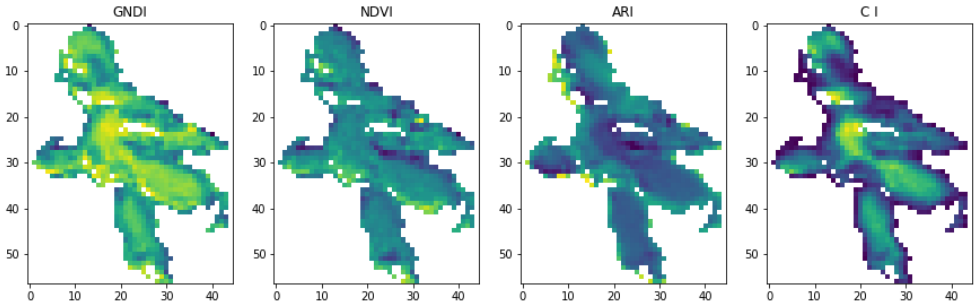

(c) Affected plant canopy plant vegetation indice

Figure. 5.6 Selected sample of preprocessed affected multispectral images. (a) Spectral bands with background not removed (b) are spectral bands with background removed, and (c) are selected sample vegetation indices of affected tomato plant canopy.

Table 5.3 Summary of selected vegetation indices

Index	Formula	$Reference$
Red-Edge Stress Vegetation Index	**RVSI** $= \frac{\text{Red} + \text{RedEdge}}{2} - RedEdge$	Gitelson et al. (2003)
Simple NIR Red Ratio Index	**NRI** $= \frac{\text{NIR}}{\text{Red}}$	Abdulridha et al. (2020)
Difference Vegetation Index	**DVI** $= \text{NIR} - \text{Red}$	Richardson and Wiegand (1977)
Modified anthocyanin content Index	**MACI** $= \frac{\text{NIR}}{\text{Green}}$	Gitelson et al. (2006*a*)
Simple Red Green Ratio Index	**RGI** $= \frac{\text{Red}}{\text{Green}}$	Gamon and Surfus (1999)
Anthocyanin content Index	**ACI** $= \text{Green} - \text{NIR}$	Sibley et al. (1999)
Chlorophyll Index	**CI** $= \frac{\text{NIR}}{\text{RedEdge}} - 1$	Dash and Curran (2004)
Green Red Index	**GRI** $= \frac{\text{Green} - \text{Red}}{\text{Green} + \text{Red}}$	Zarco-Tejada et al. (2001)
Normalized Difference Red Edge/Red	**NDRRI** $= \frac{\text{RedEdge} - \text{Red}}{\text{RedEdge} + \text{Red}}$	Ehammer et al. (2010)
Green Normalised Difference Vegetation Index	**GNDI** $= \frac{\text{NIR} - \text{Green}}{\text{NIR} + \text{Green}}$	Gitelson and Merzlyak (1996)
Normalised Difference Vegetation Index	**NDVI** $= \frac{\text{NIR} - \text{Red}}{\text{NIR} + \text{Red}}$	Raun et al. (2001)
Anthocyanin reflectance Index	**ARI** $= \text{Green}^{-1} - \text{RedEdge}^{-1}$	Gitelson et al. (2001)
Modified Anthocyanin reflectance Index	**MARI** $= \text{Green}^{-1} - \text{RedEdge}^{-1} \times \text{NIR}$	Gitelson et al. (2006*b*)

the calculated vegetation index and plant infected and non-infected with *T. absoluta*. We trained three gradient boosting classifier, XGBoost (Chen and Guestrin 2016), LightGBM (Ke et al. 2017) and CatBoost (Dorogush et al. 2018). In this research, used treeexplainer algorithm method (Lundberg et al. 2020) to explain the gradient boosting classifier result from which the attributions of each feature can be analyzed based on the sharpley additive explanations (SHAP).

Gradient boosting originally is an idea of "boosting" or improving a single weak model by combining it with a number of other weak models in order to generate a collectively strong model. Gradient boosting is an extension of boosting where the process of additively generating weak models that are trained in an additive manner where at each time step, it grows into another tree to minimize the residual of the current model and is formalised as a gradient descent algorithm over an objective function. Gradient

boosting as a supervised learning algorithm ,this means that it takes a set of labelled training instances as input and builds a model that aims to correctly predict the label of each training example based on other non-label information that we know about the example (known as features of the instance). The purpose of this is to build an accurate model that can automatically label future data with unknown labels.

We trained XGBoost, LightGBM and CatBoost binary classifiers using the scikit-learn library with the same settings to compare their performances. All the model were tuned using a 3-fold cross-validation grid-search method (Chang and Lin 2011). And the model best parameters used for,

- CatBoost are: depth - 5, iterations -350, learning rate -0.02 , l2 leaf reg -10, border count -17, and thread count -7.
- LightGBM are: colsample bytree - 4, learning rate - 3, max depth - 6, minimum number of child weight - 71, number of leaves - 7, subsample - 0.937.
- XGBoost are: colsample bytree - 2, learning rate - 5, max depth - 6, min child weight - 0 and subsample - 0.825.

The datasets were randomly split to 80% for training and 20% for validation. After training and fine-tuning all the models, the accuracy of the model was evaluated and reported as accuracy and validation.

5.2.5 Determination of suitable image indices using TreeExplainer

The features (vegetation index) used in the models, a TreeExplainer with path-dependent feature pertubation was used to define what features could be used in determining *T. absoluta* status of plants. The TreeExplainer algorithm we used based

on SHAP method. SHAP values from game theory apply to local explanations of predictions machine learning model. SHAP values are computed by introducing each feature, one at a time, into a conditional expectation function of the model's output. The calculation of SHAP is based on shapley values (Shapley 1953, Strumbelj and Kononenko 2010, Lundberg et al. 2018) which is an important method from coalition game theory to calculate how features contribute to determining the plant status (here affected and not affected with *T. absoluta*).The formula of Shapley values is,

$$\varnothing_j = \sum_{S \subseteq N \backslash i} \frac{|S|!(p - |S| - 1)!}{p!} \left(f_x \left(S \cup \{x_j\} \right) - f_x(S) \right), \tag{5.1}$$

Where $N \backslash i = \{x_1, \ldots, x_p\} \setminus \{x_j\}$, $\varnothing_j$ represent the contribution of the jth feature, x is the feature values' vector of the instance to be explained and p is the number of features.f_x (S) represent the prediction of feature values in subset S that are marginalized over features that are not included in S ((Molnar (2019)).

SHAP values show how the used vegetation index and reflance maps (here referred to as metrics) is used to classify the plant canopy into affected and non-infected *T. absoluta*. This is represented either positively or negatively. SHAP was calculated using the SHAP python package [1]. SHAP summary plots and SHAP dependency plots were created to visualize the contribution of the used metrics. SHAP Summary plots sort features by the sum of SHAP value magnitudes over all samples to show the different features' contribution to classification of plant canopy. SHAP dependency plots represent how a specific feature effects determining the plant canopy class by plotting SHAP value together with values of the metric for all the used dataset.

[1]https://github.com/slundberg/shap

5.3 Results and Discussion

5.3.1 Gradient boosting results

In this section, we present classification scores obtained after training the gradient boosting methods presented in subsection 5.2.4 on the vegetation index dataset presented in subsection 5.2.3. All vegetation index (Table 5.3) and the four reflectance maps (Red, Green, Red Edge and NIR) of respective plant canopy of both affected and non-affected with *T. absoluta* were all used in gradient boosting methods shown as Xgboost, LightGBoost and CatBoost_model_1 , we refered to this dataset as dataset 1. Using evaluation method based on accuracy and valition, results showed that the CatBoost model had the highest accuracy of 79.4% and validation of 72.2% as shown in Figure 5.7.

Using dataset 2 which had vegetation index NRI, GNDI, NDVI, MARI and the all reflectance map: Red, Green, NIR, Red Edge. The selected vegetation index were based on only the CatBoost model (here CatBoost_model_2). We further, used SHAP values to determine which metrics were of importance in classification of plant canopy (SHAP results also explained in proceesing section). We only selected only the vegetation index (here GNDI, NDVI, MARI and NRI) and used in CatBoost_model_3 which had the best accuracy and validation of 0.794 and 0.777, respectively.

5.3.2 Vegetation index based on SHAP summary plots

A combination of feature importance plot with SHAP dependence plot are presented in the summary plots of Figure 5.8 (a) – (f). The input parameters (here the used metrics as vegetation index and reflectance map) are placed on the y-axis based on their

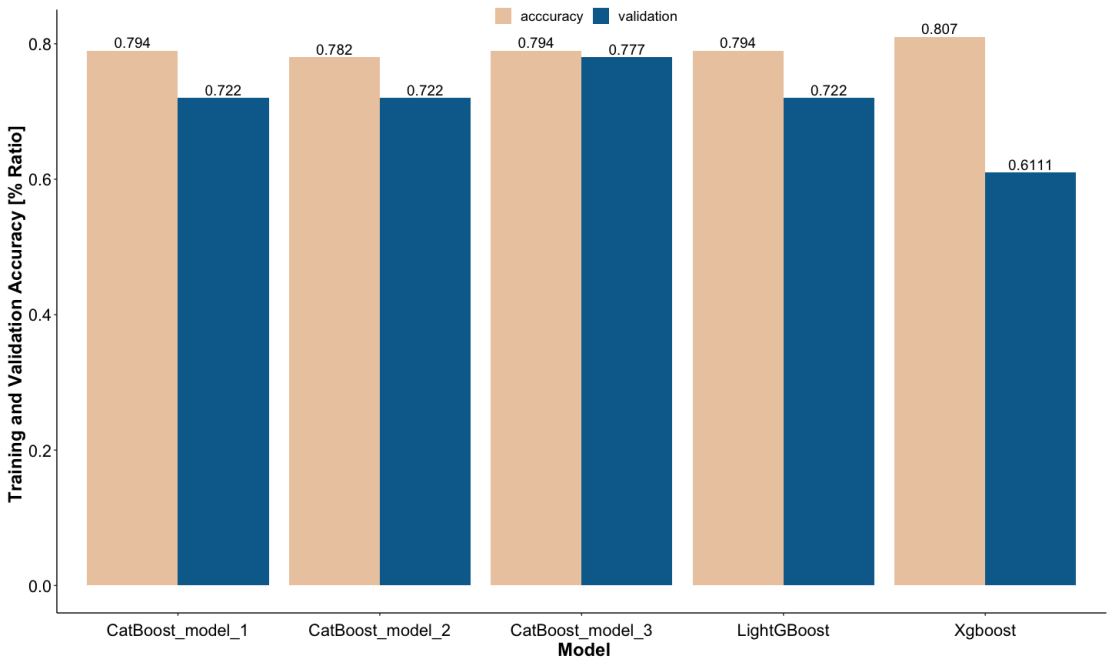

Figure. 5.7 Training and validation accuracies of Gradient Boosting Models. Xgboost and LightGBoost and CatBoost_model_1 used all the selected indices and bands. CatBoost_model_2 used GNDI, NDVI, NIR, RED, MARI, GREEN, NRI and RED indices. CatBoost_model_3 used NDVI, GNDI, NRI and MARI indices

influence and impact to the model, the most influential variable being kept at the top. The x-axis represents the SHAP value and the value of the feature is shown in color; blue to pinkish-red that represents the low to high importance. The more the data points falling in a particular range of SHAP value, the more the input variable contribute to classification of plant canopy infected and non-infected *T. absoluta*.

We show the result of CatBoost model 1, the feature importance based on SHAP values as shown in summary plot Figure 5.8, the vegetation index and reflectance map with high impact to plant canopy classification were revealed. We see a mix of vegetation index and reflectance map with importance. NDVI, GNDI, NRI as the top vegetation index with high impact to the model. We then selected only NDVI, GNDI, NRI and MARI and all four reflectance map (NIR, Red, Red Edge and Green) and used these selected features in another model and again determined the SHAP values to reveal the most important features Figure 5.8.

Results showed that the GNDI and NDVI as the most important feature. We see these features SHAP values with high positive values and negative values widely distant which may explain the plant canopy infected and non-infected *T. absoluta* distinct characteristics revealed in the indices. We further only considered on four vegetation index in order model and showed the SHAP values. Results reaffirmed that NDVI and GNDI are the most important features. It can be seen that more positive SHAP values for NDVI and GNDI. By using the summary plot, and understanding what features impact the classification model, these features can be used specifically in determining plant canopy infected and non-infected *T. absoluta*.

5.4 Conclusion

In this research,tomato plant canopy images were taken with a Sequoia (Parrot) multispectral camera, preprocessed using Pix4D software, ENVI and developed programs, results of the vegetation with four spectral bands (red, green, red edge, NIR) were used to extract only plant canopy pixels. The vegetation index images of individual tomato plants were classified using gradient boosting, XGBoost, LightGBM, CatBoost.

Result, showed that the CatBoost model of vegetation index NDVI, GNDI, NRI, and MARI images can detect diseased leaves with an accuracy of 79.4%.

Furthermore, the Tree Explainer algorithm adopting on SHAP values showed that NDVI and GNDI were the indicators with the highest contribution to the model, and that NIR reflection information was effective in identifying tomato pest damage.

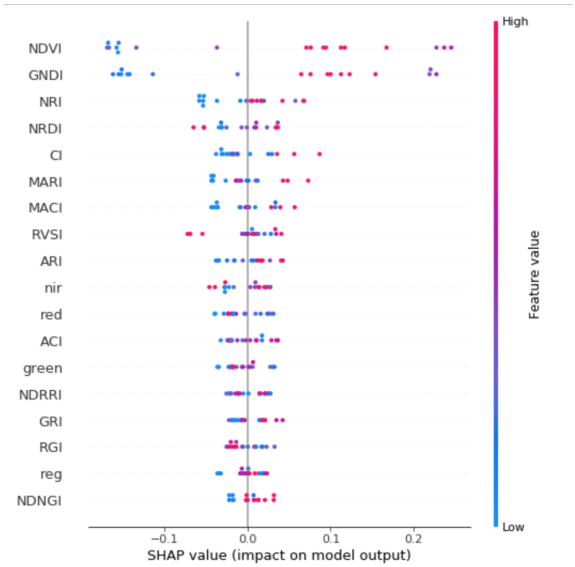

(a) Summary Plots for CatBoost_model_1

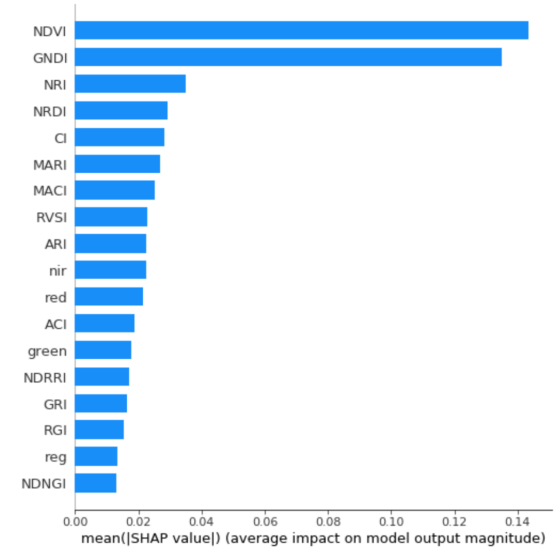

(b) Feature importance SHAP value CatBoost_model_1

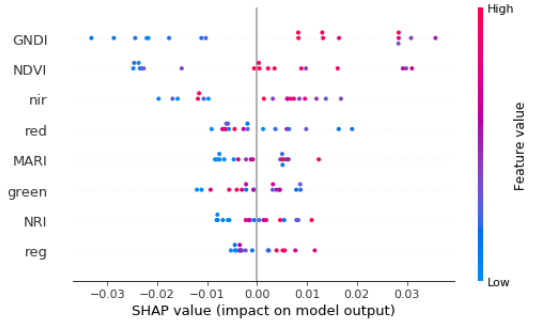

(c) Summary Plots for CatBoost_model_2

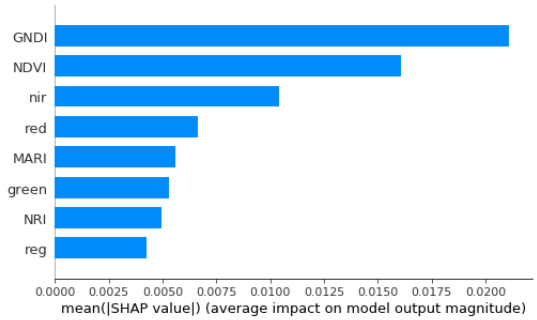

(d) Feature importance SHAP value CatBoost_model_2

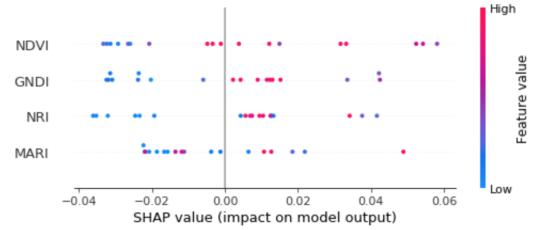

(e) Summary Plots for CatBoost_model_3

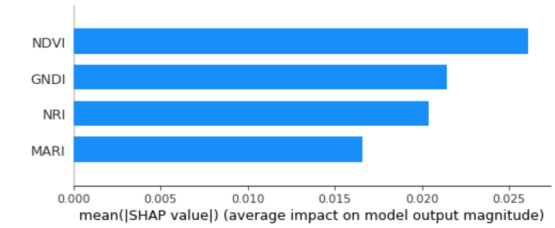

(f) Feature importance SHAP value CatBoost_model_3

Figure. 5.8 Summary Plots of used metrics of vegetation indice and spectral bands of affected (herein Non-healthy) and non-affected (herein healthy)with *T. absoluta* for CatBoost models i.e CatBoost_model_1, CatBoost_model_3 and CatBoost_model_3.

CHAPTER 6

CONCLUSIONS AND RECOMMENDATION

6.1 Conclusion

In this research, having realized the potentiality of vegetables to contribute to the required 60% increase in agriculture production to feed the projected 9.1 billion world population by 2050 despite its high vulnerable to crop failure owing to challenges of drought, adverse weather conditions e.t.c. We also realized the how economically small scale farmers as the main contributors have been affected mostly due to several loss incured during production. Therefore, we tackled the problems using recent technological advancements such as ICT techniques and artificial intelligence that have shown potential to contribute increased production in agriculture.

We showed the important to understand and develop more applicable techniques by integration of ICT and artificial intelligence to enhance vegetable production especially tomato production.

This research approach was undertaken in two main projects that focused on

development of a data driven emerging technological transfer to tackle marginalized low resource small scale tomato farmers. We categorised as labor constrained and ICT constrained small-scale farmers in Japan and sub-Sahara African Tanzania respectively. Our definition of resource constrained small-scale farmers pointed directly to two different aspect i.e., labor and technical knowledge. We therefore approached these aspects based on two different research locations.

The first main work as discussed in Chapter 2, smart agriculture application in labor constrained small scale horticulture farming in Japan. In this work, we focused at the problem of abiotic factors - micro-climate. Using ICT technological transfer of smart agriculture system, we deployed wireless sensor network that composed of commercial inexpensive wireless sensor network and developed database for crop environment monitoring and management. The results of this work, was clearly on the success use of the collected data using several consolidated methods. Deploying simple algoriths such as GDD method, we would further recommended the research community to try out other methods. However, in the context of inexpensice wireless sensors to meet farmers need in enhancing increased production.

The second work was a study to tackle ICT constrained small-scale farmers using artificial intelligence techniques. In Chapter 3, we studied the use of alternative approaches of emerging technology in ICT constrained farmers challenged by *T. absoluta* damage threats. We studied how *T. absoluta* would have impact on crop harvest and also did a comprehensive farmers awareness of *T.absoluta* damage. Results of conducted farm field survey and experiments implicated a need for an early detection approach. The set farm experiments were limited to our knowledge learnt from commonly practiced agriculture techniques. However, The first hand information

acquired from farms was very important in designing the proceeding approaches on the challenging *T. absoluta* threats,

Owing to the results of Chapter 3, we further studied and recommended artificial intelligence techniques as suitable for image classification and quantification of *T. absoluta* affected tomato. Using CNN models was the very first step, that could contribute to devise alternative methods to support phytosanitary management measures in *T. absoluta* control. We developed CNN models based on RGB images suitable for classification and for quantification. We used pretrained transfer techniques based on VGG16, VGG19, ResNet50 and InceptionV3 architecture to train deep CNN models using in-house experiment RGB images collected.

In the last work of Chapter 5, tomato plant canopy images were taken with a Sequoia (Parrot) multispectral camera, images were preprocessed using Pix4D software, ENVI and developed programs, results of the vegetation indices with four spectral bands (red, green, red edge, NIR) were used to extract only plant canopy pixels. The vegetation indices images of individual tomato plants were classified using gradient boosting algorithms; XGBoost, LightGBM, CatBoost. Result, showed that the CatBoost model of vegetation indices NDVI, GNDI, NRI, and MARI images can detect *T. absoluta* affected plant leaves with an accuracy of 79.4%. Furthermore, with the Tree Explainer algorithm adopting on SHAP values showed that NDVI and GNDI were the indicators with the highest contribution to the CatBoost best models. This Chapter, enlightened and eliminated the fact that approaches such as deep learning and machine learning should not only be be based on RGB images, but also multispectral images. We further showed how important NIR spectral bands was of significant importance in detecting *T. absoluta* infected plants.

6.2 Recommendation

Chapter 2 study showed that micro-climate environment challenges could be minimized when recommended well controlled and evenly distributed micro-climate environment are maintained. This understanding could help in regulation of heating and cooling facilities for optimum growing environment. It should be noted that this research was limited to estimation of quality. With a simplified system appropriate, we recommend integration of the system in tomato quality estimation. For the case of small scale farmers in Japan, quality plays a very important role in tomato market and eventually earns more income. Small-scale farmers struggle to produce tomato fruits of high quality. A very first step would be based on the proper management and control of micro-climate environment conditions in green houses. Therefore, with proper micro-climate management, the crop growth would be attained at their favorable conditions. Eventually good quality tomato fruits would be achieved.

From the results of Chapter 5, we saw not only the use of RGB images but also the use of NDVI and GNDI indices in detecting *T. absoluta* affected plants, we therefore recommended the use of NIR reflection information as suitable for detection of tomato plant reactions to pathogen (*T. absoluta*) which could be used in monitoring plant growth and alert when economic danger thresholds arise.

Further more, scaling up our approach, we would consider generation of damage maps based on *T. absoluta* damage status. However, this would require, a well defined system that integrates collected images of tomatoes in the field. In relation to our approach, the developed models would be used in mobile apps in defining and quantifying *T. absoluta* attack levels. Further, the results would be shared by agriculture experts in a

localized area. Such information, would also be useful to other agriculture experst such as entomologist e.t.c.

REFERENCES

Abadi, M. (2016), Tensorflow: learning functions at scale, *in* 'Proceedings of the 21st ACM SIGPLAN International Conference on Functional Programming', pp. 1–1.

Abdulridha, J., Ampatzidis, Y., Qureshi, J. and Roberts, P. (2020), 'Laboratory and uav-based identification and classification of tomato yellow leaf curl, bacterial spot, and target spot diseases in tomato utilizing hyperspectral imaging and machine learning', *Remote Sensing* **12**(17), 2732.

Agarap, A. F. (2018), 'Deep learning using rectified linear units (relu)', *arXiv preprint arXiv:1803.08375* .

Akima, H. (1978), 'A method of bivariate interpolation and smooth surface fitting for irregularly distributed data points', *ACM Transactions on Mathematical Software (TOMS)* **4**(2), 148–159.

Arora, R., Basu, A., Mianjy, P. and Mukherjee, A. (2016), 'Understanding deep neural networks with rectified linear units', *arXiv preprint arXiv:1611.01491* .

Aurelio, Y. S., de Almeida, G. M., de Castro, C. L. and Braga, A. P. (2019), 'Learning from imbalanced data sets with weighted cross-entropy function', *Neural Processing Letters* **50**(2), 1937–1949.

Bauer, A., Frank, A. and Black, A. (1984), 'Estimation of spring wheat leaf growth rates and anthesis from air temperature 1', *Agronomy Journal* **76**(5), 829–835.

Bhadane, G., Sharma, S. and Nerkar, V. B. (2013), 'Early pest identification in agricultural crops using image processing techniques', *International Journal of Electrical, Electronics and Computer Engineering* **2**(2), 77–82.

Bhatnagar, V., Singh, G., Kumar, G. and Gupta, R. (n.d.), 'Internet of thingsin smart agriculture: Applications and open challenges'.

Blasco, J., Aleixos, N., Gómez, J. and Moltó, E. (2007), 'Citrus sorting by identification of the most common defects using multispectral computer vision', *Journal of food engineering* **83**(3), 384–393.

Bottou, L. (2010), Large-scale machine learning with stochastic gradient descent, *in* 'Proceedings of COMPSTAT'2010', Springer, pp. 177–186.

Bottou, L. (2012), Stochastic gradient descent tricks, *in* 'Neural networks: Tricks of the trade', Springer, pp. 421–436.

Brahimi, M., Boukhalfa, K. and Moussaoui, A. (2017), 'Deep learning for tomato diseases: classification and symptoms visualization', *Applied Artificial Intelligence* **31**(4), 299–315.

Chang, C.-C. and Lin, C.-J. (2011), 'Libsvm: A library for support vector machines', *ACM transactions on intelligent systems and technology (TIST)* **2**(3), 1–27.

Chen, T. and Guestrin, C. (2016), Xgboost: A scalable tree boosting system, *in* 'Proceedings of the 22nd acm sigkdd international conference on knowledge discovery and data mining', pp. 785–794.

Chermiti, B., Abbes, K., Aoun, M., Ben Othmane, S., Ouhibi, M., Gamoon, W. and Kacem, S. (2009), 'First estimate of the damage of tuta absoluta (povolny)(lepidoptera: Gelecheiidae) and evaluation of the efficiency of sex pheromone traps in greenhouses of tomato crops in the bekalta region, tunisia', *African Journal of Plant Science and Biotechnology* **3**, 49–52.

Chidege, M., Al-zaidi, S., Hassan, N., Julie, A., Kaaya, E. and Mrogoro, S. (2016), 'First record of tomato leaf miner tuta absoluta (meyrick)(lepidoptera: Gelechiidae) in tanzania', *Agriculture and Food Security* **5**(1), 1–7.

Dahl, G. E., Sainath, T. N. and Hinton, G. E. (2013), Improving deep neural networks for lvcsr using rectified linear units and dropout, *in* '2013 IEEE international conference on acoustics, speech and signal processing', IEEE, pp. 8609–8613.

Dash, J. and Curran, P. (2004), 'The meris terrestrial chlorophyll index'.

DeChant, C., Wiesner-Hanks, T., Chen, S., Stewart, E. L., Yosinski, J., Gore, M. A., Nelson, R. J. and Lipson, H. (2017), 'Automated identification of northern leaf blight-infected maize plants from field imagery using deep learning', *Phytopathology* **107**(11), 1426–1432.

Deng, J., Socher, R., Fei-Fei, L., Dong, W., Li, K. and Li, L.-J. (2009), Imagenet: A large-scale hierarchical image database, *in* '2009 IEEE Conference on Computer Vision and Pattern Recognition(CVPR)', Vol. 00, pp. 248–255.
URL: *https://ieeexplore.ieee.org/abstract/document/5206848/*

Denis, P. R., Lilian, M., Mgaya, R., Never, Z., Loyani, K. L., Sawahiko, h. and Dina, M. (2020), 'A Deep Learning Dataset for Tomato Pest Leafminer TUTA ABSOLUTA'.
URL: *https://doi.org/10.5281/zenodo.4305416*

DESA, U. (2018), 'World population projected to reach 9.7 billion by 2050| un desa|

united nations department of economic and social affairs', *UN Dep. Econ. Soc. Aff. https://www. un. org/devel opmen t/desa/en/news/popul ation/world-popul ation-pros p ects-2017. html.* **7**.

Dinham, B. (2003), 'Growing vegetables in developing countries for local urban populations and export markets: problems confronting small-scale producers', *Pest management science* **59**(5), 575–582.

Dorogush, A. V., Ershov, V. and Gulin, A. (2018), 'Catboost: gradient boosting with categorical features support', *arXiv preprint arXiv:1810.11363* .

Ehammer, A., Fritsch, S., Conrad, C., Lamers, J. and Dech, S. (2010), Statistical derivation of fpar and lai for irrigated cotton and rice in arid uzbekistan by combining multi-temporal rapideye data and ground measurements, *in* 'Remote Sensing for Agriculture, Ecosystems, and Hydrology XII', Vol. 7824, International Society for Optics and Photonics, p. 782409.

Estay, P. (2000), 'The south american tomato pinworm tuta absoluta (meyrick)'.

Ferentinos, K. P. (2018), 'Deep learning models for plant disease detection and diagnosis', *Computers and Electronics in Agriculture* **145**, 311–318.

Fitz-Rodríguez, E., Kubota, C., Giacomelli, G. A., Tignor, M. E., Wilson, S. B. and McMahon, M. (2010), 'Dynamic modeling and simulation of greenhouse environments under several scenarios: A web-based application', *Computers and electronics in agriculture* **70**(1), 105–116.

Fujino, N., Ogawa, K. and Minowa, M. (2016), 'Wireless network technologies to support the age of iot', *Fujitsu Sci. Tech. J* **52**(4), 68–76.

Gamon, J. and Surfus, J. (1999), 'Assessing leaf pigment content and activity with a reflectometer', *The New Phytologist* **143**(1), 105–117.

Gebremariam, G. (2015), 'Tuta absoluta: A global looming challenge in tomato production, review paper', *Journal of Biology, Agriculture and Healthcare* **5**(14), 57–62.

Ghazi, M. M., Yanikoglu, B. and Aptoula, E. (2017), 'Plant identification using deep neural networks via optimization of transfer learning parameters', *Neurocomputing* **235**, 228–235.

Gitelson, A. A., Keydan, G. P. and Merzlyak, M. N. (2006*a*), 'Three-band model for noninvasive estimation of chlorophyll, carotenoids, and anthocyanin contents in higher plant leaves', *Geophysical research letters* **33**(11).

Gitelson, A. A., Keydan, G. P. and Merzlyak, M. N. (2006*b*), 'Three-band model for

noninvasive estimation of chlorophyll, carotenoids, and anthocyanin contents in higher plant leaves', *Geophys. Res. Lett.* **33**(11), L11402.

Gitelson, A. A. and Merzlyak, M. N. (1996), 'Signature analysis of leaf reflectance spectra: algorithm development for remote sensing of chlorophyll', *Journal of plant physiology* **148**(3-4), 494–500.

Gitelson, A. A., Merzlyak, M., Zur, Y., Stark, R. and Gritz, U. (2001), 'Non-destructive and remote sensing techniques for estimation of vegetation status'.

Gitelson, A. A., Viña, A., Arkebauer, T. J., Rundquist, D. C., Keydan, G. and Leavitt, B. (2003), 'Remote estimation of leaf area index and green leaf biomass in maize canopies', *Geophysical research letters* **30**(5).

Guimapi, R. Y., Mohamed, S. A., Okeyo, G. O., Ndjomatchoua, F. T., Ekesi, S. and Tonnang, H. E. (2016), 'Modeling the risk of invasion and spread of tuta absoluta in africa', *Ecological Complexity* **28**, 77–93.

He, K., Zhang, X., Ren, S. and Sun, J. (2016), Deep residual learning for image recognition, *in* 'Proceedings of the IEEE conference on computer vision and pattern recognition', pp. 770–778.

Ito, H. and Saito, T. (1962), 'Studies on the flower formation in the strawberry plants', *Tohoku journal of agricultural research* **13**, 191–203.

Jeong, H.-J., Park, K.-S. and Ha, Y.-G. (2018), Image preprocessing for efficient training of yolo deep learning networks, *in* '2018 IEEE International Conference on Big Data and Smart Computing (BigComp)', IEEE, pp. 635–637.

Jones, J. (2013), 'Instructions for growing tomatoes in the garden and green-house', *GroSystems, Anderson, SC, USA* **716**.

Kameoka, S., Isoda, S., Hashimoto, A., Ito, R., Miyamoto, S., Wada, G., Watanabe, N., Yamakami, T., Suzuki, K. and Kameoka, T. (2017), 'A wireless sensor network for growth environment measurement and multi-band optical sensing to diagnose tree vigor', *Sensors* **17**(5), 966.

Kameoka, T. and Hashimoto, A. (2015), 'Effective application of ict in food and agricultural sector—optical sensing is mainly described—', *IEICE transactions on communications* **98**(9), 1741–1748.

Ke, G., Meng, Q., Finley, T., Wang, T., Chen, W., Ma, W., Ye, Q. and Liu, T.-Y. (2017), Lightgbm: A highly efficient gradient boosting decision tree, *in* 'Advances in neural information processing systems', pp. 3146–3154.

Ketkar, N. (2017), Introduction to keras, *in* 'Deep learning with Python', Springer, pp. 97–111.

Kharel, T. P., Ashworth, A. J., Owens, P. R. and Buser, M. (2020), 'Spatially and temporally disparate data in systems agriculture: Issues and prospective solutions', *Agronomy Journal* **112**(5), 4498–4510.

Krizhevsky, A., Sutskever, I. and Hinton, G. E. (2012), 'Imagenet classification with deep convolutional neural networks', *Advances in neural information processing systems* **25**, 1097–1105.

KUBOTA REPORT, Business and CSR Activities 2016 (n.d.), https://www.kubota.co.jp/news/2014/2014-20j.html. Accessed: 2016-06-20.

LeCun, Y., Bengio, Y. and Hinton, G. (2015), 'Deep learning', *nature* **521**(7553), 436.

LeCun, Y., Bengio, Y. et al. (1995), 'Convolutional networks for images, speech, and time series', *The handbook of brain theory and neural networks* **3361**(10), 1995.

Lee, S. H., Chan, C. S., Mayo, S. J. and Remagnino, P. (2017), 'How deep learning extracts and learns leaf features for plant classification', *Pattern Recognition* **71**, 1–13.

Liu, B., Zhang, Y., He, D. and Li, Y. (2017), 'Identification of apple leaf diseases based on deep convolutional neural networks', *Symmetry* **10**(1), 11.

Lu, Y., Yi, S., Zeng, N., Liu, Y. and Zhang, Y. (2017), 'Identification of rice diseases using deep convolutional neural networks', *Neurocomputing* **267**, 378–384.

Lundberg, S. M., Erion, G., Chen, H., DeGrave, A., Prutkin, J. M., Nair, B., Katz, R., Himmelfarb, J., Bansal, N. and Lee, S.-I. (2020), 'From local explanations to global understanding with explainable ai for trees', *Nature Machine Intelligence* **2**(1), 2522–5839.

Lundberg, S. M., Erion, G. G. and Lee, S.-I. (2018), 'Consistent individualized feature attribution for tree ensembles', *arXiv preprint arXiv:1802.03888* .

Lundberg, S. M. and Lee, S.-I. (2017), A unified approach to interpreting model predictions, *in* I. Guyon, U. V. Luxburg, S. Bengio, H. Wallach, R. Fergus, S. Vishwanathan and R. Garnett, eds, 'Advances in Neural Information Processing Systems 30', Curran Associates, Inc., pp. 4765–4774.
URL: *http://papers.nips.cc/paper/7062-a-unified-approach-to-interpreting-model-predictions.pdf*

MAFF: (Ministry of Agriculture Fishery and Forestry, Japan, 2018) (n.d.), http://www.maff.go.jp/j/kanbo/kihyo03/gityo/smart$_{a}gri_{t}echnology/attach/pdf/smartagri_{c}atalog - 3.pdf$. $Accessed : 2019 - 01 - 20$.

Maginga, T. J., Nordey, T. and Ally, M. (2018), 'Extension system for improving the management of vegetable cropping systems', *Journal of Information Systems Engineering and Management* **3**(4).

Mandic, D. P. (2004), 'A generalized normalized gradient descent algorithm', *IEEE signal processing letters* **11**(2), 115–118.

Matsane, S. and Oyekale, A. (2014), 'Factors affecting marketing of vegetables among small-scale farmers in mahikeng local municipality, north west province, south africa', *Mediterranean Journal of Social Sciences* **5**(20), 390.

McMaster, G. S. and Wilhelm, W. (1997), 'Growing degree-days: one equation, two interpretations', *Agricultural and forest meteorology* **87**(4), 291–300.

Miller, P., Lanier, W. and Brandt, S. (2001), 'Using growing degree days to predict plant stages', *Ag/Extension Communications Coordinator, Communications Services, Montana State University-Bozeman, Bozeman, MO* **59717**(406), 994–2721.

Ministry of Agriculture, N. B. o. S. (2016/17), '2016/17 annual agriculture sample survey initial report'.

Mkonyi, L., Rubanga, D., Richard, M., Zekeya, N., Sawahiko, S., Maiseli, B. and Machuve, D. (2020), 'Early identification of tuta absoluta in tomato plants using deep learning', *Scientific African* **10**, e00590.

Mohamed, E., Mohamed, M. and Gamiel, S. (2012), 'First record of the tomato leafminer, t uta absoluta (m eyrick)(l epidoptera: G elechiidae) in s udan', *EPPO bulletin* **42**(2), 325–327.

Mokoatsi, B., Tesfamichael, S., Araya, H. and Mofokeng, M. (2017), 'Visibe and infrared spectral characterisation of chinese cabbage (brassica rapa l. subspecies chinensis), grown under different nitrogen, potassium and phosphorus concentrations.', *International Archives of the Photogrammetry, Remote Sensing and Spatial Information Sciences* **42**.

Molnar, C. (2019), 'Interpretable machine learning', *Lulu. com* .

Moussa, S., Sharma, A., Baiomy, F. and El-Adl, F. E. (2013), 'The status of tomato leafminer, tuta absoluta (meyrick)(lepidoptera: Gelechiidae) in egypt and potential effective pesticides', *Academic Journal of Entomology* **6**(3), 110–115.

Netatmo (n.d.), www.Netatmo.com. Accessed: 2016-05-20.

Nicolosi, G., Volpe, R. and Messineo, A. (2017), 'An innovative adaptive control system to regulate microclimatic conditions in a greenhouse', *Energies* **10**(5), 722.

Ouppaphan, P. (2017), Corn disease identification from leaf images using convolutional neural networks, *in* '2017 21st International Computer Science and Engineering Conference (ICSEC)', IEEE, pp. 1–5.

Pathy, A., Meher, S. and Balasubramanian, P. (2020), 'Predicting algal biochar yield using extreme gradient boosting (xgb) algorithm of machine learning methods', *Algal Research* **50**, 102006.

Perez, L. and Wang, J. (2017), 'The effectiveness of data augmentation in image classification using deep learning', *arXiv preprint arXiv:1712.04621* .

Ramcharan, A., Baranowski, K., McCloskey, P., Ahmed, B., Legg, J. and Hughes, D. P. (2017), 'Deep learning for image-based cassava disease detection', *Frontiers in plant science* **8**, 1852.

Rangarajan, A. K., Purushothaman, R. and Ramesh, A. (2018), 'Tomato crop disease classification using pre-trained deep learning algorithm', *Procedia computer science* **133**, 1040–1047.

Raun, W. R., Solie, J. B., Johnson, G. V., Stone, M. L., Lukina, E. V., Thomason, W. E. and Schepers, J. S. (2001), 'In-season prediction of potential grain yield in winter wheat using canopy reflectance', *Agronomy Journal* **93**(1), 131–138.

Richardson, A. J. and Wiegand, C. (1977), 'Distinguishing vegetation from soil background information', *Photogrammetric engineering and remote sensing* **43**(12), 1541–1552.

Rubanga, D. P., Loyani, L. K., Richard, M. and Shimada, S. (2020), 'A deep learning approach for determining effects of tuta absoluta in tomato plants', *arXiv preprint arXiv:2004.04023* .

Ruder, S. (2016), 'An overview of gradient descent optimization algorithms', *arXiv preprint arXiv:1609.04747* .

Schreinemachers, P., Simmons, E. B. and Wopereis, M. C. (2018), 'Tapping the economic and nutritional power of vegetables', *Global food security* **16**, 36–45.

Selvaraju, R. R., Cogswell, M., Das, A., Vedantam, R., Parikh, D. and Batra, D. (2019), 'Grad-cam: Visual explanations from deep networks via gradient-based localization', *International Journal of Computer Vision* **128**(2), 336–359.
URL: *http://dx.doi.org/10.1007/s11263-019-01228-7*

Shao, S., McAleer, S., Yan, R. and Baldi, P. (2018), 'Highly accurate machine fault diagnosis using deep transfer learning', *IEEE Transactions on Industrial Informatics* **15**(4), 2446–2455.

Shapley, L. S. (1953), 'A value for n-person games', *Contributions to the Theory of Games* **2**(28), 307–317.

Shiberu, T. and Getu, E. (2015), 'Estimate of yield losses due to t. absoluta meyrick (lepidoptera: Gelechiidae) on tomato crops under glasshouse and field conditions in western shewa of central ethiopia'.

Sibley, J. L., Ruter, J. M. and Eakes, D. J. (1999), 'Bark anthocyanin levels differ with location in cultivars of red maple', *HortScience* **34**(1), 137–139.

Simonyan, K. and Zisserman, A. (2014), 'Very deep convolutional networks for large-scale image recognition', *arXiv preprint arXiv:1409.1556* .

Singh, M. C., Yousuf, A. and Singh, J. (2016), 'Greenhouse microclimate modeling under cropped conditions: A review', *Res. Environ. Life Sci* **9**, 1552–1557.

Snyder, R. L., Spano, D., Cesaraccio, C. and Duce, P. (1999), 'Determining degree-day thresholds from field observations', *International Journal of Biometeorology* **42**(4), 177–182.

Strumbelj, E. and Kononenko, I. (2010), 'An efficient explanation of individual classifications using game theory', *The Journal of Machine Learning Research* **11**, 1–18.

Suga, T. and Okuyama, S. (2016), 'Fujitsu's approach to iot business and its related technologies', *FUJITSU SCIENTIFIC and TECHNICAL JOURNAL* **52**(4), 8–16.

Szegedy, C., Vanhoucke, V., Ioffe, S., Shlens, J. and Wojna, Z. (2016), Rethinking the inception architecture for computer vision, *in* 'Proceedings of the IEEE conference on computer vision and pattern recognition', pp. 2818–2826.

Tomatonews (2019 (accessed July 9, 2019)), *The Global Tomato Processing in 2018*. **URL:** *http://www.tomatonews.com/en/background*$_4$7.$html$

Tonnang, H. E., Mohamed, S. F., Khamis, F. and Ekesi, S. (2015), 'Identification and risk assessment for worldwide invasion and spread of tuta absoluta with a focus on sub-saharan africa: implications for phytosanitary measures and management', *PloS one* **10**(8), e0135283.

Uchoa-Fernandes, M., Della Lucia, T., Vilela, E. et al. (1995), 'Mating, oviposition and pupation of scrobipalpuloides absoluta (meyr.)(lepidoptera: Gelechiidae).', *Anais da Sociedade Entomologica do Brasil* **24**(1), 159–164.

Wang, G., Sun, Y. and Wang, J. (2017), 'Automatic image-based plant disease severity estimation using deep learning', *Computational intelligence and neuroscience* **2017**.

Zahedi, S. R., Zahedi, S. M. et al. (2012), 'Role of information and communication technologies in modern agriculture', *International Journal of Agriculture and Crop Sciences* **4**(23), 1725–1728.

Zarco-Tejada, P. J., Miller, J. R., Noland, T. L., Mohammed, G. H. and Sampson, P. H. (2001), 'Scaling-up and model inversion methods with narrowband optical indices for chlorophyll content estimation in closed forest canopies with hyperspectral data', *IEEE Transactions on Geoscience and Remote Sensing* **39**(7), 1491–1507.

Zekki, H., Gauthier, L. and Gosselin, A. (1996), 'Growth, productivity, and mineral composition of hydroponically cultivated greenhouse tomatoes, with or without nutrient solution recycling', *Journal of the American Society for Horticultural Science* **121**(6), 1082–1088.

Zhang, K., Wu, Q., Liu, A. and Meng, X. (2018), 'Can deep learning identify tomato leaf disease?', *Advances in Multimedia* **2018**.

Zou, F. and Shen, L. (2018), 'On the convergence of adagrad with momentum for training deep neural networks', *arXiv preprint arXiv:1808.03408* **2**(3), 5.

LIST OF PUBLICATIONS AND DATASETS

1. **D.P Rubanga**, K HATANAKA, S. SHIMADA (2018) Development of a Simplified smart Agriculture system for small-scale greenhouse farming, Sensors and Materials.

2. **D.P Rubanga**, K HATANAKA, S. SHIMADA (2018) Spatiotemporal Analysis of Small Scale Greenhouse Microclimate Based on Smart Agriculture System, AGROFOR.

3. R Saville, K Hatanaka, **DP Rubanga**, 2020. A Study on Factors Affecting High Quality Fruit Tomato Production in a Greenhouse by Utilizing Low Cost Smart Agriculture Framework. Indonesian Journal of Computing, Engineering and Design (IJoCED) 2 (2), 58-70.

4. Mkonyi, L., **Rubanga, D.**, Richard, M., Zekeya, N., Shimada, S., Maiseli, B. and Machuve, D. (2020), 'Early identification of tuta absoluta in tomato plants using deep learning', Scientific African 10, e00590.

5. **Rubanga, D. P.**, Loyani, L. K., Richard, M. and Shimada, S. (2020), A deep learning approach for determining effects of *Tuta absoluta* in tomato plants, arXiv preprint arXiv:2004.04023 .

6. **Rubanga, D. P**., Mkonyi, L., Richard, M., Zekeya, N., Loyani, L. K., Shimada, S. and Machuve, D. (2020), A Deep Learning Dataset for Tomato Pest Leafminer *TUTA ABSOLUTA*. URL: https://doi.org/10.5281/zenodo.4305416

7. **Rubanga, D. P.**, Shimada,S., Ayako S,. Early Stage Detectation of Tomato Pest *Tuta absoluta* Utilizing Deep Learning and Gradient Boosting based on Multispectral Imaging (Submitting)

Appendices

Appendix A

Farm survey - Questionnaire

The farm field survey was conducted in 9 villages of Tanzania where tomato production was commonly practiced. A total of 332 small-scale farmers were interviewed between August 2020 and October 2020. The questionnaire included is a Swahili language version that was designed for the farmers since Swahili language is the native language.

Dodoso

Utafiti juu ya wakulima wenye uelewa juu ya teknolojia zinazoibuka ili kukabiliana na changamoto za Tuta absoluta(Kantangaze) kwenye nyanya: Utafiti wa uchunguzi wa Tanzania.

Arusha: Ngarenanyuki/engarenanyukie, ngabobo, nduruma
Morogoro: Kipera, Maharak hia-Doma, Mlali
Iringa: Ilula, Sadani na Kalenga, Ruaha mbuyuni

* Required

1. Jini la kijiji *

Check all that apply.

- [ ] Arusha - Ngarenanyuki/Engarenanyukie
- [ ] Arusha - ngabobo
- [ ] Arusha - nduruma
- [ ] Morogoro - kipera
- [ ] Morogoro - maharaka-Doma
- [ ] Morogoro - Mlali
- [ ] Iringa - Ilula
- [ ] Iringa -Kalenga
- [ ] Iringa - Ruaha Mbuyuni

2. Jinsia

Mark only one oval per row.

	18 -24	24-30	40-50	50-60	60-70	Juu ya 70
F	◯	◯	◯	◯	◯	◯
M	◯	◯	◯	◯	◯	◯

3. Elimu

Mark only one oval.

- S/MSINGi
- S/SEKONDARI
- UFUNDI STADI/CERTI/DIP
- ELIMU YA JUU - BSC
- ELIMU YA JUU/ZAIDI MSc/PhD
- SIJAENDA SHULE

4. Uzoefu wa nyanya *

Mark only one oval.

- 0-1 miaka
- 2-5 miaka
- 5- 10 miaka
- 10-20 miaka
- zaidi ya miaka 20

5. Wastani wa usambazaji wa ardhi ya mazao (nyanya na mazao mengine) kwa miaka 5 iliyopita katika ekari katika msimu mwaka mzima. * Asimilia (%) Distribution of tomato compared to other crops

Check all that apply.

	0%	30%	50%	80%	100%
miaka 10 nyuma	☐	☐	☐	☐	☐
miaka 5 nyuma	☐	☐	☐	☐	☐
miaka 4 nyuma	☐	☐	☐	☐	☐
miaka 2 nyuma	☐	☐	☐	☐	☐
Kwa sasa	☐	☐	☐	☐	☐

6. Ni majira gani (mwezi) Je, kawaida hupandwa nyanya *

_____

7. Eneo na ukubwa wa shamba (Eka) *

_____

8. Msimu uliyopita ulivuna kiasi gani cha nyanya (**tenga moja huingia ndoo 2 za lita 20) *

_____

9. Ni aina gani ya nyanya ulipanda *

_____

10. Jinsi ya kufikia nafasi ya shamba. *

Check all that apply.

- [ ] pikipiki
- [ ] baiskeli
- [ ] gari
- [ ] punda
- [ ] miguu

11. Changamoto kubwa/matatizo *

Check all that apply.

- [ ] magonjwa
- [ ] wadudu
- [ ] Wanyama wasumbufu

12. Nini suluhisho la juu zaidi kwa matatizo tajwa hapo juu. *

Check all that apply.

- [ ] Matumizi ya kemikali
- [ ] mazoezi ya kiagronomia
- [ ] Matumizi ya mitishamba(mimea dawa)
- [ ] Njia mchanganyiko

13. Chanzo cha habari – ni jinsi gani unaweza kutatua changamoto? *

Check all that apply.

- [ ] Kutumia uzoefu wa zamani
- [ ] kutumia afsa ugani
- [ ] wakulima wengine
- [ ] wataalamu wa kilimo.

14. Ni chanzo gani Cha habari hutumika? *

Check all that apply.

- [ ] redio
- [ ] runinga/TV
- [ ] majirani
- [ ] Afisa ugani

15. Ni aina gani ya simu ambayo unatumia? *

Mark only one oval.

- ◯ simu ya mkononi
- ◯ simu ya mezani
- ◯ hakuna simu

16. Kituo cha karibu kwa huduma za simu Kama kuchaji simu ,je, simu huchajiwa nyumbani au kwa jirani, *

Check all that apply.

- [ ] kituo kipo
- [ ] jirani
- [ ] Nyumbani

17. Huduma za kurejesha tena muda wa maongezi ,je zipo Karibu? *

Mark only one oval.

- ◯ karibu
- ◯ mbali

18. Je, matumizi makubwa ya simu yako ni yapi? *

Check all that apply.

- [ ] Kupata habari kutoka kwa wakulima
- [ ] Kwa madhumuni ya muamala
- [ ] Kwa mawasiliano binafsi

19. Ni kwa njia gani umetumia simu yako kutatua changamoto zinazowakabili katika kilimo? *

_____

20. Je, unashirikisha vipi taarifa za mashambulio (magonjwa, wadudu) *

Check all that apply.

- [ ] Ana kwa ana
- [ ] Mawasiliano ya simu

21. Je,ni wapi unakouza mazao yako *

Check all that apply.

- [ ] sokoni
- [ ] watu wa kati
- [ ] mwingine

22. Mbinu ya malipo *

Check all that apply.

- [ ] pesa taslimu
- [ ] Pesa kupitia benki
- [ ] pesa kwa njia ya mtandao

23. Itachukua muda gani kutoka msimu wa mavuno mpaka kuuza mazao yako? *

Mark only one oval.

- ◯ wiki 0-1
- ◯ wiki 1-2
- ◯ wiki 2- 3

24. Unashirikisha habari za mashambulizi (magonjwa, wadudu) kwa wakulima wengine? *

Mark only one oval.

- ◯ ndiyo
- ◯ hapana

25. Kama ndiyo kwa nani na kwa namna gani *

Check all that apply.

- ☐ maadishi
- ☐ neno kwa neno
- ☐ wakulima wengine
- ☐ wataalamu wa kilimo

26. Mara ngapi kutembelea shamba; wakati wa hatua ipi ya ukuaji wa mazao: ..maua, matunda, mavuno.

Mark only one oval per row.

	1	3	7	14	21	30
planting	◯	◯	◯	◯	◯	◯
vegetative	◯	◯	◯	◯	◯	◯
flowering	◯	◯	◯	◯	◯	◯
fruiting	◯	◯	◯	◯	◯	◯
harvesting	◯	◯	◯	◯	◯	◯

27. Uharibifu wa kantangaze; nini hufikiriwa zaidi Kama uharibifu? *

Mark only one oval.

- ◯ Uharibifu halisia wa majani
- ◯ maua
- ◯ matunda kutobolewa

28. Jinsi gani unaweza kutambua-kuona uharibifu huo wa kantangaze? *

_____

29. Nini mikakati ya sasa mmechukua kumdhibiti Kantangaze? *

Check all that apply.

- ☐ kutega tuta wakubwa
- ☐ Kuzingatia uharibifu wa uzalishwaji (kuharibu uzazi)
- ☐ matumizi ya wadudu rafiki (mahasimu na parasitoid), microbial na vimelea pathogens
- ☐ Viwatilifu (kemikali)
- ☐ Njia za kienyeji (za wakulima)
- ☐ Njia mchanganyiko

Appendix B

Sample Dataset of Tomato Images

In this section, we show the detail layout of the in-house experiment set in Morogoro region, Tanzania, and also sample images taken.

As shown in Figure B.1, layout of the in-house experiment plot. Each block with plots of 2.72m^2 size. Agriculture practice was sprinkler irrigation, furrow irrigation and drip irrigation.

As shown in Figure B.2, sample images of tomato taken at different dates in different in-house blocks. The figure labelled with different dates. Labels such as BLK1_PL003 represent, block name (BLK1) and plant number (PL003).

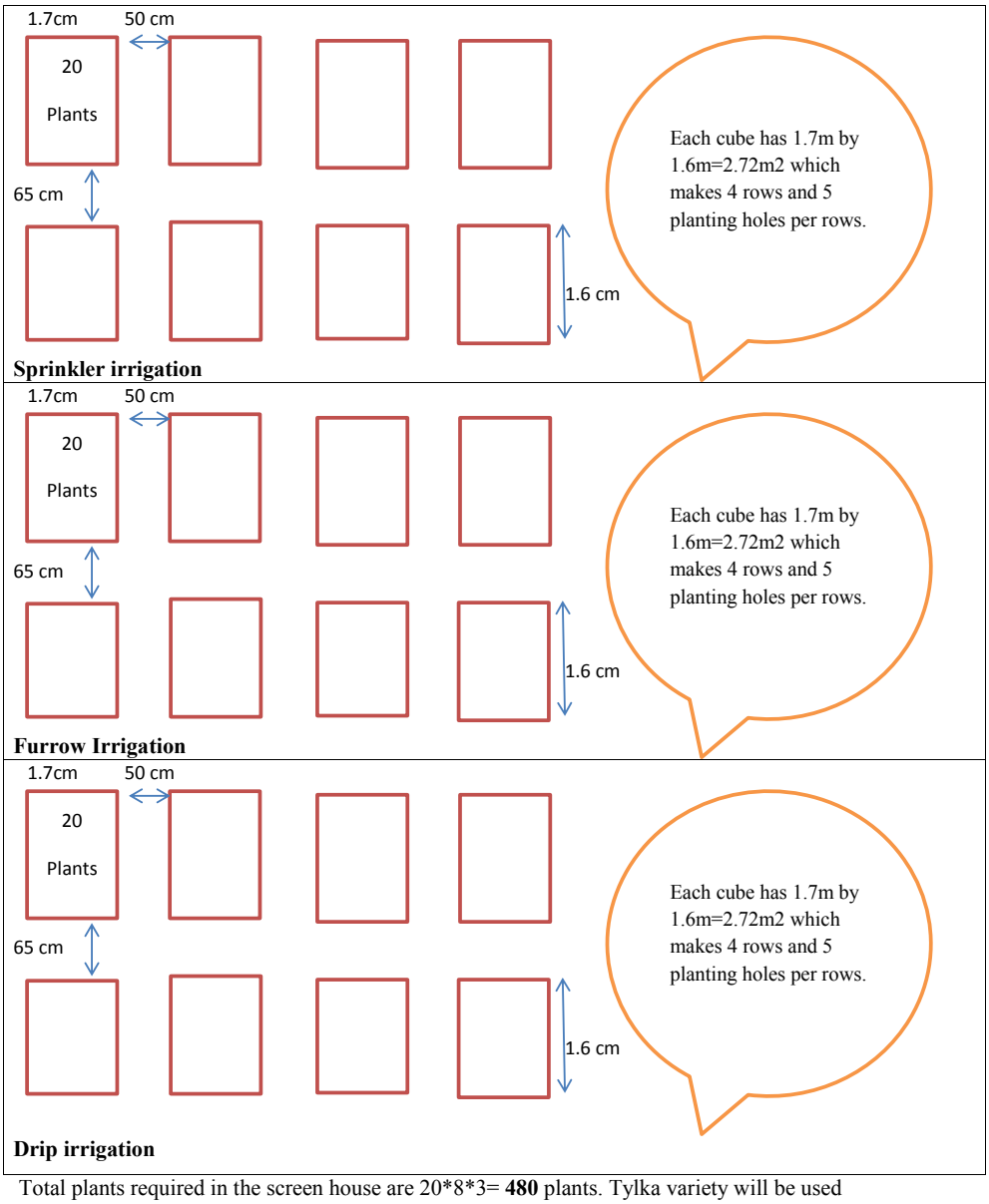

Total plants required in the screen house are 20*8*3= **480** plants. Tylka variety will be used

Figure. B.1 Morogoro in-house experiment layout description.

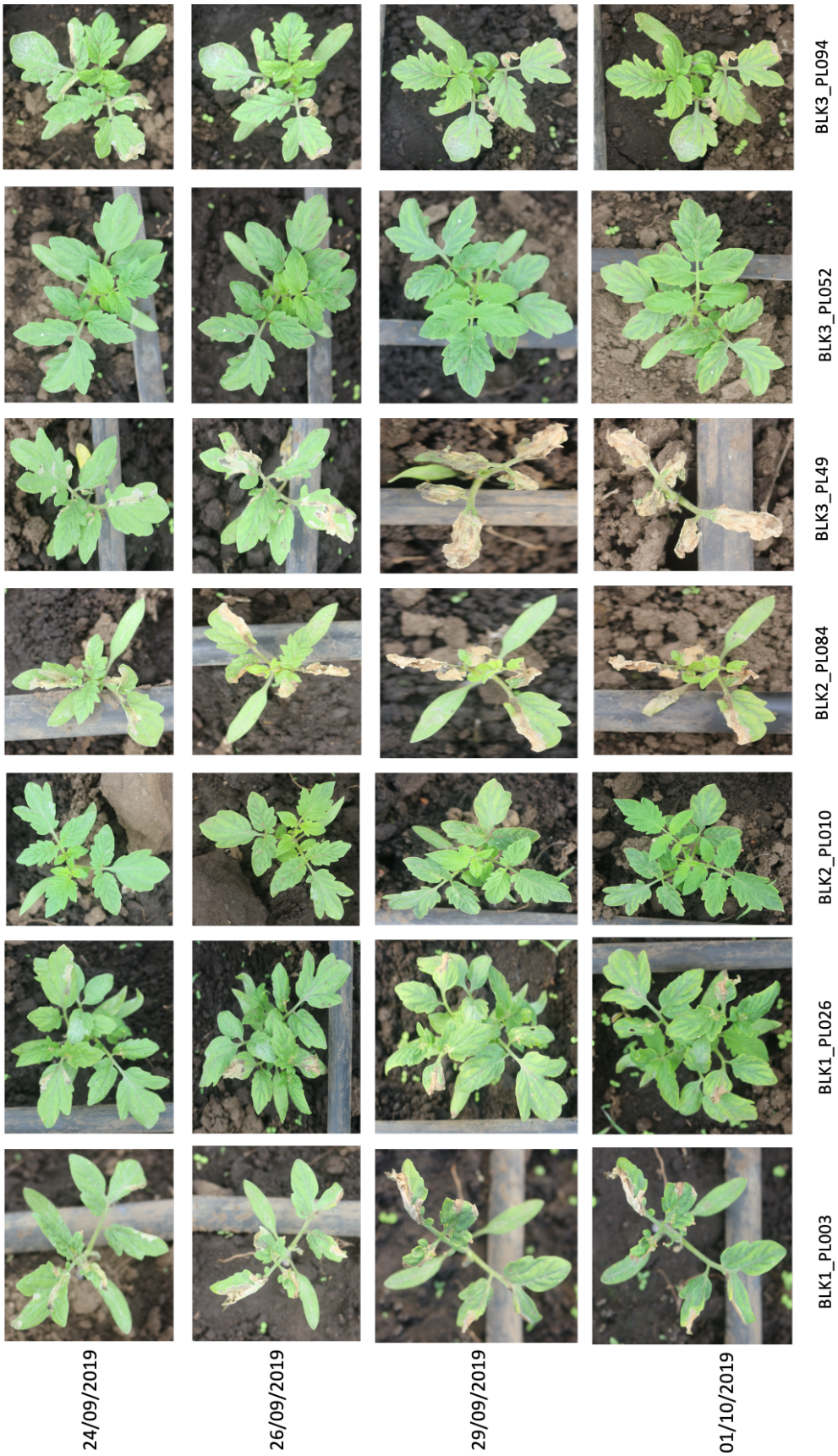

Figure. B.2 Sample dataset of tomato Images

Appendix C

EXIF Meta details of sample Images of cameras useds

Table C.1 Sample EXIF Meta data of Images taken using a PENTAX Camera during image data collection experiments in October to December 2019.

Parameter	unit/value
Exif Image Size	4,608 × 2,592
Camera Model Name (Make)	PENTAX Optio WG-2 GPS (PENTAX)
Orientation	Horizontal (normal)
Software	Optio WG-2 GPS Ver 1.00
Modify Date	2019:10:01 15:31:33
Y Cb Cr Positioning	Co-sited
ISO	125
Exif Version	230
Date/Time Original	2019:10:01 15:31:33
Create Date	2019:10:01 15:31:33
Components Configuration	Y, Cb, Cr, -
Exposure Compensation	0
Metering Mode	Multi-segment
Flash	Auto, Did not fire
Exposure Time	1/50
F Number	3.5
Focal Length	5.0 mm
Saturation	Normal
Contrast	Normal
Sharpness	Normal
Maker Note Pentax 5	(9,720 bytes binary data)
Flashpix Version	100

Continued on next page

Table C.1 – continued from previous page

Parameter	unit/value
Color Space	sRGB
Interoperability Index	R98 - DCF basic file (sRGB)
Interoperability Version	100
Custom Rendered	Normal
Exposure Mode	Auto
White Balance	Auto
Digital Zoom Ratio	1
Focal Length In 35mm Format	28 mm
Scene Capture Type	Standard
Subject Distance Range	Close
GPS Version ID	2.3.0.0
GPS Latitude (Ref)	3.375163 degrees (South)
GPS Longitude (Ref)	36.873670 degrees (East)
GPS Altitude Ref	Above Sea Level
GPS Altitude	1144 m
GPS Satellites	11
GPS Measure Mode	3-Dimensional Measurement
GPS Map Datum	WGS-84
Print Image Matching	(350 bytes binary data)
Compression	JPEG (old-style)
Resolution	72 pixels/inch
Thumbnail Length	7,042
Thumbnail Image	(7,042 bytes binary data)

Table C.4 Sample EXIF Meta data of Images taken using a Parrot Sequoia multispectral camera during image data collection experiments in October to December 2019.

Parameter	unit/value
Bits Per Sample	16
Compression	Uncompressed
Photometric Interpretation	BlackIsZero
Image Description	735 nm
Make	Parrot
Camera Model Name	Sequoia
Strip Offsets	8
Orientation	Rotate 180
Samples Per Pixel	1
Strip Byte Counts	2,457,600
Min Sample Value	0
Planar Configuration	Chunky
Software	v1.7.1
Modify Date	2019:02:11 07:41:02
Exposure Time	1/333
F Number	2.2
Spectral Sensitivity	735 nm
ISO	100
Date/Time Original	2019:02:11 07:41:02
Shutter Speed Value	1/333
Aperture Value	2.2
Max Aperture Value	2.2
Focal Length	4.0 mm
Image Number	46
Maker Note Unknown Text	0.2%00
Sub Sec Time	665,480
Sub Sec Time Original	665,480
Sub Sec Time Digitized	528,739
Focal Plane X Resolution	266.6666559
Focal Plane Y Resolution	266.6666559
Focal Plane Resolution Unit	mm
Exposure Mode	Auto
Focal Length In 35mm Format	30 mm
Image Unique ID	B1A262A49BD644A6885B1CBBEADA0C8B

Continued on next page

Table C.4 – continued from previous page

Parameter	unit/value
Serial Number	PI040378AE7I005972
GPS Version ID	2.2.0.0
GPS Latitude Ref	South
GPS Latitude Longitude	3.375265 degrees 36.873702 degrees
GPS Longitude Ref	East
GPS Altitude Ref	Above Sea Level
GPS Altitude	1150.422671 m
GPS Time Stamp	41:00.5
GPS Status	Measurement Active
GPS Speed Ref	km/h
GPS Speed	0.13166818
GPS Map Datum	WGS-84
GPS Date Stamp	2019:02:11
Black Level Repeat Dim	2 2
Black Level	5777 5734 5696 5694
Camera Serial Number	PI040378AE7I005972
Image Size	1,280 × 960
Original Raw File Name	IMG_190211_074102_0046_REG.TIF

Table C.2 Sample EXIF Meta data of Images taken using a CANON Camera during image data collection experiments in October to December 2019.

Parameter	**unit/value**
Exif Image Size	"1,275 × 1,431"
Camera Model Name (Make)	Canon EOS Kiss X7 (Canon)
Orientation	Horizontal (normal)
Exposure Time	1/50
F Number	4.5
Exposure Program	Program AE
ISO	160
Sensitivity Type	Recommended Exposure Index
Recommended Exposure Index	160
Exif Version	230
Date/Time Original	2019:10:02 15:39:04
Components Configuration	"Y, Cb, Cr, -"
Shutter Speed Value	1/49
Aperture Value	4.56
Exposure Compensation	0
Max Aperture Value	4.5
Metering Mode	Multi-segment
Flash	"On, Fired"
Focal Length	33.0 mm
Flashpix Version	100
Color Space	sRGB
Focal Plane X Resolution	2899.328859
Focal Plane Y Resolution	2894.472362
Focal Plane Resolution Unit	inches
Custom Rendered	Normal
Scene Capture Type	Standard
Lens Model	EF-S18-55mm f/3.5-5.6 IS STM
Lens Serial Number	00001aca3b
Lens Info	18-55mm f/0
Create Date	2019:10:02 15:39:04
Resolution	72 pixels/inch

Table C.3 Sample EXIF Meta data of Images taken using a Samsung Camera during image data collection experiments in October to December 2019.

Parameter	**unit/value**
Exif Image Size	320 × 240
Camera Model Name (Make)	SM-G570F (samsung)
Software	G570FXXU1CRH9
Y Cb Cr Positioning	Centered
Exposure Time	1/140
F Number	1.9
Exposure Program	Program AE
ISO	40
Exif Version	220
Date/Time Original	2019:02:15 10:48:03
Components Configuration	Y, Cb, Cr, -
Shutter Speed Value	1/140
Aperture Value	1.9
Brightness Value	5.23
Exposure Compensation	0
Max Aperture Value	1.9
Metering Mode	Center-weighted average
Flash	No Flash
Focal Length	3.6 mm
Image Size	512 × 384
Maker Note Unknown	(98 bytes binary data)
User Comment	
Flashpix Version	100
Color Space	sRGB
Interoperability Index	R98 - DCF basic file (sRGB)
Interoperability Version	100
Focal Length In 35mm Format	27 mm
Scene Capture Type	Standard
Image Unique ID	W13LSJA00AM W13LSKK01SB
Compression	JPEG (old-style)
Orientation	Horizontal (normal)
Resolution	72 pixels/inch
Thumbnail Length	33,027
Thumbnail Image	(33,027 bytes binary data)